Reconfigurable antennas for mobile phone and WSN applications

Le-Huy Trinh

UNIVERSITE DE NICE-SOPHIA ANTIPOLIS

ECOLE DOCTORALE STIC

SCIENCES ET TECHNOLOGIES DE L'INFORMATION ET DE LA COMMUNICATION

T H E S E

pour l'obtention du grade de

Docteur en Sciences

de l'Université de Nice-Sophia Antipolis

Mention : Electronique

présentée et soutenue par

Le Huy TRINH

RECONFIGURABLE ANTENNAS FOR MOBILE PHONE AND WSN APPLICATIONS

Thèse dirigée par Jean-Marc RIBERO

soutenue le 15 Juillet 2015

Jury :

M. T. P. VUONG	Professeur des Universités, INP de Grenoble	Membre
M. C. DELAVEAUD	Ingénieur, CEA-LETI de Grenoble	Rapporteur
M. L. CIRIO	Professeur des Universités, UPEM	Rapporteur
M. L. LIZZI	Maître de conférences, UNSA	Co-Encadrant
M. F. FERRERO	Maître de conférences, UNSA	Co-Directeur
M. J. M. RIBERO	Professeur des Universités, UNSA	Directeur
M. P. RATAJCZAK	Ingénieur, Orange Labs	Invité
M. F. CANNEVA	Ingénieur, Ethertronics	Invité

For my wife and my family
Nice, 15/07/2015

TABLE OF CONTENTS

TABLE OF ACRONYMS

CA	Carrier Aggregation	**LTE**	Long Term Evolution
CE	Coupling Element	**MEMS**	Micro Electro-Mechanical Systems
DTC	Digitally Tunable Capacitor	**MIMO**	Multiple Input Multiple Output
EM	Electromagnetics	**MN**	Matching Network
GSM	Global System for Mobile Telecommunications	**PCB**	Printed Circuit Board
HB	High-Band	**PIFA**	Planar Inverted F Antenna
IFA	Inverted F Antenna	**SMD**	Surface Mount Device
LB	Low-Band	**UMTS**	Universal Mobile Telecommunications System

ACKNOWLEDGEMENT

First of all, I would like to extend my sincere thanks to my advisor Prof. Jean-Marc Ribero and Mr. Fabien Ferrero for their valuable support and brilliant ideas. Throughout this thesis, they have always found the time for me to guide and encourage my research activities. I also very much appreciate their dynamism and their competences that made this thesis work a success. It has been my real pleasure to work with Jean-Marc and Fabien. Acknowledgement

I would also like to thank Mr. Leonardo Lizzi and Prof. Robert Staraj who helped me so much with their stimulating technical discussions and constructive publication reviewing.

I am grateful to the committee members of my jury, Prof. Tan Phu Vuong, Prof. Laurent Cirio and Mr. Christophe Delaveaud for their valuable inputs and time spent reading this thesis.

I would like to express my appreciation to my colleagues and friends at LEAT and also at Orange Labs La Turbie, for all the unforgettable enjoyable moments and their helps. I wish to extend my warmest thanks to all my friends in France and Vietnam for all the wonderful time we spend together.

Finally, last but not least, I want to express my special gratitude to my parents and my wife for their unconditional support, love and trust. They, together with another members in my big family, make my life full of kindness and happiness with their encouragement.

ABSTRACT

In recent years, telecommunication technologies have witnessed exponential growth, especially in the cellular communications and wireless sensor networks segment. To meet the demand for increasing transmission capacity, improving the signal to noise ratio of cellular communication channels and expanding the operating band of the equipment is necessary. For example, when 4G standard was designed and deployed, several new bands were added. The expansion of the operating band poses a huge challenge, especially in the low frequency band, because of the large wavelength. The design of a wireless system that has one or more multi-standard antennas integrated in a mobile device is very difficult. Passive antenna has reached a limit, and the use of frequency reconfigurable antenna to extend operational bandwidth is a promising solution. Besides, in wireless sensor networks application, directional reconfigurable antenna has the potential to reduce collisions, increase communication distance and optimize consumption, when compared with traditional omnidirectional antenna.

The main objective of this work was to design and optimize the reconfigurable antenna for cellular communications and wireless sensor network. The manuscript is divided in five chapters. The first chapter will introduce the evolution of telecommunications from the past to the present, issues, motivation and challenges that should be solved in the future. Some possible solutions are proposed and will be presented in detail in the following chapters.

Chapter 2 will give an overview of active components that were integrated in the reconfigurable antenna. The characteristics, advantages and disadvantages of these components are highlighted. Besides, a recent component, digitally tunable capacitor (DTC), is introduced. This device is a good candidate to be integrated in the antenna for cellular communication and wireless sensor network applications. An example of reconfigurable frequency antenna for white space antenna is presented.

In chapter 3, several antennas are proposed with multiband, MIMO and frequency reconfigurable antenna features for future cellular communication systems. These radiating structures can be used to extend the operating frequency band of the communication system, optimize spectral efficiency and improve signal to noise channel level. Geometry of these antennas is introduced together with the results of simulation and measurement.

Afterwards, chapter 4 will address the design of reconfigurable directional antennas for WSN applications. The simulation results and measurement results are also presented in this chapter. Thanks to the use of beam steering antennas, power consumption of WSN system will be optimized.

Finally, chapter 5 will summarize the work performed in this thesis, and will put into perspective the proposed solutions with the challenges given in chapter 1. Besides, perspectives on this work will be highlighted.

CHAPTER I
INTRODUCTION

For the several centuries, technologies to support long-distance communication have been strongly studied and developed. In Vietnam, ancient Vietnamese people were known to exchange information over a long distance by using an instrument called Trong Dong (Figure 1.1). This is a type of drum that made with copper. Trong Dong was mainly used in war against enemies of Van Lang (the first semi-legendary nation of ancient Vietnamese people in the early 3rd century BC). Thanks to good acoustic wave propagation, Van Lang commander were able to transmit orders to its soldiers. Afterwards, Trong Dong has become an important symbol of ancient Vietnamese people. Year by year, the primitive tool has been replaced by modern electronic devices. Currently, mobile phone, computer, Internet became common commodity in Vietnamese daily life.

Figure 1.1: Trong Dong of ancient Vietnamese people

In Vietnam, the first development has been started later than many countries in the world. In the 80s, the telecommunications system was put into use in Vietnam [1]. However, it serves primarily for the government and military communications. By 1992, Vietnam Posts and Telecommunications (VNPT) has launched telecommunications services to the public. By 1993, the first mobile network in Vietnam under the name MobiFone was put into operation. At this time, the cellular communication concept was relatively unfamiliar and there was very few users because of the limited coverage and high cost of mobile devices. Furthermore, the subscription charges and the cost were very expensive, about $200 registration fee per subscriber and the monthly subscription charge was about $30. By 2007, one year after Vietnam joined the WTO, telecommunications market grew strongly and become the second fastest growing area in ASEAN telecommunications market.

On the Internet segment, the number of user increased strongly between 2008 and 2012, from 20.8 million to 33.4 million (94 million inhabitants in Vietnam). However, between 2012 and 2014, this growth has slowed down and reached 35.6 million users in 2014 because of limited coverage in countryside. Besides, the number of people using broadband Internet is less than the ordinary Internet users. But with rapid growth at present, we expect 12.8 million new broadband subscribers in Vietnam in 2015, representing a growth rate of 13.5%.

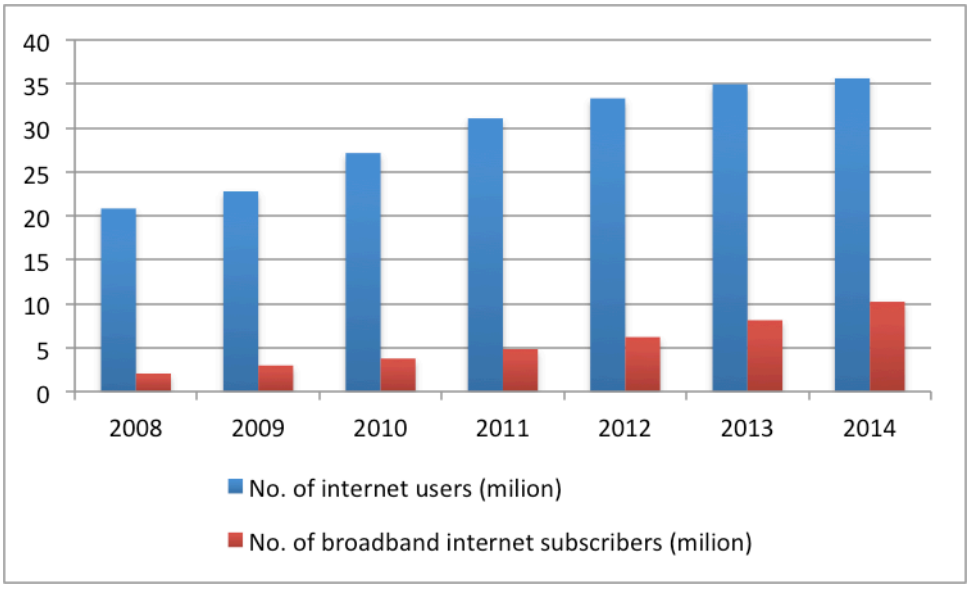

Figure 1.2: Evolution of Internet in Vietnam

Regarding mobile communications segment, Vietnam's high mobile penetration rate has finally taken a toll on the country's growth momentum as the growth rate in the second half of 2010 slowed significantly. From 2008 to 2014, the number of mobile subscribers increased from 69 million to 224.4 million. Because Vietnamese subscribers constantly switch providers and hold onto multiple SIM cards at any one time, hence 224.4 million only represents the number of SIM sales, not the number of actual subscribers. In 2009, 3G communication services was supported and supplied in Vietnam. Within six years, the number of 3G subscribers grew from 4 million to 38 million, this trend is predicted to continue to increase because the cost of 3G in Vietnam at quite cheap compared to other countries.

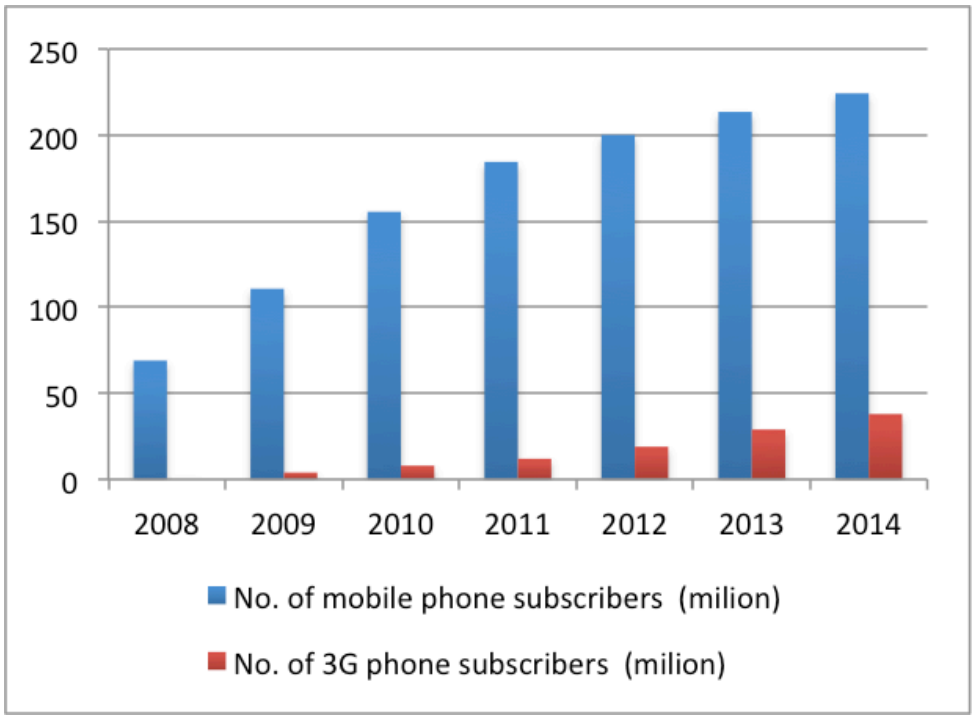

Figure 1.3: Evolution of mobile phone in Vietnam

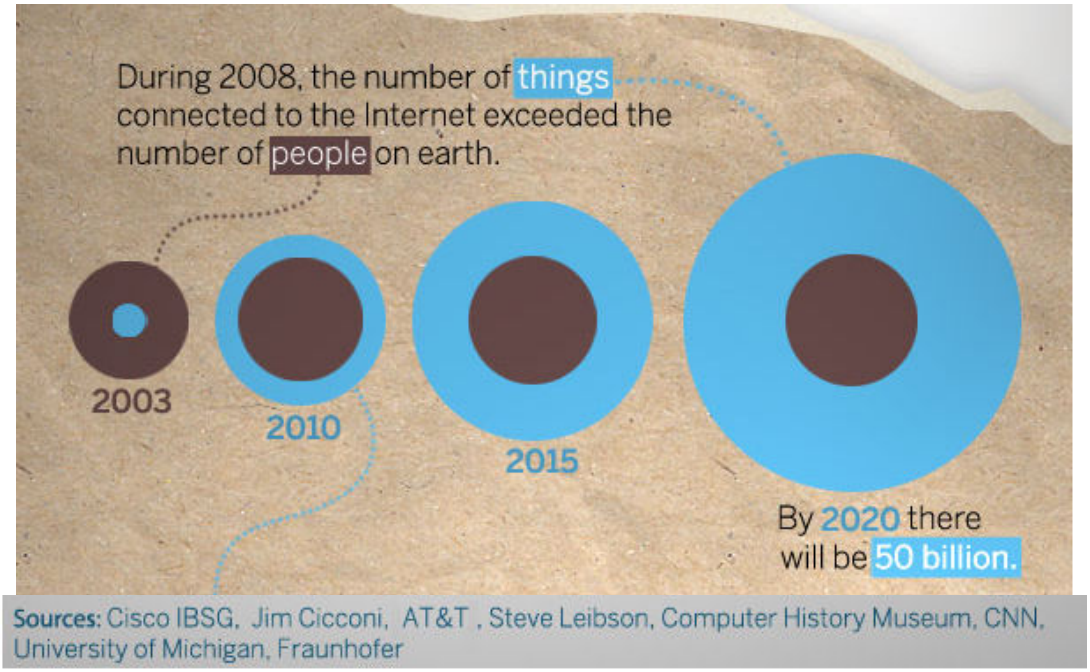

Figure 1.4: The evolution of connected devices from 2003 to 2020.

To satisfy the demand for telecommunications services, the telecommunications equipment provider gave a lot of diverse products towards different customer groups (mobile phone, tablet, laptop, etc). Due to the strong development of semiconductor technology, the cost of equipment for telecommunications was strongly reduced, so that customers have the ability to possess multiple wireless devices simultaneously. In 2008, an important achievement was marked, as the number of devices connected to the Internet has surpassed the number of people on earth. The first element to explain the exponential growth should be mentioned is the rapid rise of the middle class. According to statistics in 2010, the researchers estimated the rapid growth of the middle class in the world, from 2009 to 2030; the number of people in the middle class will increase from 1.8 billion to 4.9 billion. Especially in Asia, in 2009, middle class accounted for 28%, and this study predicts that this number will increase further to 66% in 2030.

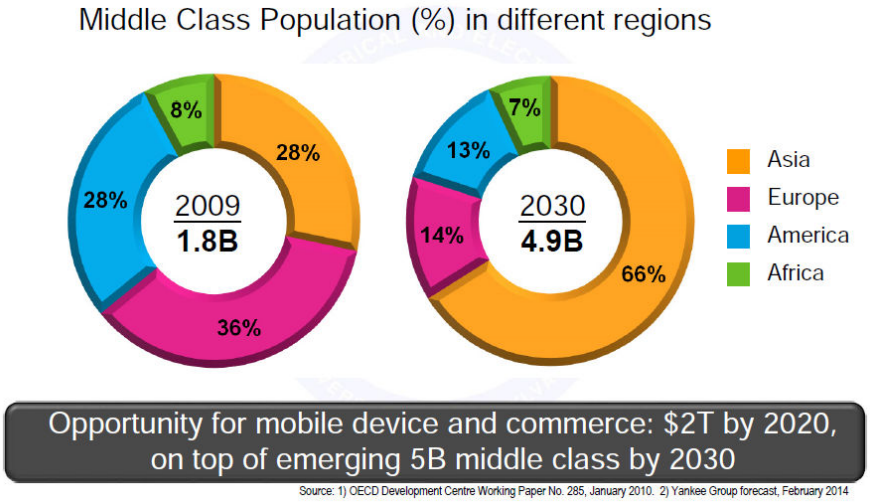

Figure 1.5: Evolution of middle class population en different regions

Another reason should be mentioned is the demands for multiple connected devices for a same user. Previously, wireless devices were expensive equipment such as desktop computers, laptops, fixed phones, and mobile phones. Up to the present time, devices such as smart phones, tablets, smart watch appear to give new services for data transmission, entertainment, health monitoring, etc. And then, in the future, everyone will use more than tens of connected devices, which will provide support for a better life (smart home, smart car, etc…).

Figure 1.6: The variety of devices from past to future

Associated with the development of the technology, the wireless network systems are becoming more ubiquitous. They not only satisfy the communication needs of person-to-person and person-to-server but also of machine-to-machine. Thus, mobile phone networks and wireless sensor networks (WSN) play important roles in telecommunications. They are focused and prioritized in industrial research and development strategy. A report from Ericson in November 2014 showed the rapid growth of mobile data traffic [2]. At the end of 2014, there were 2500 petabytes of total monthly traffic. In addition, the cellular connection speeds in 2014 was about 1700 kbps, also grew 20% in comparison with 2013.

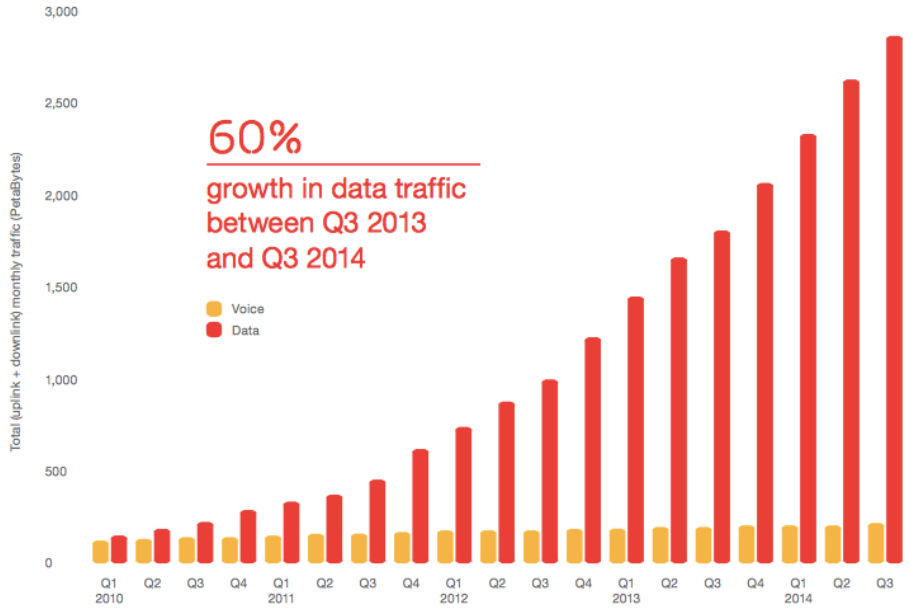

Figure 1.7: Evolution of mobile data traffic

Considering WSN, they were first developed for military applications, but now WSN are studied and deployed in new areas such as environment, health, home, automotive, etc. A report of IDTechEx predicted that the market for WSN will grow from 0.45 billion dollars in 2011 to 2 billion dollars in next 10 years [3]. These developments above posed to the researchers a lot of challenges. To improve the performance of the system, the optimizations of software, protocols and also hardware are necessary, particularly antenna systems. In this chapter, mobile phone networks and wireless sensor networks will be introduced in a general way, as well as the challenges of antenna system and proposed solutions.

1. MOBILE PHONE NETWORKS

In 1973, the first call of Martin Cooper marked the beginning of the mobile telecommunications technologies. For over 40 years, the development of cellular communication from 1G to 4G has fully met the basic needs of voice transmission as well as the data transmission.

1.1. Evolution of mobile phone networks

In 1979, the first generation was studied and deployed in Japan by Japan's Nippon Telephone and Telegraph Company. Shortly thereafter, the similar system was developed and deployed in Europe (*Nordic Mobile telephone* NMT-400) in 1981 and the US (*Advanced Mobile Phone Service* AMPS) in 1983. Basically, first generation mobile system provided voice transmission by using frequencies around 900 MHz and analog modulation schemes.

Second-generation (2G) system was introduced at the end of the 1980s. It was based on low-band data signaling and also aimed primarily toward the voice market but, unlike the first generation system, it used digital modulations. Shifting from analog to digital enabled several improvements in systems performance. System capacity was improved through the use of spectrally efficient digital speech codecs, multiplexing several users on the same frequency channel via time division or code division multiplexing techniques. In addition, tighter frequency re-use enabled by better error performance of digital modulation, coding, and equalization techniques, which reduced the required carrier-to-interference ratio from 18dB to just a few dB. The most popular 2G wireless technologies are known as the *Global Systems for Mobile Communications* (GSM) in Europe, the *Code Division Multiple Access* (CDMA) and the *Time Division Multiple Access* (TDMA) in North America and part of Asia.

The first GSM system used a 25 MHz frequency spectrum in 900 MHz band. A *mobile station* (MS) consists of 2 main parts: the smart card called *subscriber identity module* (SIM) and the *mobile equipment* (ME). It communicates with a *base station system* (BSS) through radio interface (Um). Inside of BSS part, there are the *base transceiver station* (BTS) that handles the radio physical layer and *base station controller* (BSC) that deals with radio resource management and handover. Thanks to BSC, the BSS can connect to *network and switching system* (NSS). It consists of the circuit-switched core network, which used for traditional GSM service such as voice calls, SMS, and circuit switch data calls. Beside, NSS was extended to provide packet-switched data services known as the GPRS core network.

Thanks to this expansion, the mobile station can access to Internet services. The next step in GSM evolution was *enhanced data rates for GSM evolution* (EDGE). It allows improving data transmission rates by using a new modulation type, 8PSK. The EDGE standard has a maximum per slot data rate of 59.2kbps, a three times increase from GPRS speeds. Unlike GSM standard, CDMA uses spread spectrum multiple access technique. Thus, in CDMA standard, multiple users share the same frequency channel at the same time. Instead of time-slicing multiple users in a given frequency channel, user is given a orthogonal spreading code that is used to separate their signals at the receiver. Based on this technique, CDMA is recognized as providing clearer voice quality with less background noise, fewer dropped calls, enhanced security, greater reliability and greater network capacity. [4]

As mention in previous section, 2G systems are focus on the voice transmission. It provided significant increase in voice capacity, improved voice quality, and began support for data applications such as Internet access. However, it has the huge issue of the limited data capabilities, thus third generation (3G) was born. With this new generation, there are many enabling technologies such as wideband code division multiple access (W-CDMA), intelligent antennas, software defined radio (SDR), and advanced digital signal processing devices (DSP). These technologies allow improving the spectral efficiency and performance of 3G. This generation systems have been demonstrated a remarkable advantage compared with the previous generation. It provided much higher data rates, significant increase in voice capacity, and supporting advanced services and applications. Depending on environment conditions, quality of transmission channel is different. It can provide 2Mbps in fixed or in building environments, 384kbps in pedestrian or urban environments, and further reduced to 144kbps in wide area vehicular environments.

Long term evolution-Advanced (LTE-A) is the global standard for the fourth generation of cellular communication. Using a different radio interface together with core network improvements the capacity and speed of 4G are increased. Beside, LTE-A uses the popular orthogonal frequency division multiplex access (OFDMA), which provides the essential spectral efficiency to achieve high data rates and allows multiple users to share a common channel. On the other hand, at the higher frequencies, the receiver can obtain the signals from multiple paths. Most of the time, the light-of-sight configuration is blocked, the signals are reflected, diffracted and scattered along multiple paths before being received at the receiver. When the different signals are combined in destructive ways, the received signal suffer from abrupt dips, which are unexpected and will degrade the performance of the channel. Thanks to the use of OFDMA, the multipath effects can be mitigated. Moreover, with the modulation schemes of QPSK, 16QAM and 64QAM, LTE enable peak data rates of up to 1Gbit/s for low-mobility user in downlink (100Mbit/s for high-mobility user) and 500Mbit/s for uplink. About the hardware, multiple-input multiple-output (MIMO) is a key technique in this generation. It is a very useful tool in order to increase the spectral efficiency. LTE-A used some of the existing frequency band of 3G systems as well as the new frequency bands. The channel bandwidth allocated is variable between 1.4MHz and 20MHz. Generally, most of the frequency bands are reserved for frequency division duplexing (FDD) from LTE band 1 to

LTE band 31. LTE bands 33 through 44 are used for time division duplexing (TDD) with the same frequencies for both downlink and uplink.

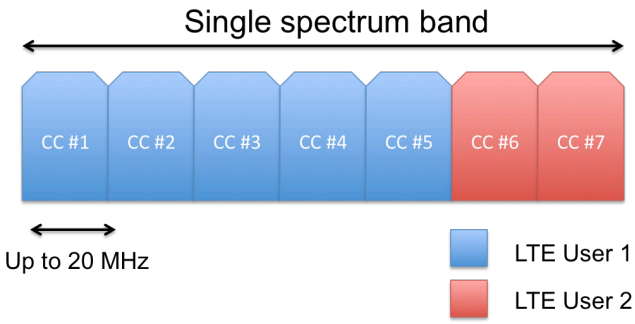

Figure 1.8: Carrier aggregation in contiguous bandwidth

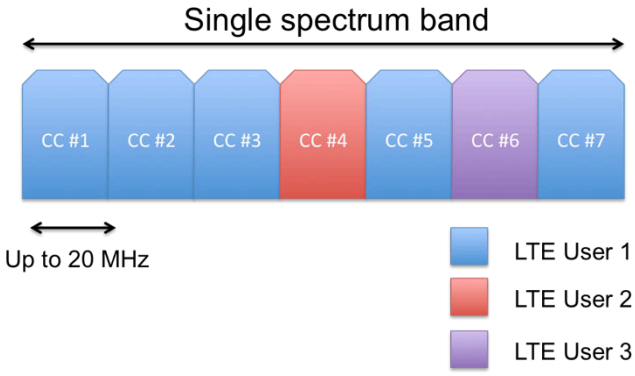

Figure 1.9: Carrier aggregation in noncontiguous bandwidth, single band

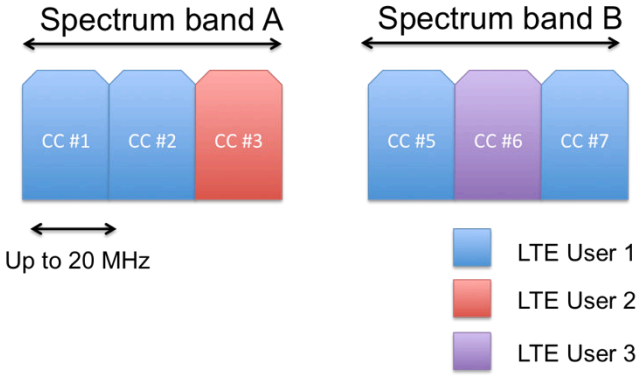

Figure 1.10: Carrier aggregation in noncontiguous bandwidth, multiple bands

More particularly, LTE-A system also supports the contiguous and the noncontiguous carrier aggregations. They mean, a single user can occupy more than one available carrier, and the component carriers can be noncontiguous in the same spectrum band or in the different spectrum bands [5]. The principle of this technique is shown in Figure 1.8, Figure 1.9, and Figure 1.10. Finally, carrier aggregation allows a service provider to offer up to 100 MHz of bandwidth per user in order to increase the performance of system.

Description	Spectrum	Advantage	Target Utilization
Low bands	470-690 MHz	**Great propagation** characteristics	Cellular coverage network
	694-790 MHZ		Mobile broadband
Low-to-mid bands	1350-1525 MHZ	**Good coverage** and **complement** below 1 GHz bands	Contribute to the need of coverage and capacity for the future development
	Bands around 2000 MHz	Possible to combine the **MSS Band**, existing **3GPP Band 1/I**, **TDD Bands 33/34** and the bands 2090-2110 MHz / 2170-2200 MHz can create a **broad contiguous frequency band**	Mobile broadband
Mid-to-high bands	3400-4200	**Large contiguous bandwidth, good frequency reuse**	Microcell and picocell network. High capacity
	4400-4990		

Table 1.1: Summaries of different possible candidate frequency bands

Up to the present moment, 5G technologies are still being studied. As mention in the WRC 2012, the consideration of additional spectrum allocations for future IMT (so-called 5G) will be discussed in the WRC-15. It will mainly focus on frequency band below 6 GHz [6], [7]. Some frequency ranges are suitable for the future deployment of IMT that were proposed such as 410-430, 470-790, 1000-1700, 2025-2110, 2200-2290, 2700-5000, 5350-5470, and 5850-6425 [8]. For each frequency band, the strategies and utilizations are different such as the lower frequency bands (for example 470-790 MHz) are suitable for providing coverage for both indoor and outdoor due to its great propagation characteristics. And higher frequency bands (for example 3400-3800 MHz) are most suitable to provide high capacity and performance for small coverage, etc. In [9], White paper from Huawei proposed a tentative spectrum for WRC-15, accompanied by the detailed analysis and the summaries for each frequency band. This document mainly discussed about possible candidate bands such as 470-694 MHz, 694-790 MHz, 1350-1525 MHz, bands around 2 GHz, 3600-4200 MHz, and 4400-4990 MHz. The main advantages and the different utilization of each band are shown in the Table 1.1.

1.2. Antenna Challenges

As mentioned in the previous section, a summary of the operating frequency range is shown in Figure 1.11. The main objective is to design antenna system for mobile devices that can operate for all existing band of mobile phone from 2G to 4G, and also for extension band planned for 5G communications. To facilitate the analysis, the operating band of the antenna is divided into three parts, (1) low-band 500-960 MHz from (2) mid-band from 1710 to 2700 MHz, and (3) high- band from 3400-4200 / 4400-5000 MHz.

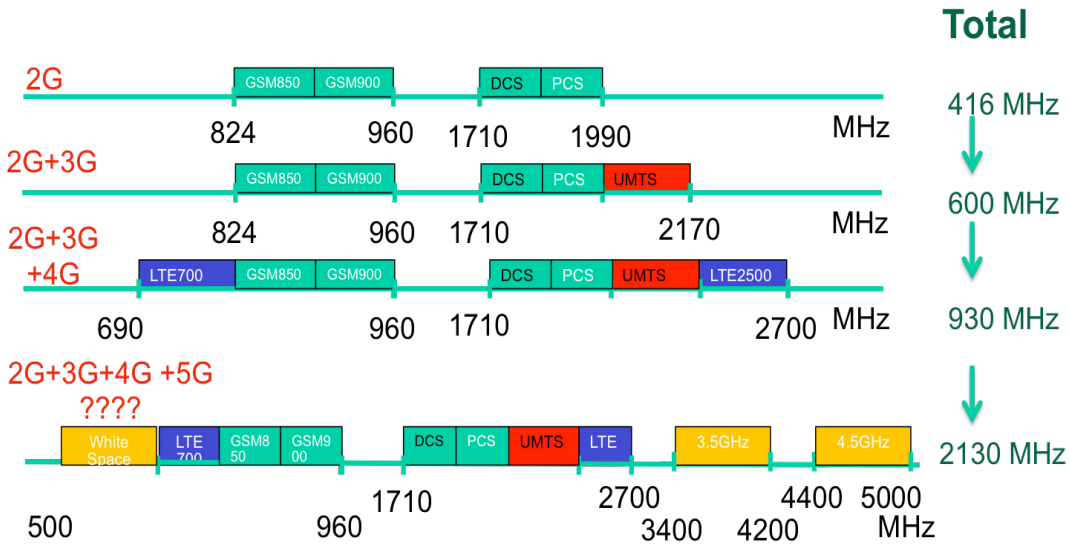

Figure 1.11: Frequency spectrum requirements for future standard antenna

Firstly, the design of a passive multi-band antenna that can cover a wide non-contiguous frequency range of 2130 MHz is not simple. Especially the broadband from 500-960 MHz is very complicated because the wavelength at the frequency of 500 MHz is large, about 600 mm, and the integration of antenna in a mobile terminal is a big challenge. Besides, following the trend of technology, the size of the antenna has to miniaturized as much as possible to make room for other electronic components such as large touchscreen, speaker, microphone, USB, battery, etc. Typically, the available space of antenna in a mobile phone is 10mm × 50mm × 7mm. Associated with the reduction in the size of the antenna, the efficiency should also be preserved. Finally, miniaturization is also needed because it will enable to integrate multiple antennas in a device to support MIMO schemes.

1.3. Proposed Solutions

As mentioned above, the design of miniaturized passive antenna operating in the frequency band 500-960 MHz is over fundamental antenna limits. Therefore, frequency reconfigurable antenna is a good solution for the low-band. Thanks to reconfigurable RF components, the resonant frequency of antenna will tune on the band requirement. For other bands in higher frequencies, parasitic elements could be integrated to create additional resonances. Using a combination of these resonances, the mid-band and high-band can be covered. The surveying and testing of reconfigurable components will be introduced in chapter 2. The proposed antennas will be presented in chapter 3 with their characteristics and also their results.

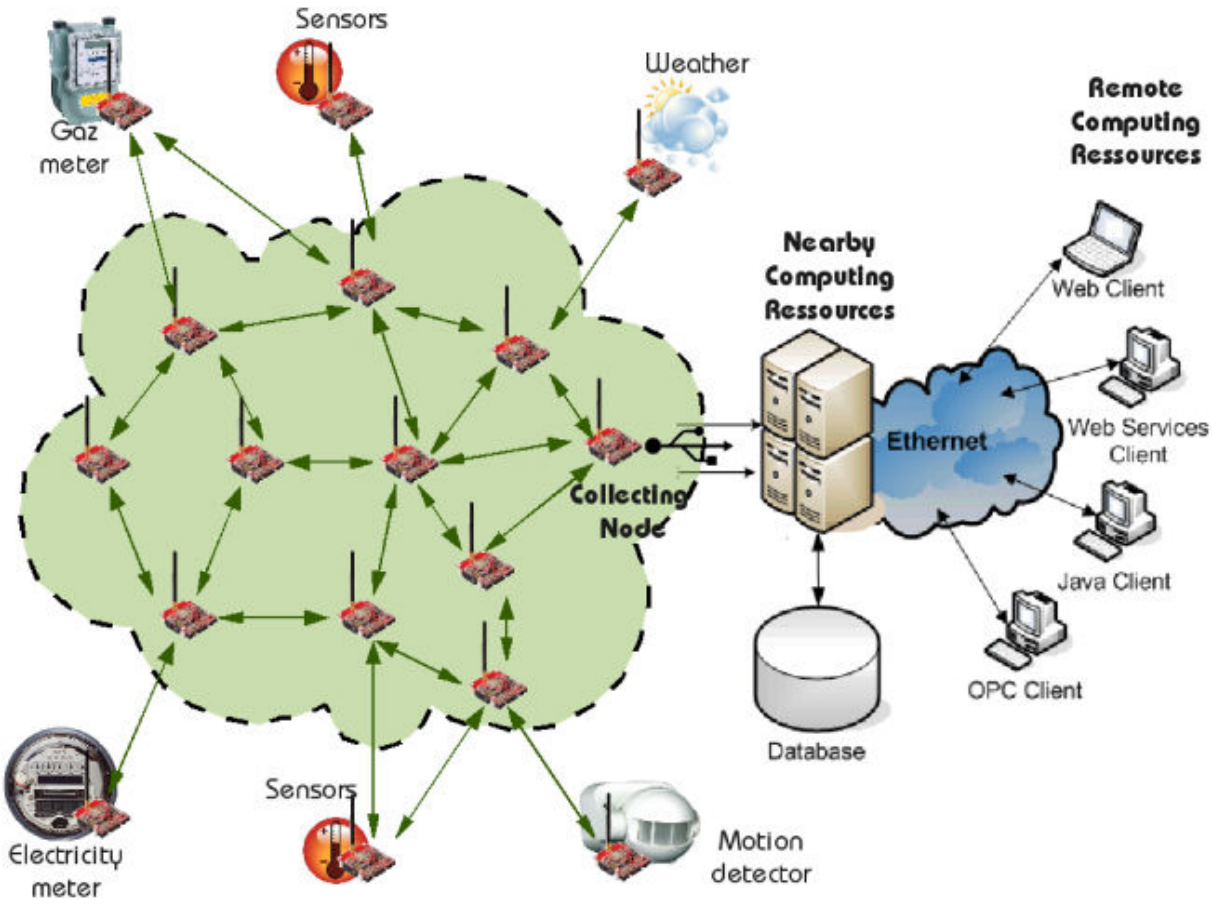

Figure 1.12: Classical structure of wireless sensor networks

In recent years, wireless sensor network (WSN) has been considered a hot trend in wireless communication technology. There have been many studies focused on the design, development and optimization of this type of system. As shown in Figure 1.12, WSN is defined as a large number of small sensing self-powered nodes, which gather information or detected special events and communicate in a wireless fashion [10]. Specially, sensing, processing and communication are mentioned as the key elements on WSN. Recent advances in nanotechnology and micro-electro-mechanical (MEMS) technologies have facilitated the development of multifunctional sensor nodes that have small size, low-cost and energy saving.

The architecture of classical wireless sensor node is shown in Figure 1.13. It consists of the main components such as:

- Sensing unit
- Processing unit
- Transceiver unit
- Power unit
- Location finding system (optional)
- Power generator (optional)
- Mobilizer (optional)

The first important requirements of WSN is the node's **lifetime**, the network should be power efficient and fulfill its task as long as possible. The energy savings can be obtained from the optimization of software or hardware used on the system. Using energy harvesting from the environment is also a good solution to increase the WSN lifetime .

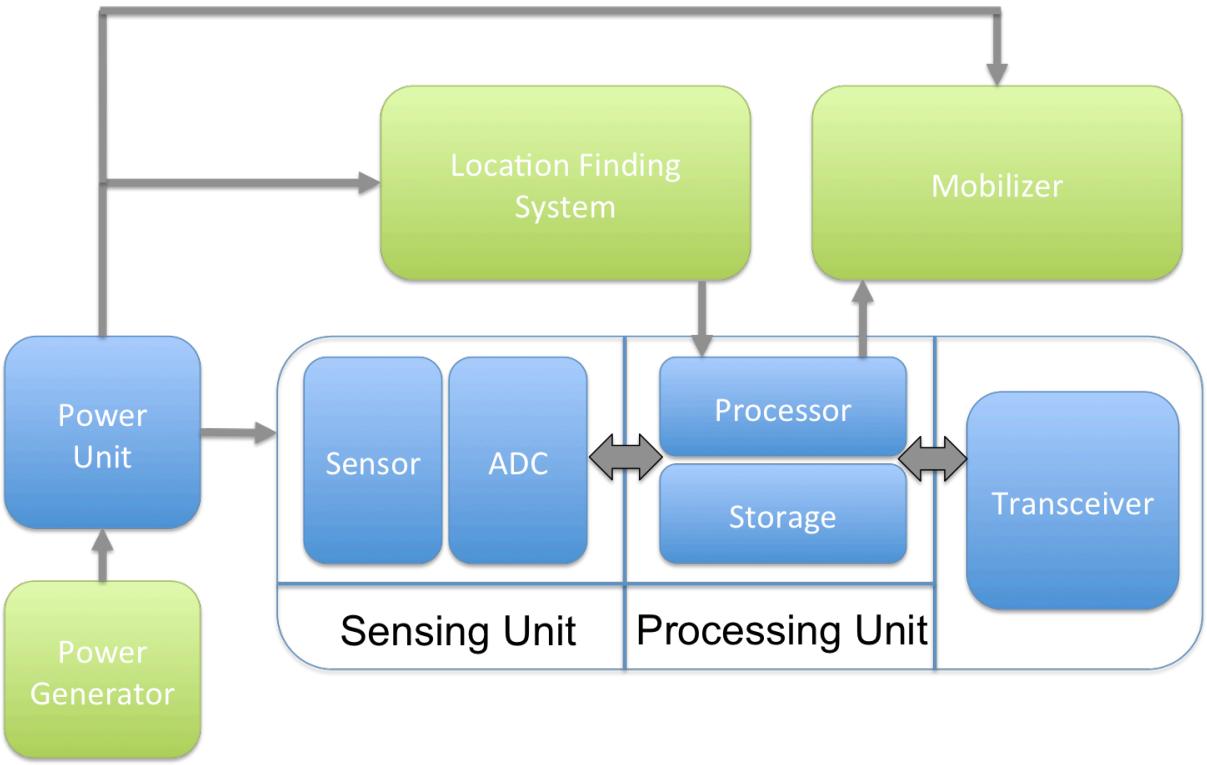

Figure 1.13: Architecture of typical wireless sensor nodes

Beside, the wireless sensor system should be based on **low cost** devices because the number of node can be up to thousands or more. The new technology such as nanotechnology and micro-electro-mechanical (MEMS) can reduce the price of WSN.

Sensor network should be very **flexible** to adapt to the different conditions and **scalable** to support large number of nodes. The system should be self-reconfigured to guarantee the network connection when the failure of individual nodes occurs. The **reprogramming** of sensor nodes is also important to update the new configuration and improve the performance of system.

Finally, a sensor network should be able protect itself an its data. For the **secure** data transmission, the encryption keys have to be established among sensor nodes.

There are many different types of sensors that are used on WSN such as:

- Temperature
- Humidity
- Vehicular movement
- Lightning condition
- Pressure
- Soil makeup

- Noise level
- The existence of certain kinds of objects
- Mechanical stress levels
- The current characteristics such as speed, direction, and size of an object

In [11], I.F. Akyildiz et al. categorized the WSN application into military, environment, health, home and other commercial areas. In addition, space exploration, chemical processing and disaster relief are also considered as the expanding categories.

2.1. Antenna Challenges

Typically, the majority of researchers are currently focusing on design of power-aware protocols and algorithms for optimizing the performance of WSN. These methods will limit the asynchronization of the nodes that can cause significant topological changes and might required re-routing of packets and re-establishing of the network.

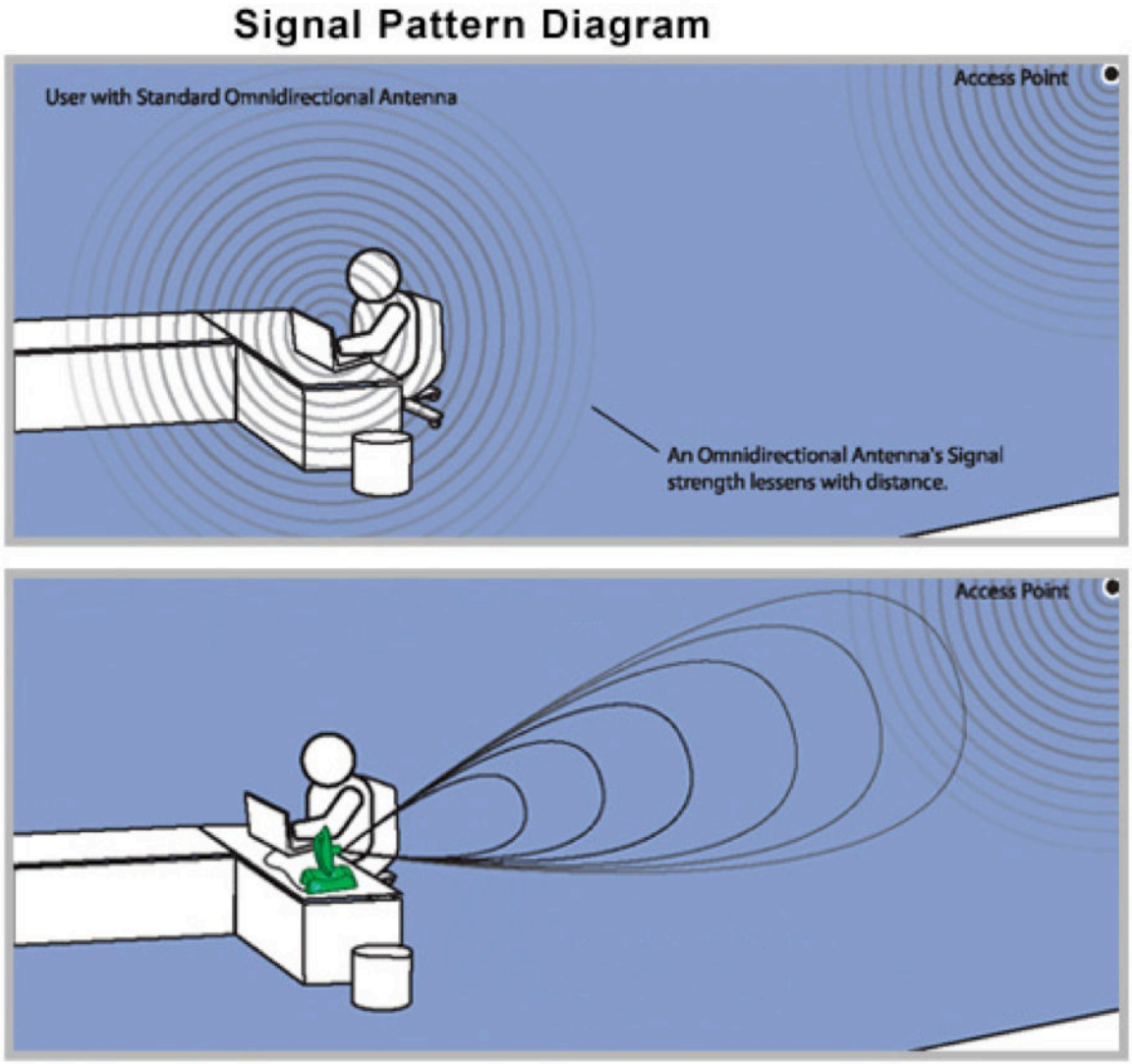

Figure 1.14: Comparison between omnidirectional and directional antennas.

In addition, the optimization of the transmission link is also a good option, especially increasing the performance of the antenna on the wireless sensor node. However, up to now, there are not many research papers focused on the antenna systems for WSN applications. Most of WSN systems use the miniature sleeve dipole antenna or printed IFA. Although the use of these antennas is relatively simple (buy-plug-play), their performances are limited (about 0 dBi of gain). This type of antenna provides an omnidirectional radiation pattern. The ability to receive signals from almost every direction (azimuth plane) is the main advantage of omnidirectional antenna. In addition, this type of antenna is very sensitive in multipath environments when the fading effect is important. In this case, the drop in the quality of transmission channels will lead to more packet errors. Thus, the packets have to be resend and the overall power consumption will increase. To solve this problem, directional antenna can be considered as an interesting solution. The main advantage of this solution is a higher gain because radiated power is focused and it propagates the signal in one or more specify directions. Besides, the effect of noise from unwanted signals is reduced, thus channel quality is improved. However, the larger dimension is a classical drawback of this antenna type. Additionally, in the networks that contain hundreds or thousands of sensor nodes, the restriction on the number of signal propagation direction is its fatal weaknesses. This is also a big reason there is very little research that refers using directional antenna in the field of WSN.

2.2. Proposed Solutions

Solving the above problems and maximizing the advantages of directional antennas are an important motivation of this thesis. Firstly, we focus on the antenna size problem. Instead of using the dipole or monopole, planar IFA and wire-plate antenna are the good candidates. Thanks to the addition of short element and optimizing the location as well as its dimension, the size of the antenna is reduced as much as possible. Then, the propagation direction limitation of fixed directional antenna has to be solved. Radiation pattern reconfigurable antenna is a good solution. The possibility of reconfiguring the antenna to radiate towards the location of the target node allows the overcome of directional antenna limitations, thus improving the performance of the WSN. The approach and proposed antenna will be presented in chapter 4 of this thesis. Through these results, we can demonstrate the huge benefits of radiation pattern reconfigurable antenna in WSN.

REFERENCE OF THIS CHAPTER

[1] Business Monitor International. (2010, December). *Vietnam telecommunications Report* [Online]. Available: http://businesstimes.com.vn/wp-content/uploads/downloads/2013/05/Vietnam-telecommunications-Report-Q1-2011.pdf

[2] Ericsson. (2014, November). *Ericsson Mobility Report* [Online]. Available: http://www.ericsson.com/res/docs/2014/ericsson-mobility-report-november-2014.pdf

[3] P. Harrop and R. Das, “Wireless sensor networks (wsn) 2012-2022,” IDTechEx, Tech. Rep., Decermber 2012.

[4] Vasco Pereira, Tiago Sousa, Paulo Mendes, Edmundo Monteiro, “Evaluation of Mobile Communications: From Voice Calls to Ubiquitous Multimedia Group Communications”, in Proc. Of the 2nd International Working Conference on Performance Modeling and Evaluation of Heterogeneous Networks, HET-NETs’04, Ilkley, West Yorkshire, U.K., July 2004.

[5] Ian F. Akyildiz , David M. Gutierrez-Estevez, Elias Chavarria Reyes: The evolution to 4G cellular systems: LTE-Advanced , Physical Communication 3,pp.4,10,21 Available on: http://www.journals.elsevier.com/physical-communication

[6] ITU-R Resolution 233, “Studies on frequency-related matters on international mobile telecommunications and other terrestrial mobile broadband applications,” Tech. Rep. 233 [COM6/8], Mar. 2012.

[7] ITU-R Administrative Circular CA/201, “To administrations of member states of ITU and radiocommunication sector members: Preparation of the draft CPM report to WRC-15,” Tech. Rep. CA/201, Jan. 2013.

[8] ITU-R Joint Task Group, “Annex 3 to joint task group 4-5-6-7 chairman’s report working document towards preliminary draft CPM text for WRC- 15 agenda item 1.1,” Tech. Rep. Document 4-5-6-7/393-E, Oct. 30, 2013.

[9] Huawei. (2013, February). *Whitepaper On Spectrum* [Online]. Available: http://www.huawei.com/ilink/en/download/HW_204545

[10] D. Puccinelli and M. Haenggi, "Wireless sensor networks: applications and challenges of ubiquitous sensing," IEEE Circuits and Systems Magazine, vol. 3, no. 3, pp. 19-29, 2005.

[11] I. F. Akyildiz, W. Su, Y. Sankarasubramaniam, and E. Cayirci, “Wireless sensor networks: a survey,” Computer Networks, vol. 38, no. 4, pp. 393–422, 2002.

CHAPTER II
ACTIVE COMPONENTS AND WHITESPACE ANTENNA EXAMPLE

In this chapter, we analyze as well as choose the reconfigurable components suitable for the antenna towards mobile phone and WSN applications. After selecting the appropriate component, a frequency reconfigurable antenna and controlled system are designed with the integration of this element. Through the measurement results, the performance of the antenna as well as the components will be confirmed. Thanks to using multiple reconfigurable resonators, a diversity antenna system is designed with the aim to minimize the effects of fading effect and exhibits performance antenna system.

1. ANALYSIS OF RECONFIGURABLE COMPONENTS

On the previous part of this manuscript, many studies and new concepts have been introduced about reconfigurable antenna. This is an antenna can reconfigure the radiation pattern, resonant frequency, or polarization. Most researchers agree and define the basic characteristics of reconfigurable antenna as follows [1]:

- Antennas integrated with electronic switches, mechanical actuators, tunable materials for reconfigurability in terms of circuital characteristics and/or radiation properties;
- Ultra Wide Band (UWB) or multiband antennas integrated with tunable filters;
- Reconfigurable/multiband arrays where the same aperture is utilized for different operational modes.

There are many methods to reconfigure the characteristics of antenna. However, researchers and industrial are often interested in the electronic components for easy integration, high reliability and small size. The electronics components have been mainly used as PIN diode, MEMS switch, optoelectronic switch, varactor diode and digitally tunable capacitor (DTC).

1.1. PIN Diode

PIN diode is a semiconductor device, which can vary its series resistor depending on the voltage applied through its cathode and anode. Ideally, this component acts as a short circuit in ON state and open circuit in OFF state. PIN diode is a low-cost component, various dimension as well as fast time switch. Typically, PIN diode can handle power on the order of 40 dBm that is enough for wireless sensor nodes or mobile phones applications. However, its main drawback is the high DC power consumption in ON state. PIN diode has been used in many type of antenna such as printed dipoles, slot antennas, microstrip patch antennas, PIFAs, and dielectric resonator antennas [2-13].

1.2. MEMS Switch

RF microelectromechanical systems (MEMS) switch is a component developed by Dr. Larry Larson at Hughes Research Labs in Malibu, California, with the support of DARPA (Defense Advanced Research Projects Agency) in 1990-1991 [14]. MEMS switches use a mechanical movement to achieve a short circuit or an open circuit. They have several features

over PIN diode or other solid-state diode such as lower insertion loss, higher isolation, low DC power consumption, and relatively high power handling. However, RF MEMS switch have also some inconvenient including high activation voltages, higher cost, lower reliability, and limited commercial availability [15]. Thanks to the wide operating frequency range, these components are used in various antenna designs as well as for different applications [16-23].

1.3. Optoelectronic Switch

Unlike the above component, instead of using the bias voltage, optoelectronic switch can be reconfigure by optical bias. Thanks to the use of fiber or direct illumination, the impedance of component can be switched between high or low value. Optoelectronic switch has shown a lot of superior advantages such as low losses, being lightweight, noise immunity, and RF-circuit isolation. Some reconfigurable antenna used this components are introduced in [24-28].

1.4. Varactor diode

Varactor diode is a variable capacitor that can vary the resistance capacitance due to the change of the bias voltage value. Based on the characteristics of the PN junction, the varactor diode is operated under reverse bias conditions and this gives rise to three regions. At either end of the diode are the P and N regions where current can be conducted. However around the junction is the depletion region where no current carriers are available. This region will produce the effect of parasitic capacitor. The size of this area is modified thanks to the changes of injected voltage. Thereby, capacitance of varactor diode will vary. The advantage of this type of components is low consumption DC and continuous tuning. However, the major drawback of these components is the low power handling, so it is often used for the received antenna, especially DVB-H applications [29-31].

1.5. Digital Tunable Capacitor (DTC)

The DTC is a DuNE™-enhanced Digitally Tunable Capacitor based on Peregrine's UltraCMOS technology. It offers high RF power handling which is up to 34 dBm and it has a low current consumption, therefore it is suitable for reconfigurable antenna, which can be used as a receiver and also a transmitter. Besides the fact that it is highly linear, the DTC also has the highest quality factor and provides a wide power supply range compatible with mobile phone power units (2.3 to 3.6 V).

Furthermore, the significant feature that makes DTC is different to a varactor diode is that this device is controlled through the widely supported 2-wire (I2C compatible) or 3-wire (SPI compatible) interfaces. Instead of controlling the voltage of the capacitor, the DTC uses this I2C or SPI interfaces to let the capacitance vary digitally in 32 states with a 5-bit addressing. For our proposed antennas, we use mainly PE64905 because it has highest value of handling power (38 dBm).

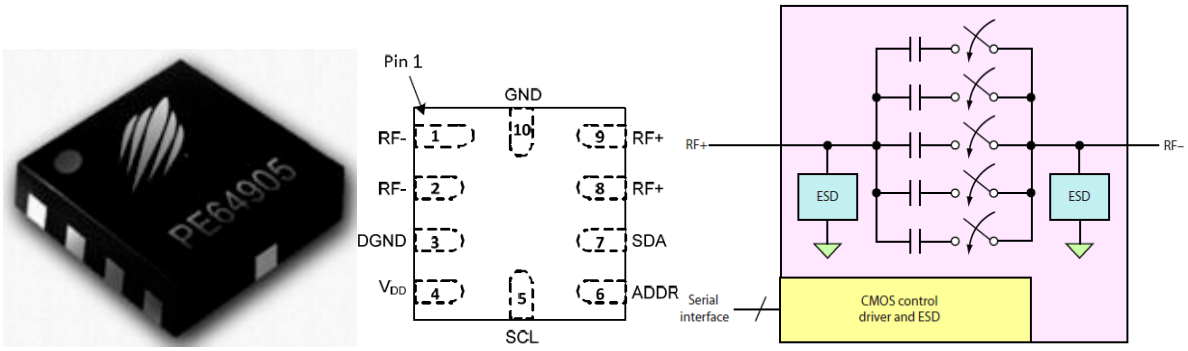

(a) (b) (c)

Figure 2.1: (a) Package type, (b) pin configuration, (c) functional block diagram of DTC

Pin #	Pin Name	Description
1	RF-	Negative RF Port
2	RF-	Negative RF Port
3	DGND	Ground
4	VDD	Power supply
5	SCL	Serial Interface Clock Input
6	ADDR	Serial Interface Address Input
7	SDA	Serial Interface Data Input
8	RF+	Positive RF Port
9	RF+	Positive RF Port
10	GND	RF Ground

Table 2.1: DTC pins description

Thanks to the use of Peregrine evolution kit, the performance of PE64905 DTC is measured and introduced in Figure 2.2. The value of capacitor is relative stable at the frequencies from 100 MHz to 1 GHz. However, at the higher frequencies, the DTC capacitance is change a lot.

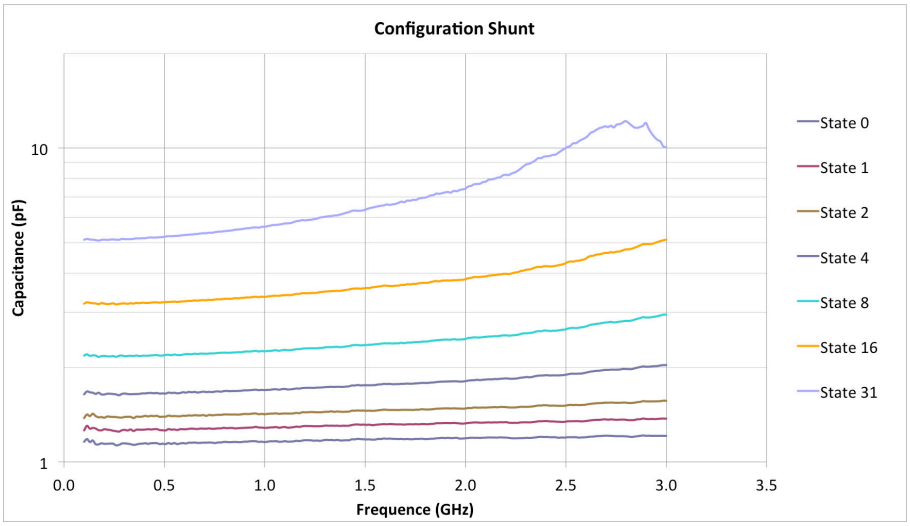

Figure 2.2: Measured capacitor values of DTC at the different configurations.

The equivalent circuit of DTC is also shown in the Fig. 2.3. But in simulation, DTC can be simplified by a capacitor in serie with a resistor. With each state, the capacitance and resistance can be found in Tab. 2.2. Comparable with other component such as varactor diode, the serie resistor value of DTC is quite higher. Thus, the antenna efficiency will be slightly reduced. However, with the advantages mentioned above, the DTC still is a good choice for the reconfigurable antenna.

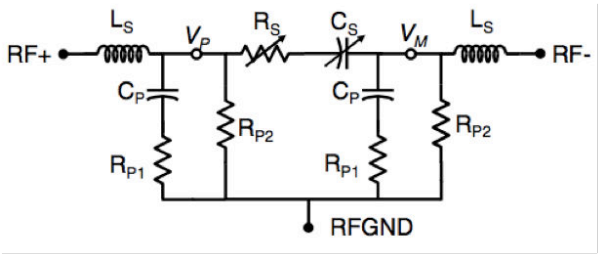

Variable	Equation (state = 0, 1, 2...31)	Units
C_S	0.129*state + 0.600	pF
R_S	20/(state+20/(state+0.7)) + 0.7	Ω
R_{P1}	7	Ω
R_{P2}	10	kΩ
C_P	0.5	pF
L_S	0.27	nH

Figure 2.3: Equivalent circuit model schematic of DTC

State		DTC Core		State		DTC Core	
Binary	Decimal	Cs(pF)	Rs(Ohm)	Binary	Decimal	Cs(pF)	Rs(Ohm)
00000	0	0.60	1.40	10000	16	2.66	1.86
00001	1	0.73	2.27	10001	17	2.79	1.80
00010	2	0.86	2.83	10010	18	2.92	1.75
00011	3	0.99	3.08	10011	19	3.05	1.70
00100	4	1.12	3.12	10100	20	3.18	1.65
00101	5	1.25	3.05	10101	21	3.31	1.61
00110	6	1.37	2.93	10110	22	3.44	1.57
00111	7	1.50	2.78	10111	23	3.57	1.54
01000	8	1.63	2.64	11000	24	3.70	1.51
01001	9	1.76	2.51	11001	25	3.83	1.48
01010	10	1.89	2.39	11010	26	3.95	1.45
01011	11	2.02	2.27	11011	27	4.08	1.42
01100	12	2.15	2.17	11100	28	4.21	1.40
01101	13	2.28	2.08	11101	29	4.34	1.37
01110	14	2.41	2.00	11110	30	4.47	1.35
01111	15	2.54	1.93	11111	31	4.60	1.33

Table 2.2: Equivalent circuit data of DTC PE64905

2. CONTROLLED SYSTEM

Typically, the mobile devices as well as wireless sensor nodes always provide the serial interface to control the slave devices such as memory, LCD, communication unit, sensor unit, etc. Thus the integration of DTC in antennas for these devices becomes feasible. Thus, in this thesis, we use the Mbed LPC1768 Microcontroller that provides the SPI or I2C signals to control the DTC.

The Mbed NXP LPC1768 Microcontroller is packaged in a 40-pin DIP, 0.1-inch pitch form-factor making it favorable for prototyping with solder less breadboard, strip board and through-hole PCBs. The special attraction about this microcontroller is that we can used it as

simple as using USB Flash because the Mbed can easily be connected to a Windows, Mac or Linux computer and it will appear as a USB drive. There are no drivers or software to install or set up the programs as the link on the board can be used to connect to the Mbed website, where we can sign up and begin designing.

There are also other characteristics about this microcontroller, as mentioned below:

- NXP LPC1768 MCU
  - High performance ARM® Cortex™-M3 Core
  - 96MHz, 32KB RAM, 512KB FLASH
  - Ethernet, USB Host/Device, 2xSPI, 2xI²C, 3xUART, CAN, 6xPWM, 6xADC, GPIO
- Prototyping form-factor
  - 40-pin 0.1" pitch DIP package, 54x26mm
  - 5V USB or 4.5-9V supply
  - Built-in USB drag 'n' drop FLASH programmer
- Mbed.org Developer Website
  - Lightweight Online Compiler
  - High level C/C++ SDK
  - Cookbook of published libraries and projects

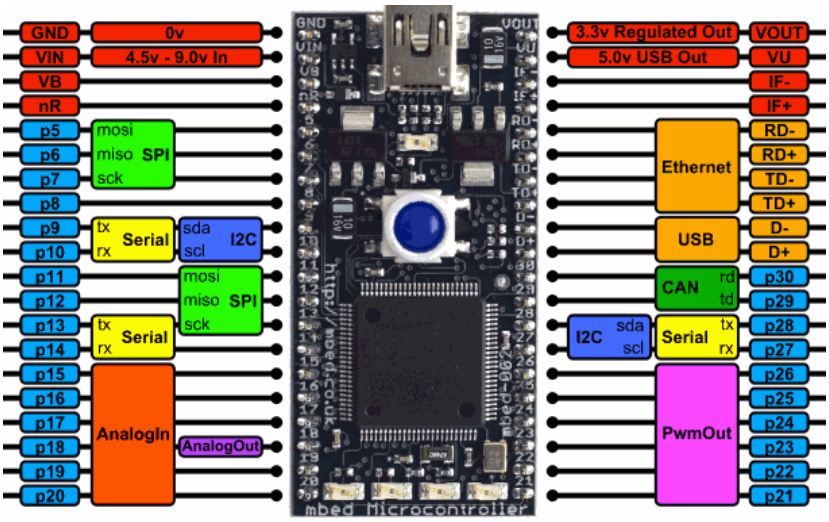

Figure 2.4: Mbed NXP LPC1768

3. RECONFIGURABLE ANTENNA FOR WHITE SPACE APPLICATIONS

3.1. State of the art

TV White Space (TVWS) refer to the unused frequency range in the TV band, where the operating frequency is ranging from 470 to 862 MHz. With the relative bandwidth about 58% and also the ability to transmit signal for long distance, this frequency band has a large potential for communication. Furthermore this White Space allocation is expected to stimulate the development of mobile multimedia technologies and services. Therefore the reconfigurable antenna is one of the best solutions to respond to this type of standard because it can be miniaturized and operated by reconfiguring the operating frequency.

Nowadays, many reconfigurable antennas have been proposed in the UHF band, including a spiral-shaped monopole to minimize the antenna size [32]. Moreover, by using an additional tunable inductor, the frequency reconfigurable concept is presented in [33]. According to [34], [35], the reconfigurable antennas are designed with RF MEMS switches to obtain a wide bandwidth and low insertion loss. Because of the switching speed is slow and it needs a high-control voltage (50-100V), these switches present then a huge inconvenient for those antennas. The reconfigurability of an antenna also has been tested using a resonator magneto-dielectric material. Two antennas are proposed with resonators and varactor diode as shown in [36] and [37]. The results proved that the antenna with magneto-dielectric material offered a large return loss bandwidth even though its size is small.

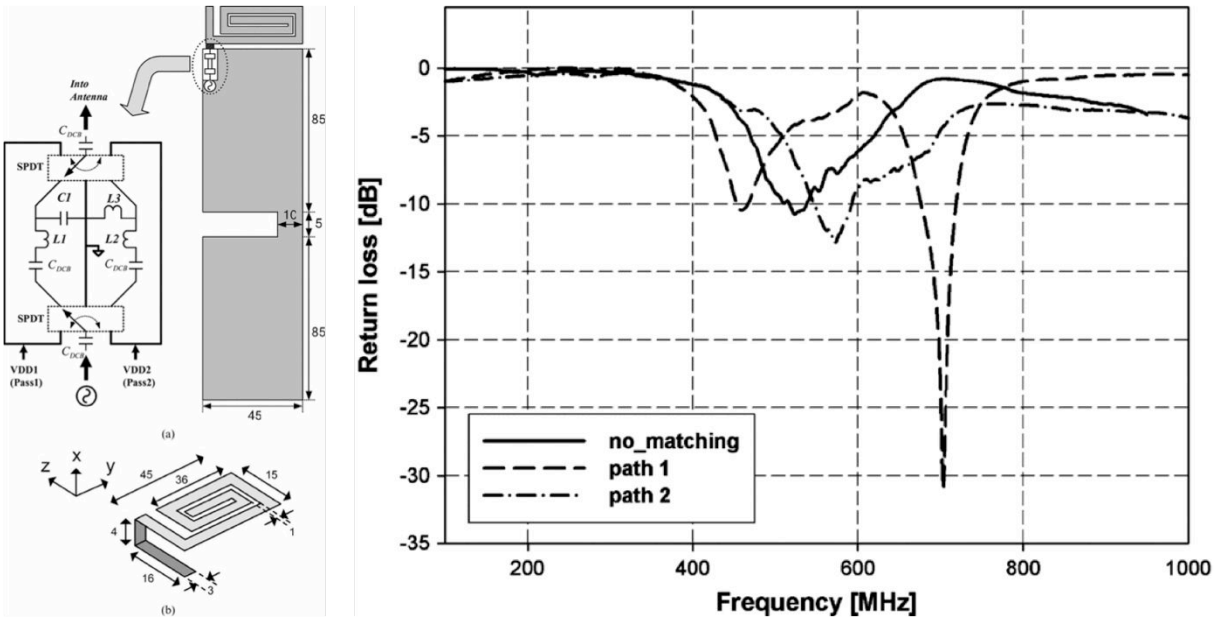

Figure 2.5: The UHF band antenna based on a spiral-shaped monopole [32].

Besides using only varactor diode to tune the frequency, the reconfigurable antennas also have been successfully implemented with the assistance of the PIN diode [38], [39]. By switching this component, a wide tuning range from 0.42 to 1.48 GHz is achieved. However because of its discrete tuning behaviour, the utilisation of PIN diode conducts to a poor quality factor. That is why the varactor diode has been employed in [40-42] to obtain a continuous tuning and to increase the efficiency in order to have a better performance. However, with low power handling, the varactor diode is not a good choice to transmit the signal. Since White Space communication functions for transmission/reception, a Digitally Tunable Capacitor (DTC) has been studied in this thesis, thanks to its high handling power (up to 34 dBm).

Section 3.2 focuses on the antenna design. Next, the simulation and measurement results are reported in sections 3.3 and 3.4. We move then to section 3.5 where the antenna diversity system is discussed, followed by the envelope correlation coefficient calculation in section 3.6. Finally a brief conclusion is given in section 4.

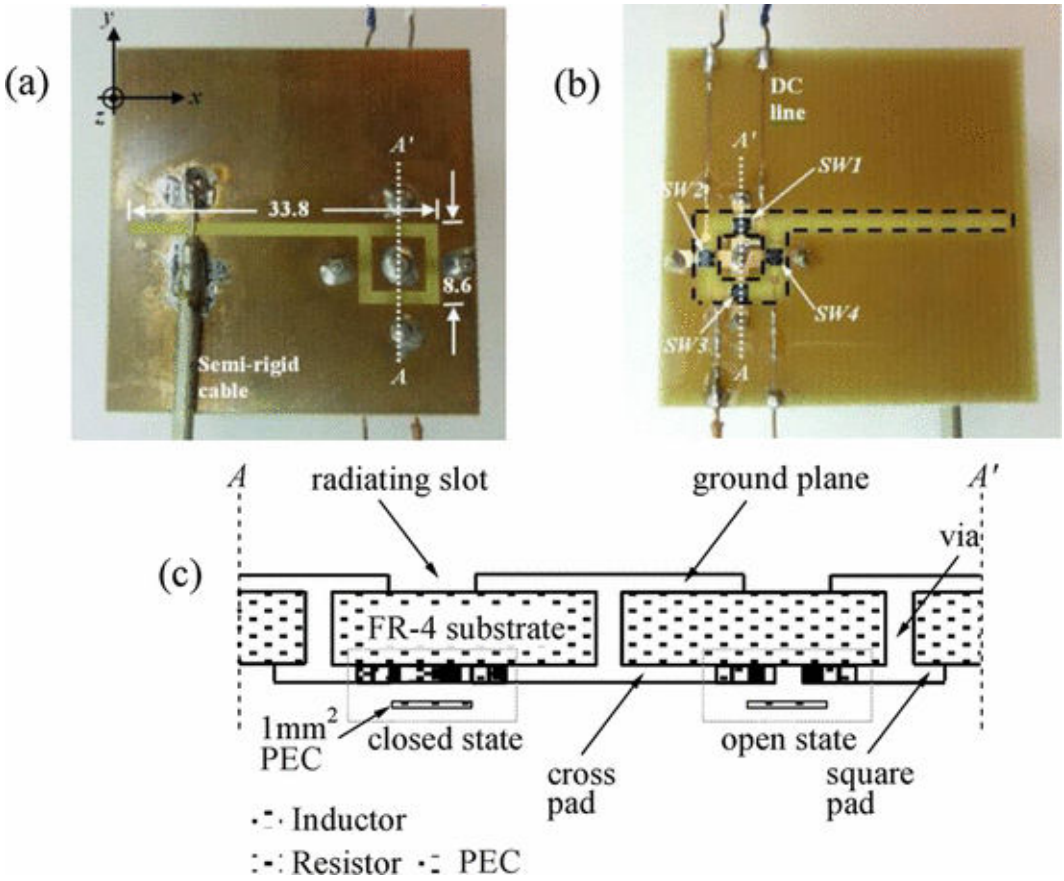

Figure 2.6: Geometry of single-pixel slot antenna: (a) upper side; (b) lower side; (c) cross-section of AA' with MEMS switches replaced by simplified models [35]

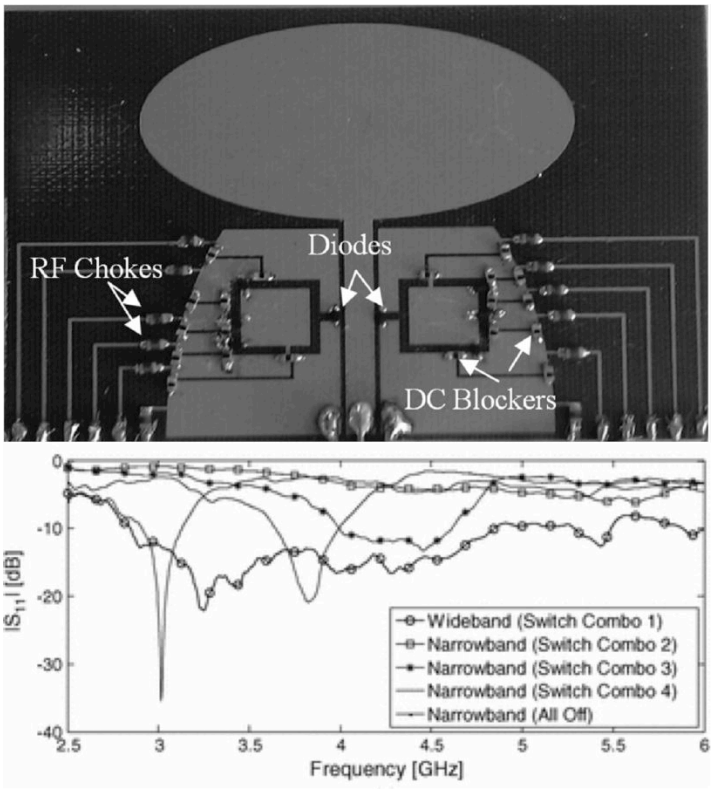

Figure 2.7: Switched monopole antenna [39]

3.2. Antenna Design

Our study is focused on a frequency reconfigurable antenna. The small size of the antenna compared to the free-space wavelength at 470MHz (0.015λ × 0.047λ × 0.013λ) brings to a limitation of the radiating efficiency.

Therefore a folded monopole structure has been chosen due to its good tradeoff between bandwidth, size and efficiency. This structure has already been presented in [36] using varactor diodes. This type of monopole was integrated into a small aperture in the corner of the printed circuit board (PCB), which is normally exhibits an impedance of 33 Ω at the resonance frequency. Thus a matching circuit is needed to optimize this impedance to 50 Ω by placing an open stub close to the ground plane as shown in Figure 2.8.

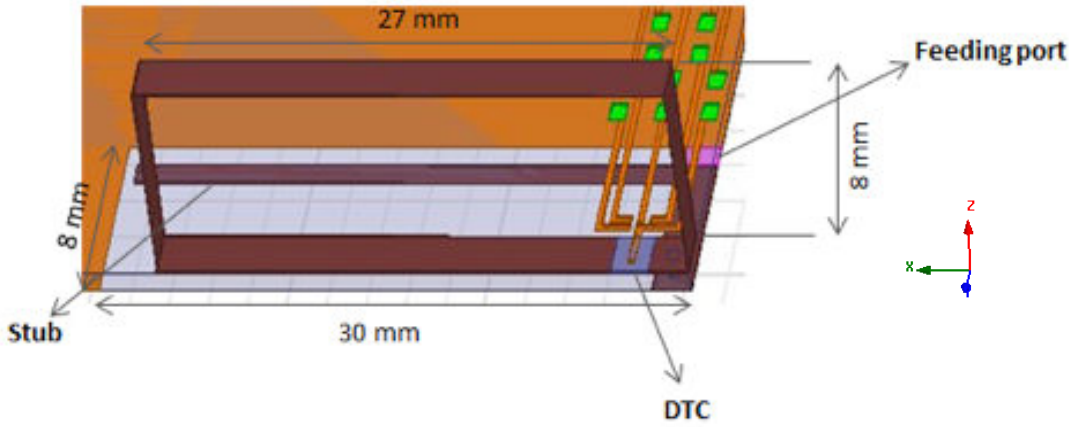

Figure 2.8: Antenna geometry

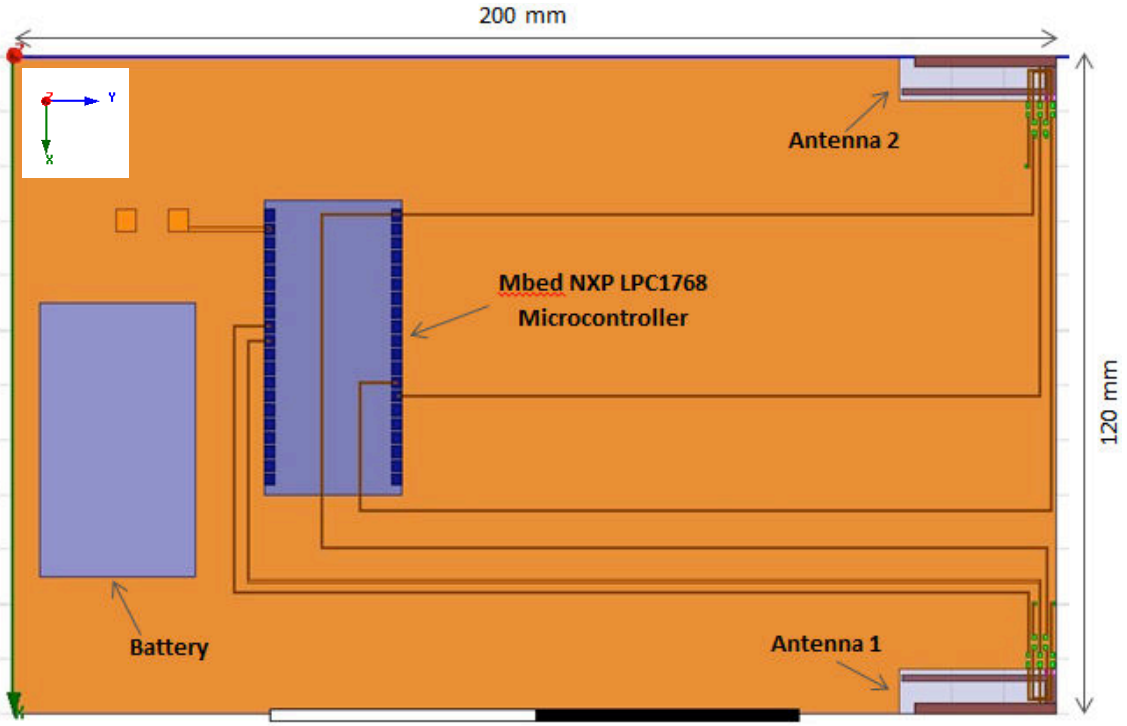

Figure 2.9: Top view of the reconfigurable antenna

The DTC has a few pins configuration. Each of these pins has to be connected by RF choke to ensure that it will not interrupt the antenna, and vice versa. By connecting this component to the pins, it will guarantee that the RF electromagnetic radiation that may distort the antenna will be blocked. The Mbed board also connect to the DTC by the microstrip line. Beside of this microcontroller, a battery is placed to provide the power for all units of system. A controlled program is written, compiled and uploaded on the flash disk of Mbed board. This program provides the I2C signal to the DTCs and pilots them. The controlled program is given in Appendix 1.

3.3. Simulation Results

The performance of the reconfigurable antenna has been analysed and optimized using HFSS. Thanks to the change of DTC value from 0.9-2.9 pF, the resonant frequency of antenna is shift between 470-700 MHz. The simulated reflection coefficients of different configurations are presented in Figure 2.10. The obtained results show the proposed antenna well operates at most of frequencies between 470-700 MHz with the reflection coefficient lower than -6dB. But, these simulated results also present the non-contiguous coverage at some of frequencies in this range. However, to resolve this problem, adding a serial capacitor (we will talk about this technique on chapter 3) or using another model of DTC, which have an appropriate value.

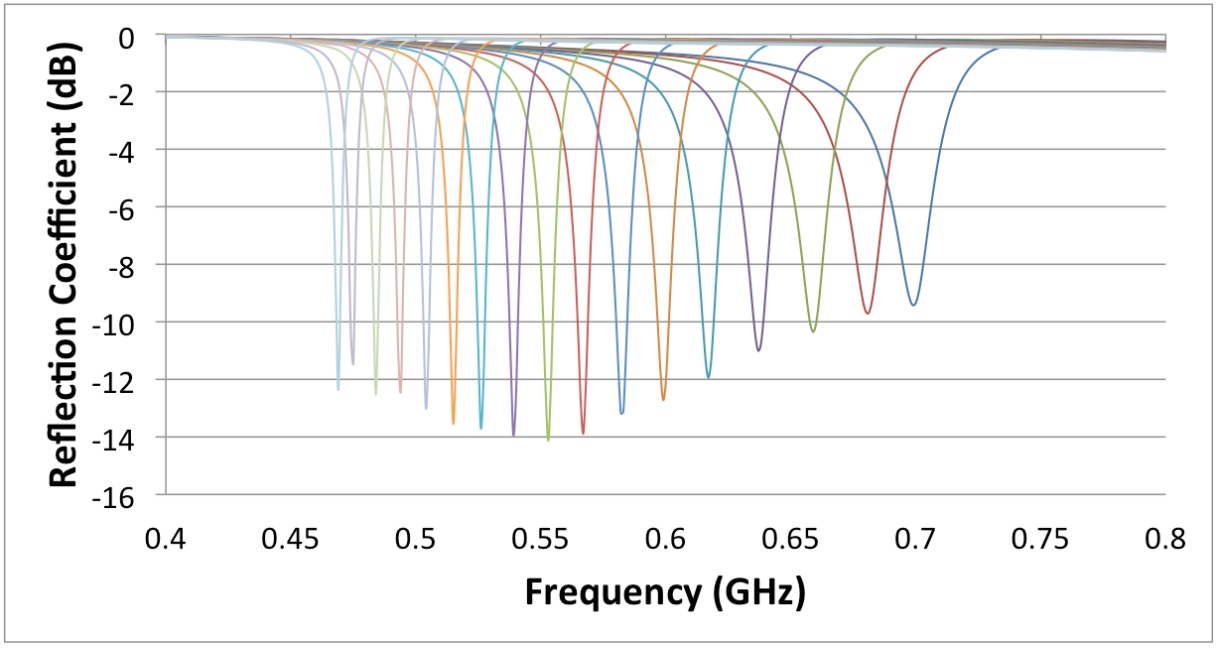

Figure 2.10: Simulated reflection coefficients at the different DTC value.

For the purpose of checking the multi antenna system performance, three configurations are also simulated, namely, (1): Antenna 1 at 470 MHz and Antenna 2 at 700 MHz, (2): Antenna 1 at 700 MHz and Antenna 2 at 470 MHz, (3): Antenna 1 and Antenna 2 at 470 MHz. The simulated reflexion coefficients are shown in the Figure 2.11, Figure 2.13 and Figure 2.15. Those results showed that the return loss is below -6 dB, thus we can say that the antennas are well matched. In order to have better performance for our antennas, we also have

to verify its isolation. For that purpose, the simulated results are shown the isolation between both antennas for each configuration in the previous figures. It is important to have a high isolation because it is the main parameters that can assure a good performance for the MIMO applications.

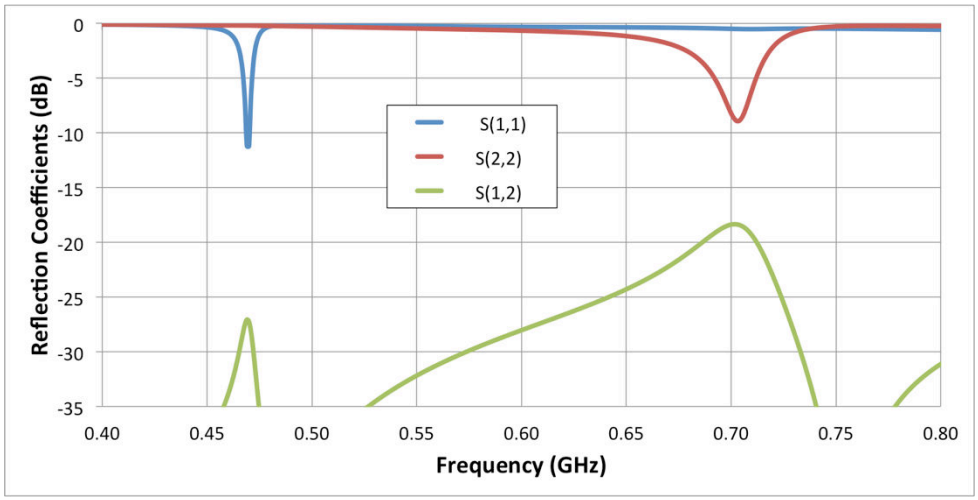

Figure 2.11: Config1 - the resonances of antenna 1 at 470 MHz and antenna 2 at 700 MHz

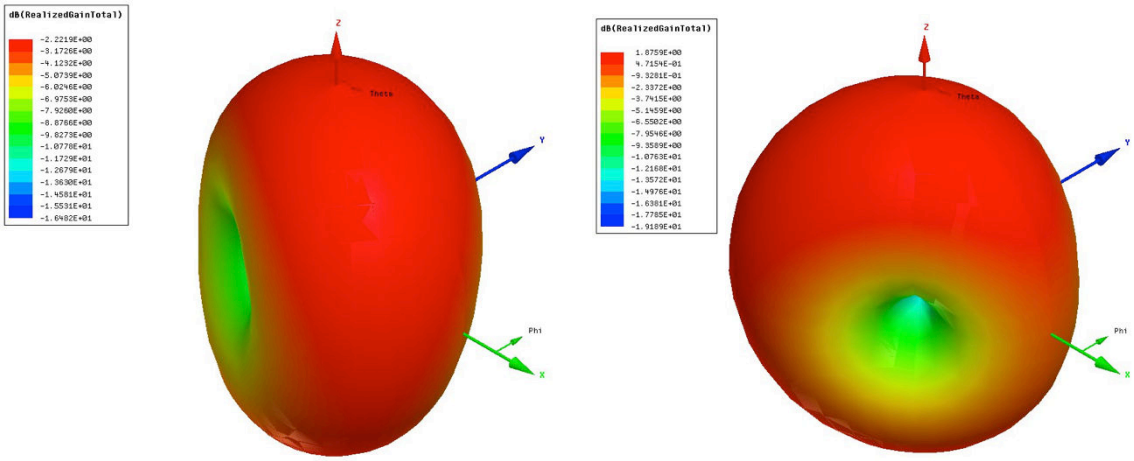

(a) (b)

Figure 2.12: The 3D realized gain of (a) antenna 1 at 470 MHz and (b) antenna 2 at 700 MHz

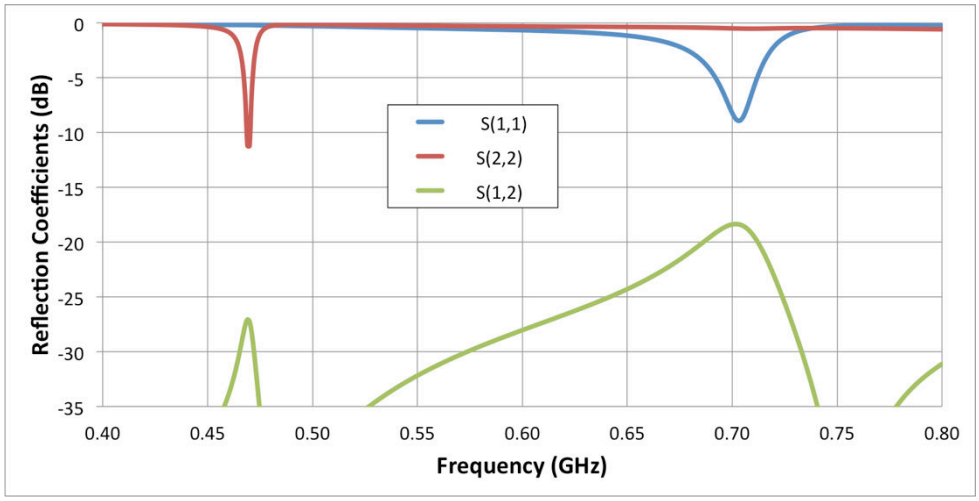

Figure 2.13: Config 2 - the resonances of antenna 1 at 700 MHz and antenna 2 at 470 MHz

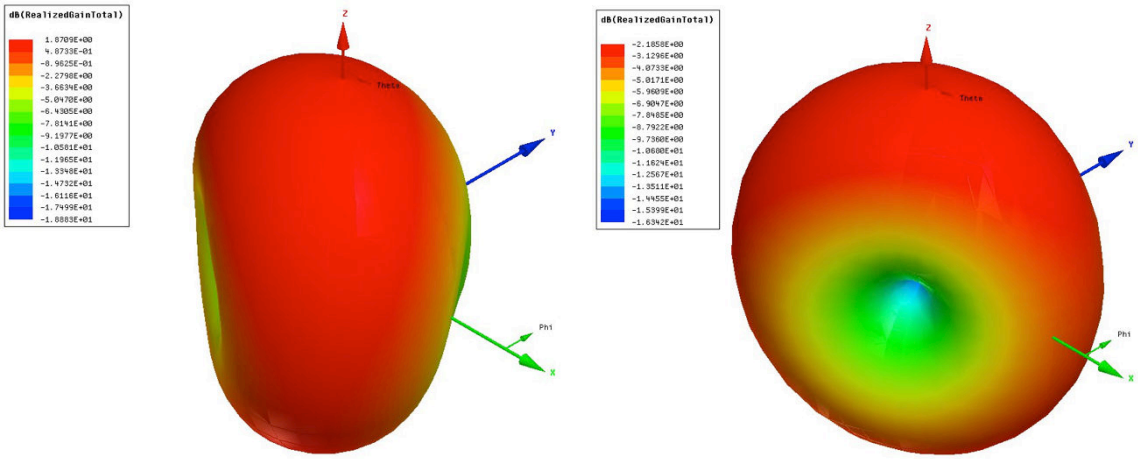

(a) (b)

Figure 2.14: The 3D realized gain of (a) antenna 1 at 700 MHz and (b) antenna 2 at 470 MHz

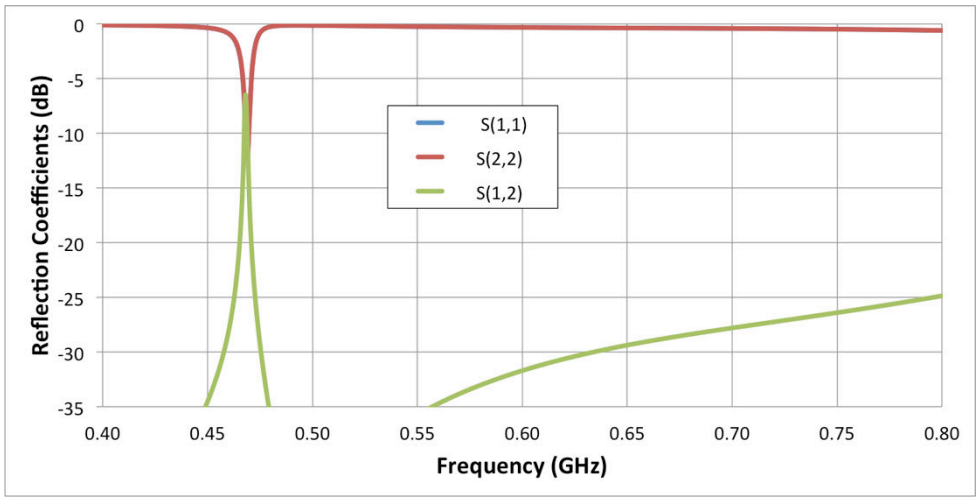

Figure 2.15: Config 3 - the resonances of antenna 1 at 470 MHz and antenna 2 at 470 MHz (The S11 and S22 results overlap each other)

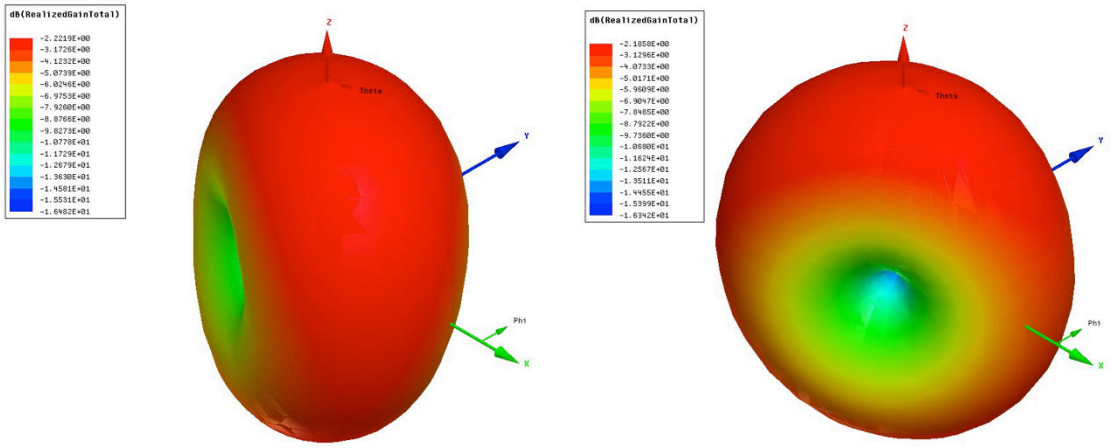

(a) (b)

Figure 2.16: The 3D realized gain of (a) antenna 1 at 700 MHz and (b) antenna 2 at 470 MHz

From the S-parameters simulated results, the configurations 1 and 2 show a good isolation that is greater than 15 dB at 700 MHz and 25 dB at 470 MHz. In theory, the obtained results are relative reasonable. Because in the configurations 1 and 2, each antenna operate at a different frequency, thus, the influence of the antenna to another will be significantly reduced. However, in configuration 3, 2 antennas operate at the same frequency, particularly, 470 MHz is the lowest frequency in the band requirement. Because the distance of 2 antennas (120 mm) rather short compared to wavelength at this frequency (about 638 mm), the isolation becomes quite low, approximately 6.3 dB. Therefore, the performance of the antenna can be affected. Nevertheless, this value may also be acceptable.

Figure 2.12, Figure 2.14 and Figure 2.16 illustrate the radiation pattern for each antenna at different frequencies. The radiation patterns are omnidirectional at 470 MHz and quasi-omnidirectional at 700 MHz. The realized gain of antenna is change from -2.2 dB to 1.87 dB at the frequencies of 470 MHz to 700 MHz, respectively. Therefore these parameters clearly indicate that this proposed antenna satisfies the specified requirement and it can be used in the mobile communication applications.

3.4. Measurement Results

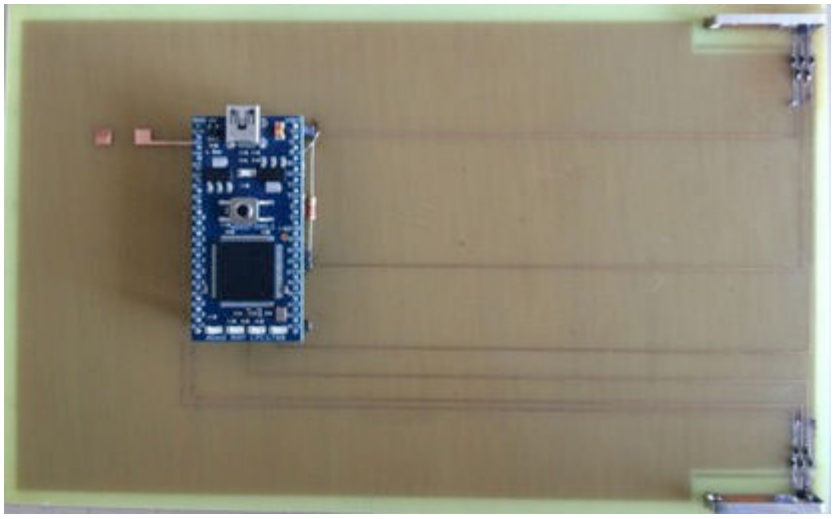

Figure 2.17: The prototype of antenna system.

Then the prototype of the antenna is realized (see Figure 2.17) and measured. Figure 2.18 shows the measured reflection coefficients of the proposed antenna. With a 0.73 pF – 3.05 pF capacitance value range of DTC, this antenna can be tuned all over White Space band with a reflection coefficient lower than -6 dB. Due to the fabrication error and the component losses, the bandwidth of antenna can be increased. However, it is not a good sign because those losses will affect the performance of antenna.

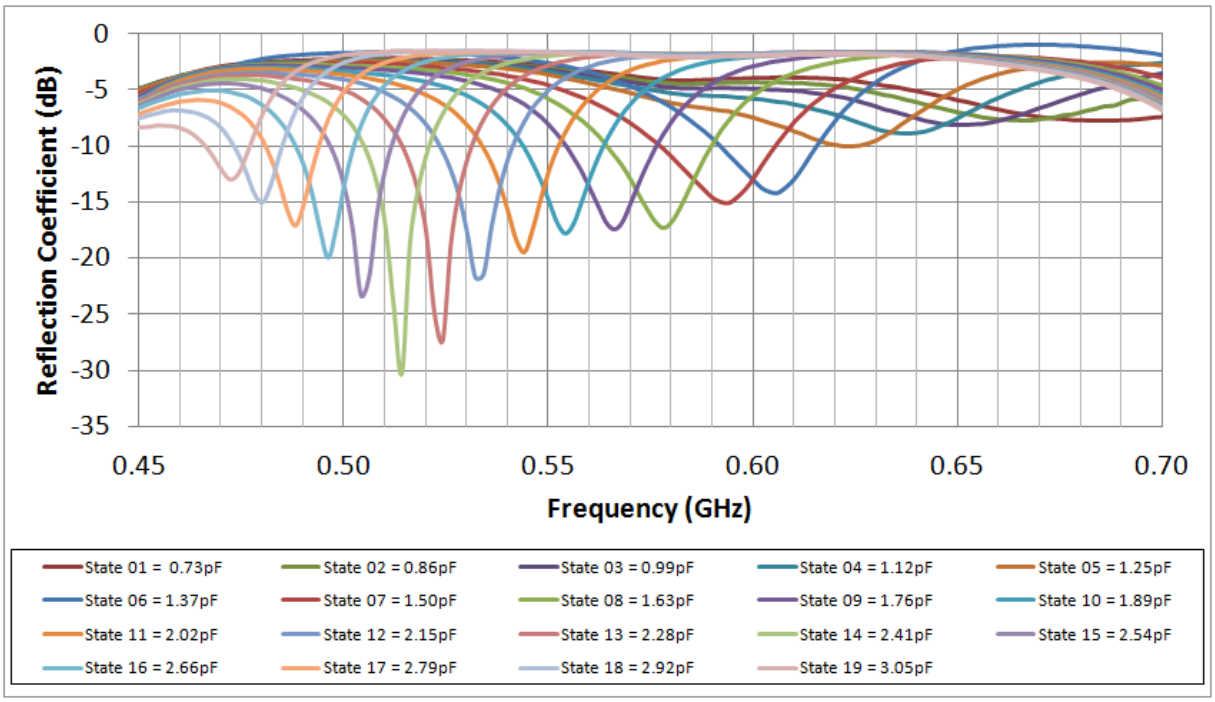

Figure 2.18: The measured reflection coefficients at the different DTC state.

The main objective of this chapter is to understand the control method and to test the characteristics of DTC component by integrating it in to a simple antenna. Firstly, the

influence of this component on the reflection coefficient is reviewed and confirmed. Thanks to the change of I2C control signals that are provided by Mbed microcontroller, the capacitor value of DTC is varied. Thus, resonant frequency of antenna can be shifted on the required frequency band. Because the operating band of the antenna is quite low, the measurement of antenna radiation field becomes difficult. However, at the end of chapter 3, the measurement of antenna efficiency, which uses DTC component will be introduced. By using the results of measurement in the easily measurable frequency and simulation results in low frequency to estimate the relative performance of the antenna.

3.5. *Approach of Antenna Diversity System*

Disadvantages of the low-frequency multi reconfigurable antenna are the narrow bandwidth, worse efficiency and low isolation. Besides, according to the development of technology, the carrier aggregation is a trend to improve the spectrum usage efficiency. Based on the MIMO reconfigurable antenna, which is presented above, an approach of antenna diversity system is proposed to solve the drawback of low-frequency reconfigurable antenna and to support for the carrier aggregation. Firstly, two reconfigurable resonators are connected to each other via a simple divider. The isolation problem between 2 antennas that is mentioned in section 3.3 has been solved. By using ADS software and the .snp file is provided from HFSS, the simulated S-parameters of proposed system is shown in the figures below.

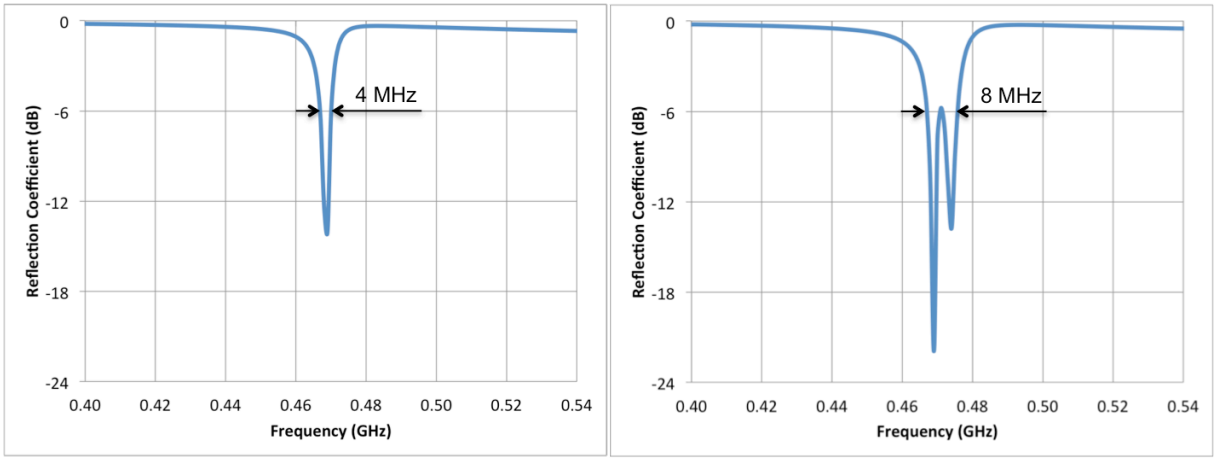

(a) Single resonator (b) Double resonators

Figure 2.19: Bandwidth enhancement of proposed approach

In terms of reflection coefficient, the proposed approach presents a good improvement of bandwidth (contiguous and non-contiguous. As introduced in Figure 2.19, thanks to the use of 2 capacitors that have slightly different value (2.9 pF and 2.82 pF), 2 resonant frequencies are created. Thanks to the combination of these resonances, the bandwidth of the antenna can be increased (from 4 MHz to 8 MHz). On the other hand, due to the flexibility of 2 reconfigurable resonators, the carrier aggregation spectrum can be easily achieved (Figure 2.20).

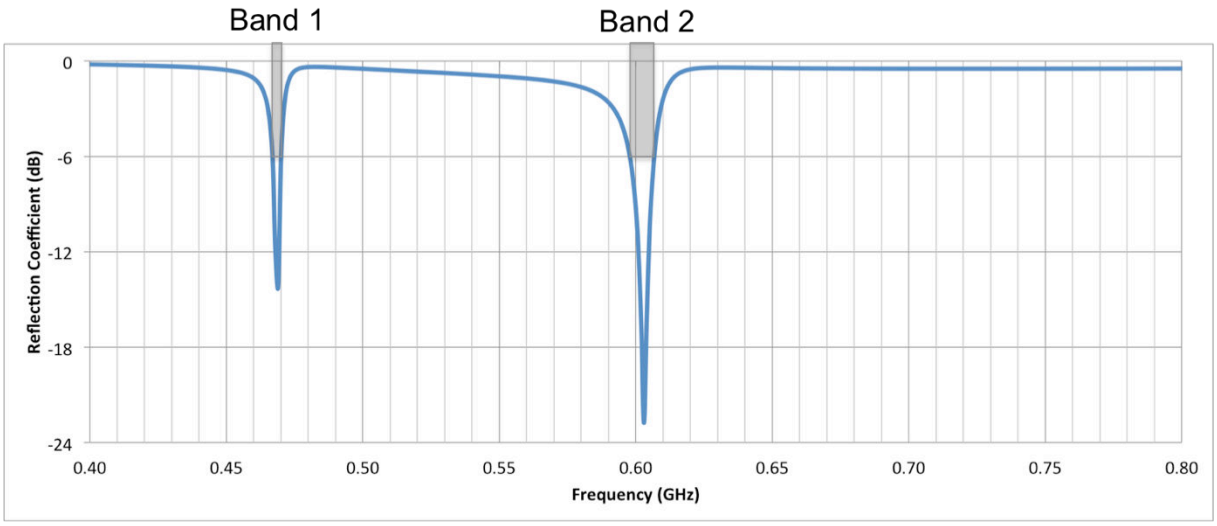

Figure 2.20: Carrier aggregation non-contiguous spectrum

In terms of radiation pattern, antenna performance is increased when two resonators operate at the same frequency. The simulation results with HFSS software prove that the radiation efficiency of antenna increased from 40% (single resonator) to 58% (double resonators) and realized gain increased from -2.18 dB (single resonator) up to -0.18 dB (double resonators).

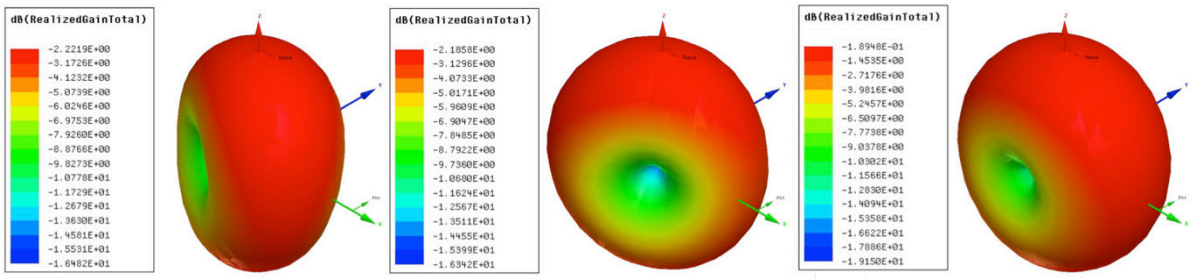

(a) (b) (c)

Figure 2.21: 3D realized gains of (a) resonator 1, (b) resonator 2 and (c) double resonators

3.6. Envelope Correlation Coefficient (ECC)

In general, the correlation between the signals received by the two antennas can be evaluated through the Envelope Correlation Coefficient (ECC), ρ_e. To achieve a reduction in signal fading and a higher level of diversity gain, ρ_e must be lower than 0.5.

	Configuration 1	*Configuration 2*	*Configuration 3*
Resonator 1	*470 MHz*	*700 MHz*	*470 MHz*
Resonator 2	*700 MHz*	*470 MHz*	*470 MHz*

Table 2.3: the description about 3 different configurations

In our case, we have 3 configurations, (1) resonator 1 at 470 MHz and resonator 2 at 700 MHz, (2): resonator 1 at 700 MHz and resonator 2 at 470 MHz, (3): resonator 1 and resonator 2 at 470 MHz. By using Scilab, the envelope correlation coefficient is calculated;

the program code is given in Appendix 2. Thanks to HFSS simulation, we exported the data in radiation pattern for each configuration into the type of table. And then, ρ_e can be calculated by comparing the data between two different configurations at the same frequency. The formula of ECC is shown below:

$$\rho_{12}^{P} = \frac{\left| \iint_{4\pi} \left(XPR \cdot E_{\theta_1}(\Omega) \cdot E_{\theta_2}^{*} + E_{\phi_1}(\Omega) \cdot E_{\phi_2}^{*} \right) d\Omega \right|^2}{\iint_{4\pi} \left(XPR \cdot G_{\theta_1}(\Omega) + G_{\phi_1}(\Omega) \right) d\Omega \cdot \iint_{4\pi} \left(XPR \cdot G_{\theta_2}(\Omega) + G_{\phi_2}(\Omega) \right) d\Omega}$$

470 MHz	*Configuration 1*	*Configuration 2*	*Configuration 3*
Configuration 1		*0.475*	*0.219*
Configuration 2	*0.475*		*0.287*
Configuration 3	*0.219*	*0.287*	

Table 2.4: The ECC value of three configurations at 470 MHz

700 MHz	*Configuration 1*	*Configuration 2*	*Configuration 3*
Configuration 1		*0.0418*	
Configuration 2	*0.0418*		
Configuration 3			

Table 2.5: The ECC value of three configurations at 700 MHz

At 470 MHz, we obtained ρ_e= 0.475 for the first and the second configurations. After that the comparison is also made for the first and third configurations and I obtained ρ_e= 0.219 while for the second and third configurations I managed to get ρ_e= 0.287. Then I compared the first and the second configurations at 700 MHz and the result was ρ_e= 0.0418. We can conclude that our ECC were verified since all ρ_e were below than 0.5.

4. CONCLUSION

This chapter presented an overview of reconfigurable components especially digitally tunable capacitor (DTC). Since this is a relatively new product, the component control unit is also unusual as the other common components. Therefore, using a microcontroller to control this component is necessary. Mbed LPC1768 Microcontroller was chosen due to the ease of use and ability to provide SPI or I2C signal, thus, we can control DTC. By using the evaluation board, the basic characteristics of PE64005 DTC is measured and compared to the information that provided by the datasheet, thereby confirming the use of this device in reconfigurable antenna is feasible.

A reconfigurable antenna that was integrated the DTC has been designed and presented. The proposed antenna operates for Whitespaces applications at the frequency of 470 - 700 MHz. An antenna prototype is fabricated and measured. The S-parameters results show a good agreement between the simulation and measurement. Based on this design, an approach is proposed. By connecting 2 resonators, the proposed antenna it has shown a significant improvement about the bandwidth, radiation efficiency as well as the spectrum usage efficiency. On the other hand, the envelope correlation coefficients at the same frequency of

different configuration are calculated by using a Scilab code. It confirms the good performance of antenna system for MIMO and diversity applications.

REFERENCE OF THIS CHAPTER

[1] N. Haider, D. Caratelli and A. G. Yarovoy, "Recent Developments in Reconfigurable and Multi-Band Antenna Technology," International Journal of Antennas and Propagation, pp. 1-24, 2013.

[2] H. J. De Los Santos, Introduction to Microelectromechanical Microwave Systems, Second Edition, Norwood, MA, Artech House, 2004.

[3] J. M. Laheurte, "Switchable CPW-Fed Slot Antenna for Multifrequency Operation," *Electronics Letters*, **37**, 25, December 2001, pp. 1498-1500.

[4] C. Luxey, I. Dussopt, J. L. Le Sonn, and J. M. Laheurte, "Dual-Frequency Operation of CWP-Fed Antenna Controlled by PIN Diodes," *IEE Electronics Letters*, **36**, 1, January 2000, pp. 2-3.

[5] N. C. Karmakar, "Shorting Strap Tunable Stacked Patch PIFA," *IEEE Transactions on Antennas and Propagation*, **AP- 53**, 2, November 2004, pp. 2877-2884.

[6] A. F. Sheta and S. F. Mahmoud, "A Widely Tunable Compact Patch Antenna," *IEEE Antennas and Wireless Propagation Letters*, **7**, 2008, pp. 40-42.

[7] D. Peroulis, K. Sarabandi, and L. P. B. Katehi, "Design of Reconfigurable Slot Antennas," *IEEE Transactions on Antennas and Propagation*, **AP-53**, 2, February 2005, pp. 645-654.

[8] M. Komuleinen, M. Berg, H. Jantunen, E. T. Salonen, and C. Free, "A Frequency Tuning Method for a Planar Inverted-F Antenna," *IEEE Transactions on Antennas and Propagation*, **AP-56**, 4, April, 2008, pp. 944-950.

[9] W. Lee, H. Kim, and Y. J. Yoon, "Reconfigurable Slot Antenna with Wide Bandwidth," IEEE International Symposium on Antennas and Propagation *Digest*, Albuquerque, NM, July 2006, pp. 3063-3066.

[10] V. K. Palukuru, M. Komulainen, M. Berg, H. Jantunen, and E. Salonen, "Frequency-Tunable Planar Monopole Antenna for Mobile Terminals," European Conference on Antennas and Propagation EuCAP 2007 Digest, Edinburgh, Scotland, November, 2007.

[11] A. Ramadan, M. Al-Husseini, Y. Tawk, K. Y. Kabalan, and A. El-Hajj, "A Novel Frequency/Pattern-Reconfigurable Microstrip Antenna for WLAN Applications," European Conference on Antennas and Propagation, EuCAP 2010, Barcelona, Spain, April 2010.

[12] F. Yang, Y. Rahmat-Samii, "Patch Antennas with Switchable Slots (PASS) in Wireless Communications: Concepts, Designs, and Applications," *IEEE Antennas and Propagation Magazine*, **47**, 2, April 2005, pp. 13-29.

[13] C. W. Jung, K. Kim, I. Kim, H. Kim, and A. Goudelev, "Reconfigurable Antenna for Concurrent Operation over Cellular and Connectivity Bands," IEEE International Symposium on Antennas and Propagation Digest, San Diego, CA, July 2008.

[14] G. M. Rebeiz, "RF MEMS: Theory, design, and technology", John Wiley & Sons, Inc., 2003.

[15] A. Petosa "An overview of tuning techniquesfor frequency-agile antennas", *IEEE AntennasPropag. Mag.*, vol. 54, pp.271 -296 2012.

[16] D. E. Anagnostou, G. Zheng, M. T. Chryssomallis, J. C. Lyke, G.E. Ponchak, J. Papapolymerou, and C. G. Christodoulou, "Design, Fabrication, and Measurements of an RF-MEMS-Based Self-Similar Reconfigurable Antenna," *IEEE Transactions on Antennas and Propagation*, **AP-54**, 2, February 2006, pp. 422-432.

[17] N. Kingsley, D. E. Anagnostou, M. Tentzeris, and J. Papapolymerou, "RF MEMS Sequentially Reconfigurable Sierpinski Antenna on a Flexible Organic Substrate With Novel DC-Biasing Technique," *IEEE Journal of Microelectromechanical Systems*, **16**, 5, October 2007, pp. 1185-1192.

[18] R. K. Gupta, U.C. Sharma, P. Ayanu, and G. Kumar, "MEMS Based Reconfigurable Dual Band Antenna" *Microwave and Optical Technology Letters*, **50**, 6, June 2008, pp. 1570-1575.

[19] T. Wu, R. L. Li, S. Y. Eom, S. S. Myoung, K. Lim, J. Laskar, S.I. Jeon, and M.M. Tentzeris, "Switchable Quad-Band Antennas for Cognitive Radio Base Station Applications," *IEEE Transactions on Antennas and Propagation*, **AP-58**, 5, May, 2010, pp. 1468-1476.

[20] W. B. Zheng, Q. A. Huang, X. P. Liao, and F. X. Li, "RF MEMS Membrane Switches on GaAs Substrate for X-Band Applications," *Journal of Microelectromechanical Systems*, **14**, 3, June 2005, pp. 464-471.

[21] C. Zhang, S. Yang, H. K. Pan, A. E. Fathy, S. El-Ghazaly, and V. Nair, "Development of Reconfigurable Mini-Nested Patches Antenna for Universal Wireless Receiver Using MEMS," IEEE International Symposium on Antennas and Propagation *Digest*, Albuquerque, NM, July 2006, pp. 205-208.

[22] P. Panaia, C. Luxey, G. Jacquemod, R. Staraj, G. Kossiavas, L. Dussopt, F. Vacherand, and C. Billard, "MEMS-Based Reconfigrable Antennas," IEEE International Symposium on Industrial Electronics Digest, Ajaccio, France, May 2004, pp. 175-179.

[23] B. A. Cetiner, G. R. Crusats, L. Jofre, and N. Biyikh, "RF MEMS Integrated Frequency Reconfigurable Annular Slot Antenna," *IEEE Transactions on Antennas and Propagation*, **AP-58**, 3, March 2010, pp 626-632.

[24] R. N. Lavallee and B. A. Lail, "Optically-Controlled Reconfigurable Microstrip Patch Antenna," IEEE International Symposium on Antennas and Propagation *Digest*, San Diego, July 2008.

[25] Y. Tawk, A. R. Albrecht, S. Hemmady, G. Balakrishnan, and C. G. Christodoulou, "Optically Pumped Reconfigurable Antenna Systems (OPRAS)," IEEE International Symposium on Antennas and Propagation *Digest*, Toronto, Canada, July, 2010.

[26] C. J. Panagamuwa, A. Chauraya, and J. C. Vardaxoglou, "Frequency and Beam Reconfigurable Antenna Using Photoconducting Switches," *IEEE Transactions on Antennas and Propagation*, **AP-54**, 2, February 2006, pp. 449-454.

[27] G. P. Jin, D.L. Zhang, and R. L. Li, "Optically Controlled Reconfigurable Antenna for Cognitive Radio Applications," *IET Electronics Letters*, **47**, 17, August 2011, pp. 948-950.

[28] I. Carraquillo-Rivera, Z. Popovic, and R. A. Rodriquez Solis, "Tunable Slot Antenna Using Varactors and Photodiodes," IEEE International Symposium on Antennas and Propagation *Digest,* Columbus, OH, June 2003, pp. 532-535.

[29] L. Huang and P. Russer, "Tunable Antenna Design Procedure and Harmonics Suppression Methods of the Tunable DVB-H Antenna for Mobile Applications," 37th European Microwave Conference EMC 2007, Munich, Germany, October, 2007

[30] I. J. Yoon, S. H. Park, and Y. E. Kim, "Frequency Tunable Antenna for Mobile TV Signal Reception," IEEE International Symposium on Antennas and Propagation *Digest*, Honolulu, HI, July 2007, pp. 5861-5864.

[31] M. Abdallah, L. Le Coq, F. Colombel, G. Le Ray, and M. Hindi, "Frequency Tunable Monopole Coupled Loop Antenna with Broadside Radiation Pattern," *IET Electronics Letters*, **45**, 23, November, 2009, pp. 1149-1151.

[32] Dong-Hyuk Choi, Yun-Taek Im, Young-Jun Cho, and Seong-Ook Park: "A Tunable Antenna for DVB-H Applications", IEEE Antennas and Wireless Propagation Letters, vol. 6, pp. 515-517, 2007.

[33] M. Y. Abou Shahine1, M. Al-Husseini, Y. Nasser, K. Y. Kabalan, and A. El-Hajj: "A Reconfigurable Miniaturized Spiral Monopole Antenna for TV White Spaces", PIERS Proceedings, Stockholm, Sweden, Aug. 12–15, 2013

[34] Dimitris E. Anagnostou, Michael T. Chryssomallis, Benjamin D. Braaten, John L. Ebel, and Nelson Sepúlveda: "Reconfigurable UWB Antenna With RF-MEMS for On-Demand WLAN Rejection", IEEE Transactions on Antennas and Propagation, vol. 62, No. 2, pp. 602-608, Feb. 2014.

[35] Chi-Yuk Chiu, Jichao Li, Sichao Song, and Ross D. Murch: “Frequency-Reconfigurable Pixel Slot Antenna”, IEEE Transactions on Antennas and Propagation, vol. 60, No. 10, pp. 4921-4924, Oct. 2012.
[36] F. Ferrero, A. Chevalier, J.M. Ribero, R. Staraj, J.L. Mattei, and Y. Queffelec: “A new magneto-dielectric material loaded, tunable UHF antenna for handheld devices”, IEEE Antennas and Wireless Propagation Letters, vol. 10, pp. 951–954, 2011.
[37] Laure Huitema, Tibault Reveyrand, Jean-Luc Mattei, Eric Arnaud, Cyril Decroze, and Thierry Monediere: “Frequency Tunable Antenna Using a Magneto-Dielectric Material for DVB-H Application”, IEEE Transactions on Antennas and Propagation, vol. 61, No. 9, pp. 4456-4466, Sept. 2013.
[38] Hui Li, Jiang Xiong, Yufeng Yu, and Sailing He: “A Simple Compact Reconfigurable Slot Antenna With a Very Wide Tuning Range”, IEEE Transactions on Antennas and Propagation, vol. 58, No. 11, pp. 3725-3728, Nov. 2010.
[39] Abubakar Tariq and Hooshang Ghafouri-Shiraz: “Frequency-Reconfigurable Monopole Antennas”, IEEE Transactions on Antennas and Propagation, vol. 60, No. 1, pp. 44-50, Jan. 2012.
[40] F. Canneva, F. Ferrero, J. M. Ribero, and R. Staraj: “Frequency Reconfigurable Antenna for DVB-H Applications”, Microwave and Optical Technology Letters, vol. 53, No. 8, pp. 1734-1736, Aug. 2011.
[41] Shih-Chia Chiu, Liang-Yu Ou Yang, Chien-Pai Lai, and Shih-Yuan Chen: “Compact CRLH Asymmetric-CPS Resonant Antenna With Frequency Agility”, IEEE Transactions on Antennas and Propagation, vol. 62, No. 2, pp. 527-534, Feb. 2014.
[42] Luyi Liu, Jonathan Rigelsford, and Richard Langley: “Tunable Multiband Handset Antenna Operating at VHF and UHF Bands”, IEEE Transactions on Antennas and Propagation, vol. 61, No. 7, pp. 3790-3796, July 2013

[43]

CHAPTER III
MOBILE PHONE ANTENNA AND MIMO APPLICATIONS

1. STATE OF ARTS

In recent years, the development of telecommunication technology has brought many challenges in the design of mobile devices, especially in the antenna area. With nowadays many different frequency bands in telecommunication systems, multi-band antenna is one of the most employed. Many studies have introduced multi-band antennas for GSM, UMTS, and Wi-Fi in a mobile phone, but as now LTE standard is announced and begin to be deployed, new frequency bands have to be covered. Due to the low frequency used by this standard, the design of an antenna that can operate over a wider frequency band and be integrated in a mobile phone form factor becomes a challenge again.

In the first generation of mobile phones, the majority of GSM handsets used an external antenna such as a helix, a monopole (also called a whip) or a helix-plus-whip combination. In 1996, a Danish company produced the first GSM phone with an internal antenna [1]. Since this date, internal antennas were gradually introduced into mobile phones to facilitate more flexibility in the industrial design and to reduce the SAR [2]. Typically, there are now mainly two kinds of internal antennas used in mobile phones: the PIFA/microstrip antenna and the ungrounded monopole type. From the advantages mentioned above, in this section, we propose a dual-broadband antenna dedicated to 2G/3G/4G mobile phone applications.

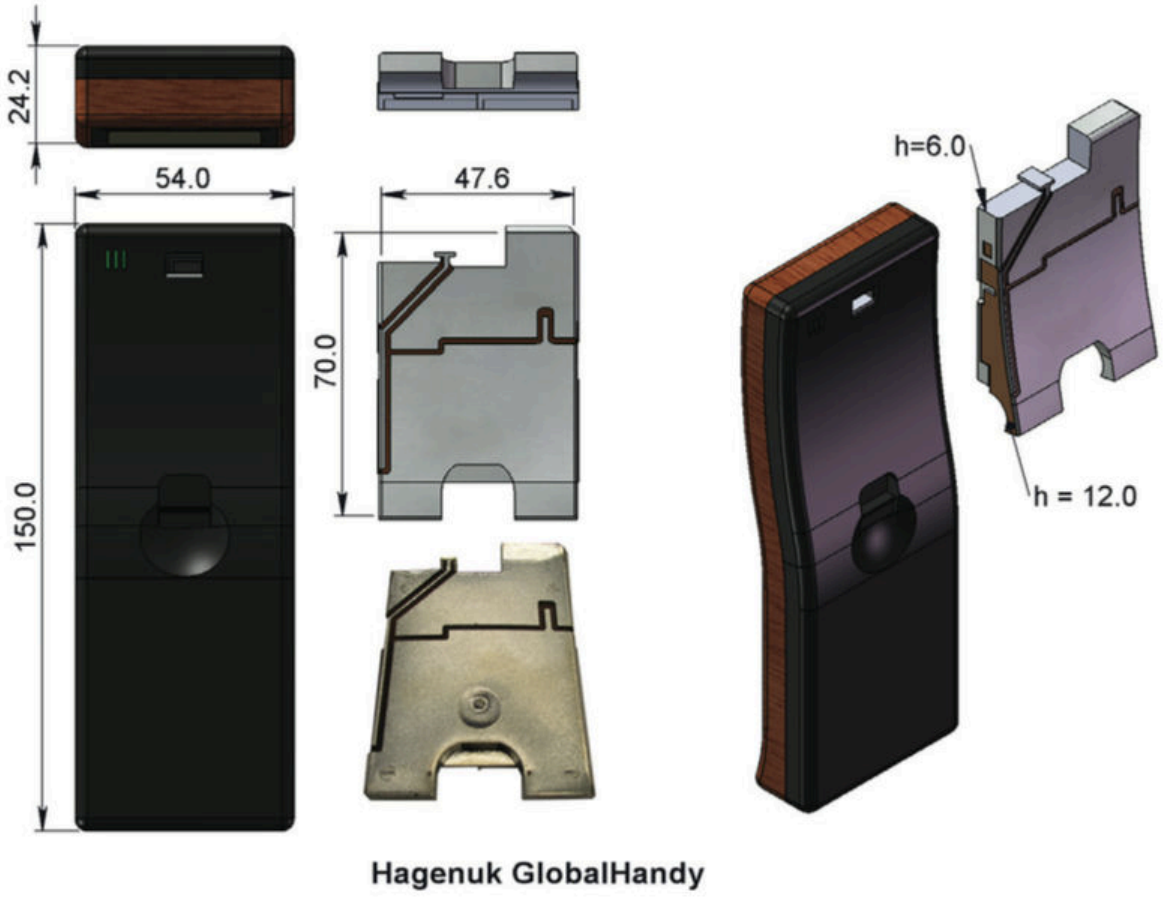

Figure 3.1: The first GSM phone with an internal antenna: Hagenuk Globalhandy [1].

Firstly, the reduction of the antenna size for integration into mobile phones has always been at forefront. In reference [3], Cheon et al. introduced a method to miniaturize an antenna using a magneto-dielectric material. The proposed antenna can operate in the low frequency LTE 700 MHz standard and in the high-frequency band from 1710-2170 MHz for DCS, PCS, W-CDMA applications. With this technique, they can reduce the size of antenna to 18×8×3 mm^3, corresponding to $\lambda_0/24\times\lambda_0/55\times\lambda_0/142$, ($\lambda_0$ being the wavelength at 700 MHz). Although the use of magneto-dielectric material helps miniaturizing the antenna size as well as keeping the bandwidth, due to the large magnetic losses (tgδ =0.0487 for the LTE band from 704-746 MHz and 0.0925 for the high- frequency band from 1710-2179 MHz), its total efficiency is relatively small especially in the low frequency band LTE 700 MHz, (about 33% to 43%). This is a notable limitation when using this type of material.

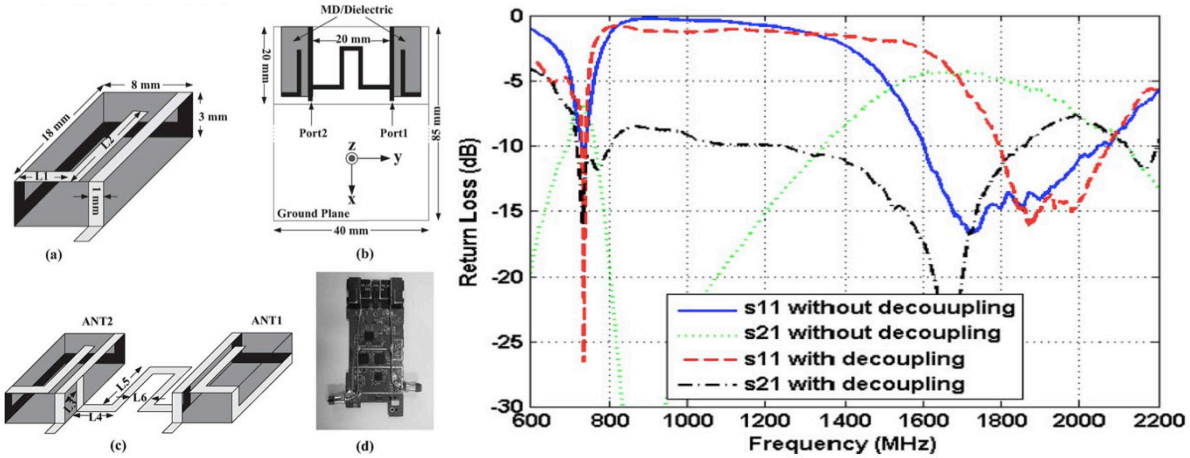

Figure 3.2: Geometries of the quad-band antenna and measured S-parameters [3].

Secondly, the selection of suitable antenna geometry is also a big challenge. There are a lot of techniques to design a multiband antenna that can cover the entire operating frequency of mobile phone application. Using parasitic coupled elements to add more resonance frequencies is a quite common method. Ku et al presented in [4] a compact multiband antenna for handset application which consists of a T-shaped driven strip coupled with a radiating structure having a small size of 50x15 mm^2. This antenna can provide two wide operating bandwidths covering 697-1012 MHz and 1598-2795 MHz for LTE/WWAN communications systems.

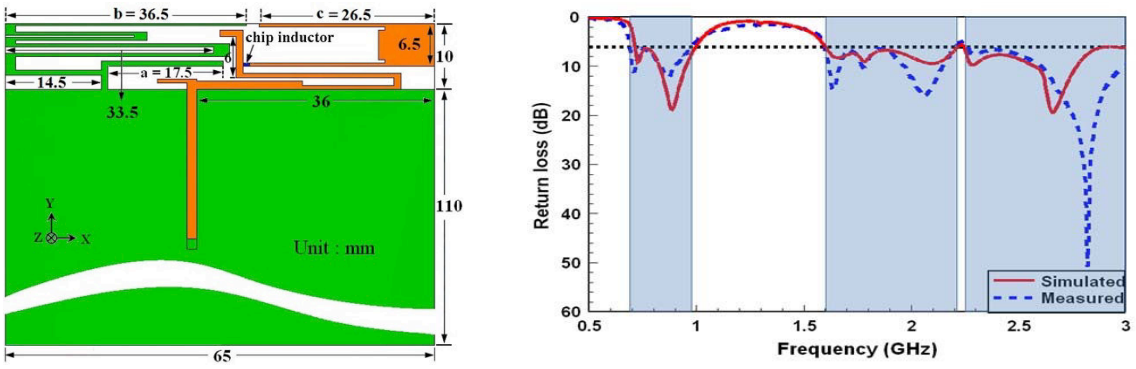

Figure 3.3: Coupled-fed and directed-fed monopole for mobile handset application [4].

Targeting the same specifications, but using parasitic coupled elements, Jeon et al. proposed a double planar inverted-E feed structure that achieves a wide impedance bandwidth (35% in the low band and 24% in the high band). The antenna is designed by inserting two branch capacitors in the feed structure of a conventional planar inverted-F antenna. With this modification, their antenna operates in the frequency bands of 698-990 MHz and 1710-2170 MHz with good efficiencies [5].

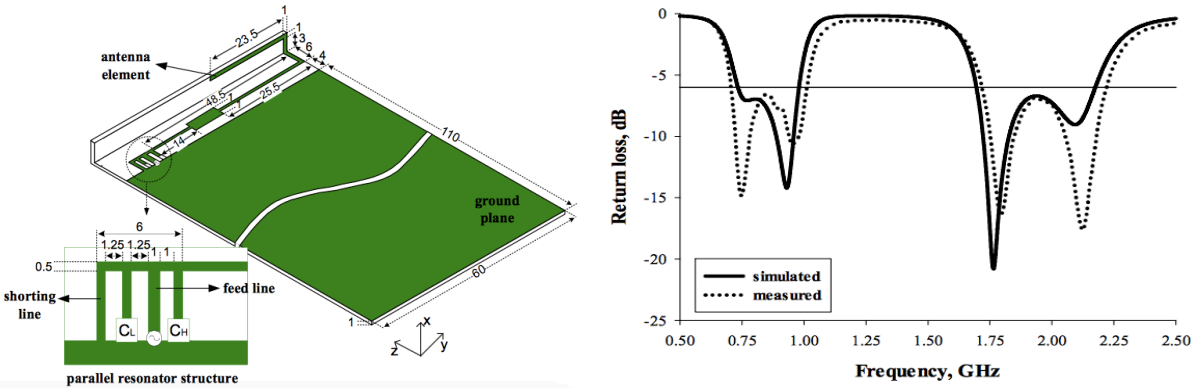

Figure 3.4: Double planar inverted-E feed structure antenna and measured S-parameters [5].

Beside, the continuing exponential growth of data traffic on mobile devices is forcing network provider and authorities to find new frequency bands. Thanks to the lower bandwidth requirement of digital television compared to the analog one, the portion of spectrum from 698 to 806 MHz has been free up in US. The 700 MHz waves have excellent propagation characteristics to easily penetrate buildings and to cover large geographic areas with few infrastructures (compare to higher frequencies) [6]. This tendency is going to be extended lower in frequency because the FCC is planning to reallocate as much as 120 MHz of 600 MHz spectrum for cellular market [7]. The arrival of these new frequency bands adds new challenges for antenna designer. First, as the compatibility with 2G and 3G is required, the number of operating band is naturally increasing. Secondly, the volume dedicated to the antenna can't be expanded, resulting in the design of smaller antennas compared to the lower used wavelength [8]. Passive antenna technology is then reaching its limits.

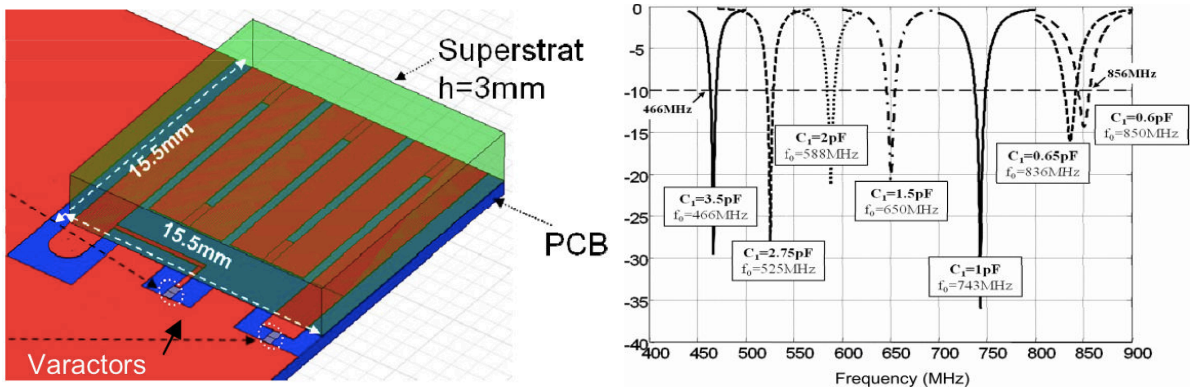

Figure 3.5: Geometry of meandered monopole with superstrate and varactors.

Nowadays, a large number of reconfigurable antennas have been considered based on different tuning techniques. Varactor diodes have been extensively used for DVB-H reception

[9], [10]. However, because of weak radiofrequency (RF) power handling of this component, its application is generally limited to receiving mode. The discrete frequency tuning by means of PIN diodes is also mentioned as a popular technique [11]. In this case, the inconvenient of varactor diodes is solved. However the high DC power consumption is a huge drawback of this semiconductor component for mobile application.

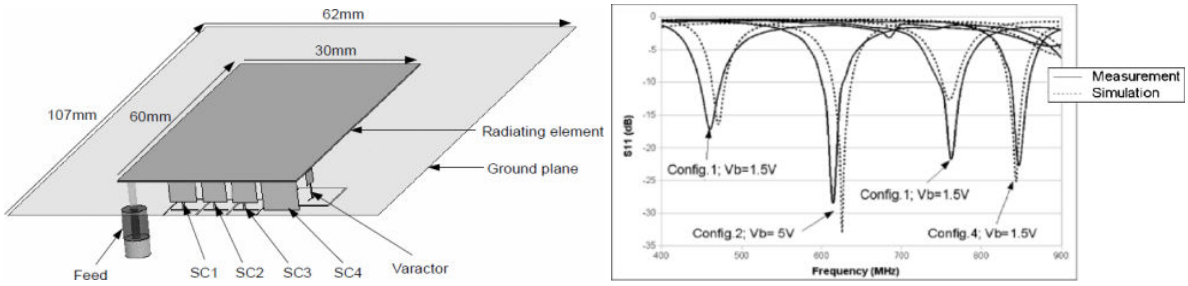

Figure 3.6: Reconfigurable antenna for DVB-H standard and measured S-parameters [10].

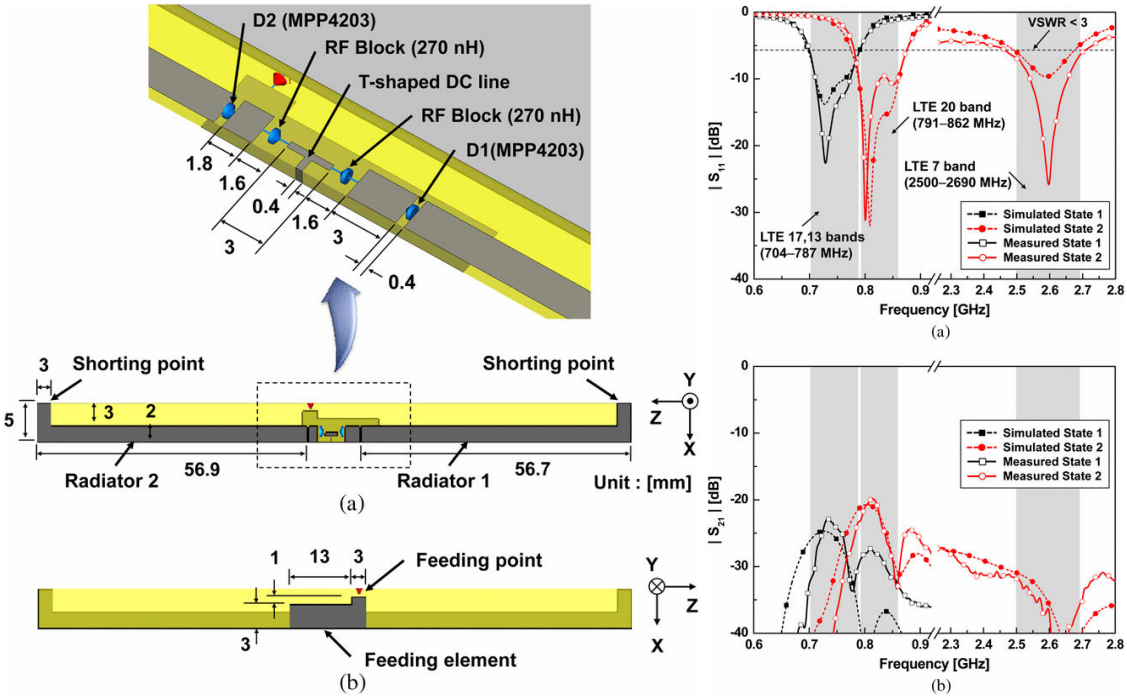

Figure 3.7: Reconfigurable multiband antenna with diodes for laptop applications [11].

2. PASSIVE MULTIBAND ANTENNA FOR 2G, 3G AND 4G APPLICATIONS

In this section, an ungrounded antenna is presented. Thanks to the use of a folded inverted-L antenna and a grounded stub to reduce the size, the antenna of dimensions 68x130x10 mm^3 can be easily integrated into mobile devices. In addition, the grounded stub acts as a parasitic coupled element that ensures that the antenna can operate in all frequency bands of mobile phone applications with a return loss less than -6 dB at frequency bands of 700-960 MHz and 1580-2700 MHz.

2.1. Antenna design

Proposed antenna's geometry is presented in Figure 3.8. It is designed on a FR-4 Epoxy substrate with overall dimensions of 68×130×1.6 mm^3. The volume occupied by the radiating element is only 68×17×10 mm^3, corresponding to $0.16\lambda_0 \times 0.04\lambda_0 \times 0.23\lambda_0$ (λ_0 calculated at 700 MHz).

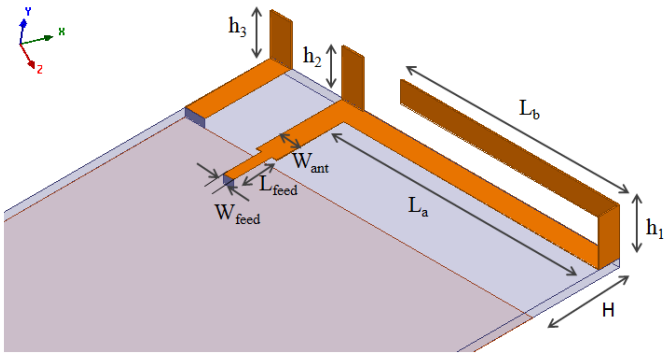

L_{feed}	W_{feed}	h_2
7.5 mm	2 mm	9mm
L_b	W_{ant}	h_1
42.2mm	4mm	9mm
L_a	H	h_3
49.7mm	17mm	8mm

Figure 3.8: Geometries of the proposed antenna for 4G, 3G and 4G standards.

The antenna design is based on the idea of dividing mobile phone's operation frequency bands into 3 separate ranges. Frequency band [700-960 MHz] is used for LTE 700/GSM 900 bands, [1710-2170 MHz] for GSM 1800/LTE 1800/UMTS bands and the last one [2400-2600 MHz] for ISM, Bluetooth, Wi-Fi and LTE 2600 applications.

Due to the division of the frequency band as above, we can estimate in advance the antenna size for the different frequency bands. Two parts compose the proposed antenna. A folded inverted-L shape antenna dedicated to operate at low frequency band from 700 MHz to 960 MHz and middle frequency band from 1570 MHz to 1730 MHz. Using a coupled grounded stub as second radiating part which contributes to higher frequency band of 1900-2700 MHz, the tri-band behavior is obtained.

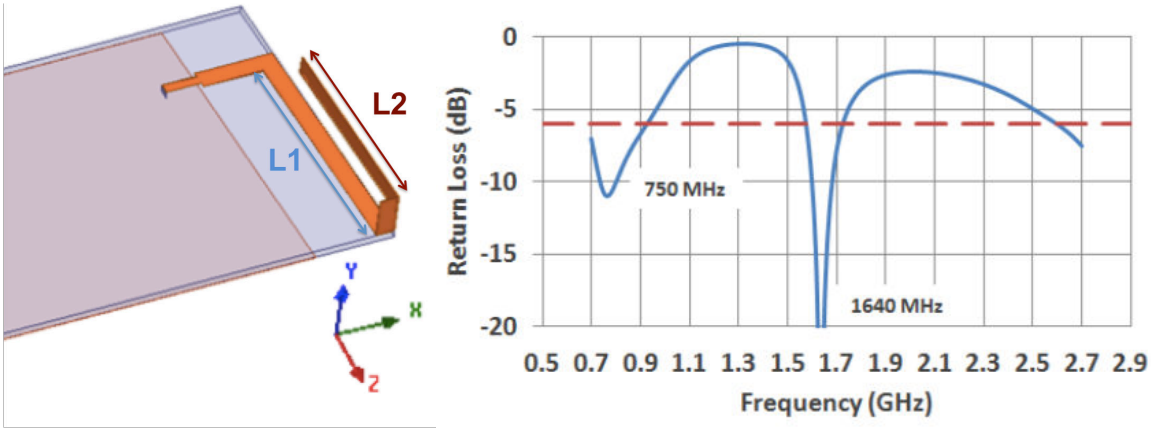

Figure 3.9: Geometry and simulated result for the folded inverted-L antenna.

The lowest frequency band is the most difficult part of the antenna according to the physics laws. Because of the relatively long (about 428 mm) antenna's wavelength at 700 MHz, the integration of the antenna on the mobile device (68×130 mm^2) is a major challenge.

Miniaturization is mandatory but the antenna size with respect to the wavelength is the parameter that will have the preponderant influence on the radiation characteristics.

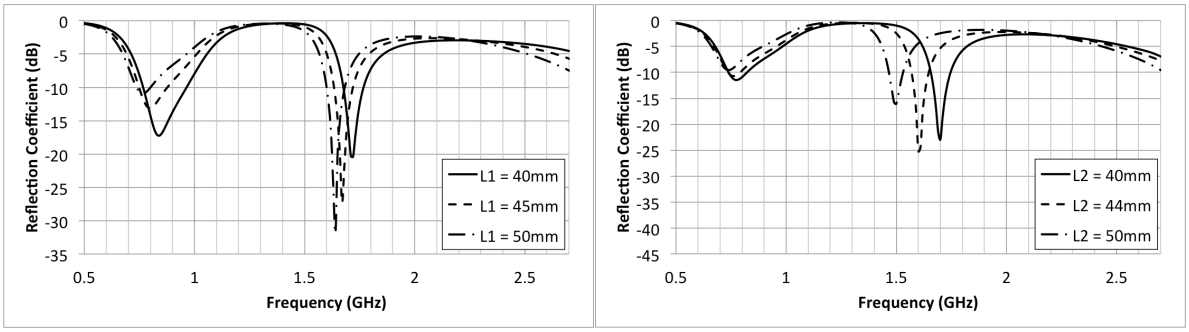

Figure 3.10: The influence of the length L1 and L2 on antenna matching.

To satisfy the size requirement listed above, and to have an omnidirectional radiation pattern as well as an acceptable bandwidth, using folded inverted-L antenna is a reasonable choice (Figure 3.11). With an overall trace length about 100 mm, which is equivalent to $\lambda_1/4$ (λ_1 being the wavelength at 750 MHz), this branch line allows us to cover the frequency band between 700 MHz and 930 MHz with a return loss less than -6 dB. Moreover, the folded shape of the antenna helps in reducing its size, as well as adding the capacitive effect in order to have one more resonance frequency at 1640 MHz. The simulation result is also shown in Figure 3.11.

Once the antenna is designed for the low band, we continue the design of the antenna for medium and high frequency bands. At these frequencies, wavelengths are much smaller, thus the antennas size will be reduced. With an additional branch in the folded inverted-L shape and an additional ground stub, a new resonance frequency appears at 2170 MHz. Thanks to the combination of this resonance frequency and the other one at 1640 MHz, we observed a return loss lower than -6 dB over all the frequency band from 1615 MHz to 2700 MHz. And it also impact on the low band to expand the operating frequency (700-960 MHz instead of 700-930 MHz). With the simulation results shown in Figure 3.12, we can conclude that the proposed antenna can be operated for all mobile-phone's applications.

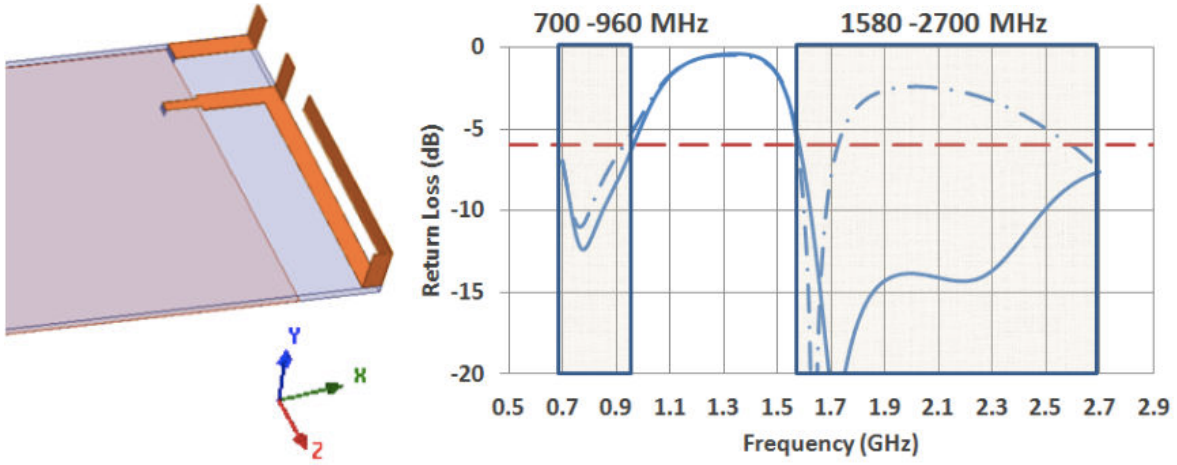

Figure 3.11: Geometry of antenna with simulated result before and after adding ground stub.

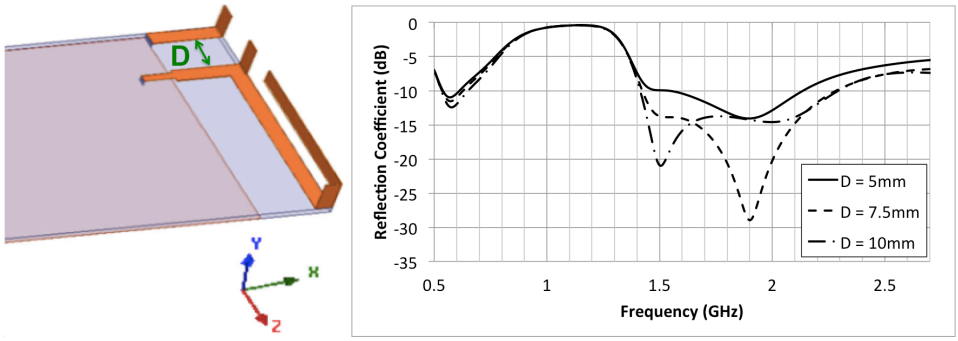

Figure 3.12: The influence of distance between 2 elements on antenna matching.

The resonance of the lower band can be observed from the current distribution shown in Figure 3.13 (a) for 700 MHz. The strong current starts from the input port to the folded inverted- L arm that is the longest ways in the proposed antenna. In Figure 3.13 (b) and Figure 3.13 (c), a strong current density appears simultaneously at feed line, at on-air branch of the folded inverted-L shape and at the ground stub. It shows the combination effect of two resonance frequencies 1640 MHz and 2170 MHz. Finally, Figure 3.13 (d) shows the current that is mainly located on the ground stub, able to create a resonance frequency in the high band. This simulated results shows the validation of our explication above.

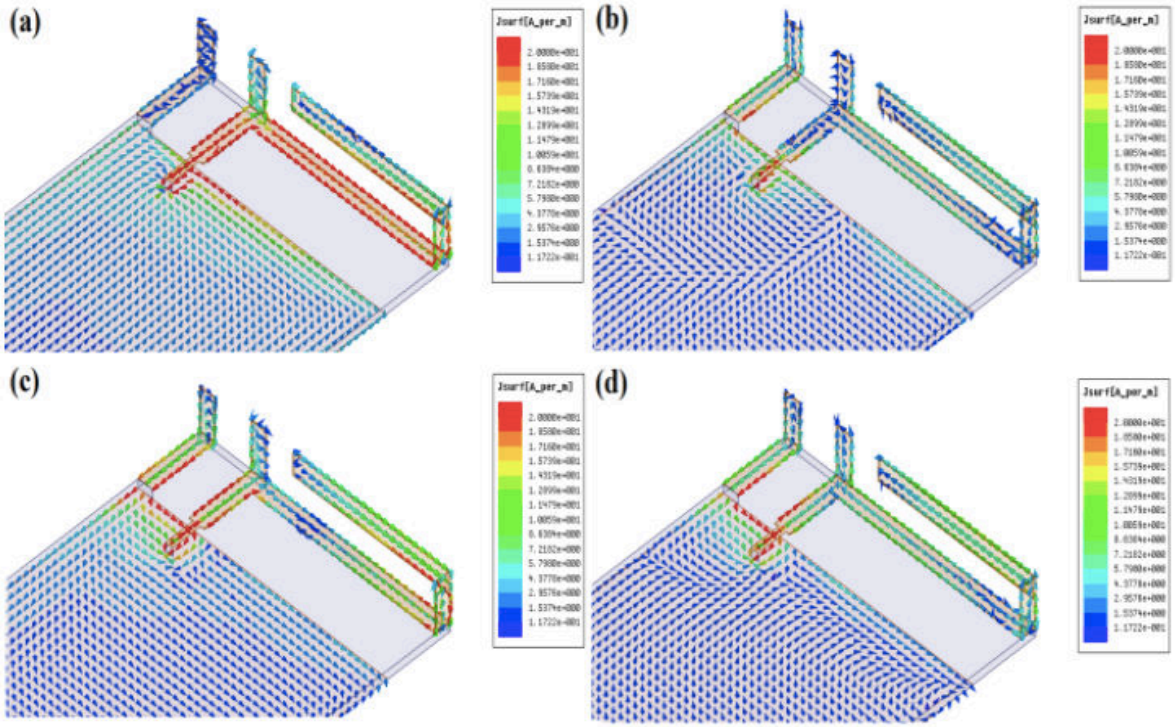

Figure 3.13: Simulated current distribution at different frequencies at (a) 700 MHz, (b) 1710 MHz, (c) 2170 MHz, (d) 2700 MHz.

2.2. Results and discussion

According to the parameters given in the previous section, a prototype of the proposed antenna was fabricated on a FR-4 Epoxy substrate of permittivity 4.4 and dimension of

68×130×1.6 mm^3, comparable with modern Printed Circuit Board (PCB) of modern mobile phones. The volume of the antenna is 68×17×10 mm^3.

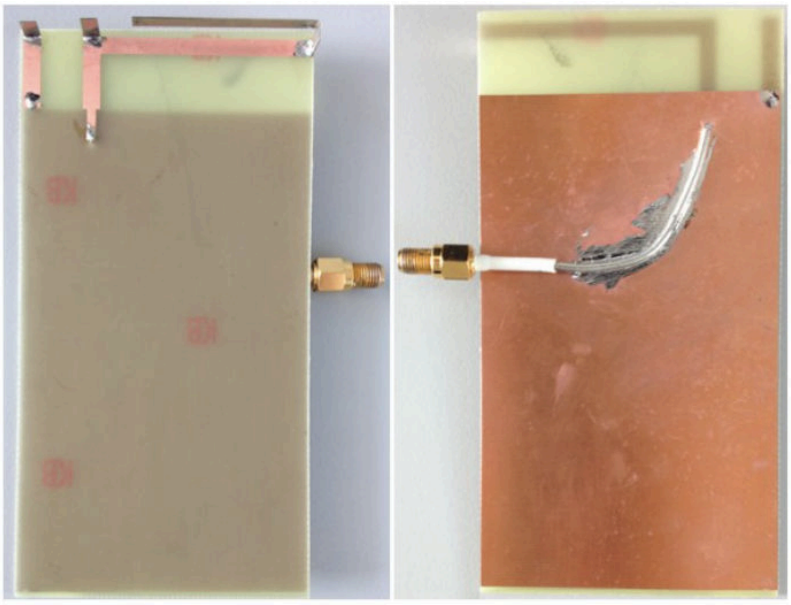

Figure 3.14: The prototype of the proposed antenna on a FR-4 Epoxy.

By using the Rohde & Schwarz ZVL Network Analyzer, the measured and simulated reflection coefficients are presented in Figure 3.15. Both results show good agreement. From the measurement, we observe that the impedance bandwidth ($|S_{11}|$<– 6 dB) is 260 MHz from 700 MHz to 960 MHz (15.7%). In the high-frequency band, the frequency bandwidth is 185 MHz from 1615 MHz to 2700 MHz, which represents 25.1% with a reflection coefficient S_{11} less than -10 dB.

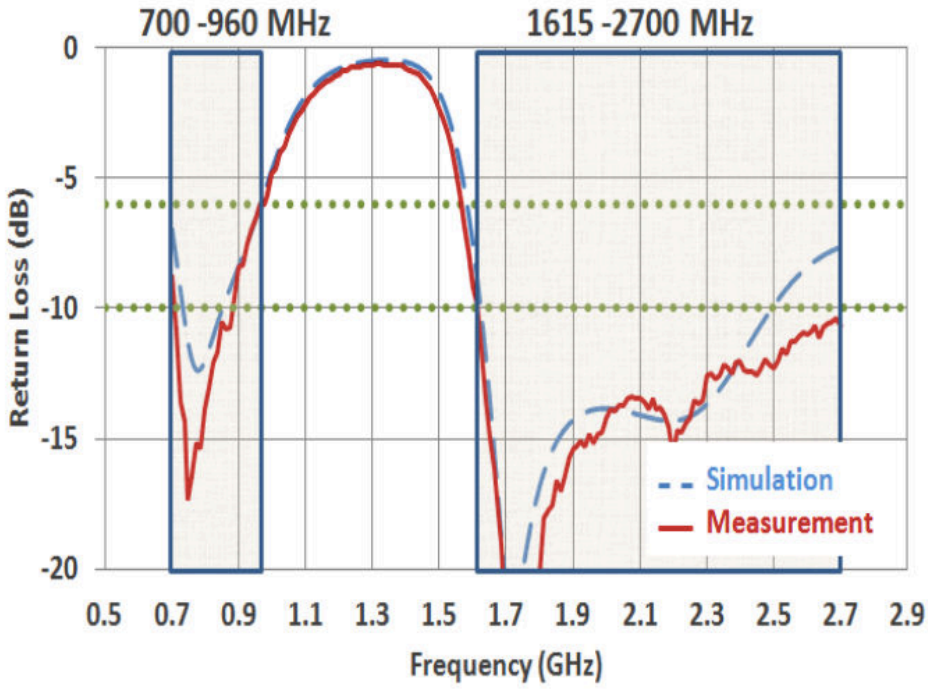

Figure 3.15: The simulated and measured reflection coefficients of the proposed antenna.

Radiation patterns of the prototype were also measured using the StarLab-Satimo chamber of Orange Labs center in La Turbie. These results are shown in Figure 3.16. Only four representative frequencies (f = 700 MHz, 1710 MHz, 2170 MHz and 2700 MHz) are presented. Due to the results in the Figure 3.16 below, we can conclude that the proposed antenna radiates as a dipole at low frequency band and as a quasi-omnidirectional radiating element at high frequency band. The measured radiation efficiency and gain are also depicted in Figure 3.17. It can be seen that the antenna efficiency is from 55% to 83% in the lower band and from 77% to 95% higher band. In addition, the measurement results are also presented antenna has the good gain, from 1 dB to 2.1 dB in the lower band and 2.4 dB to 4 dB in the higher band.

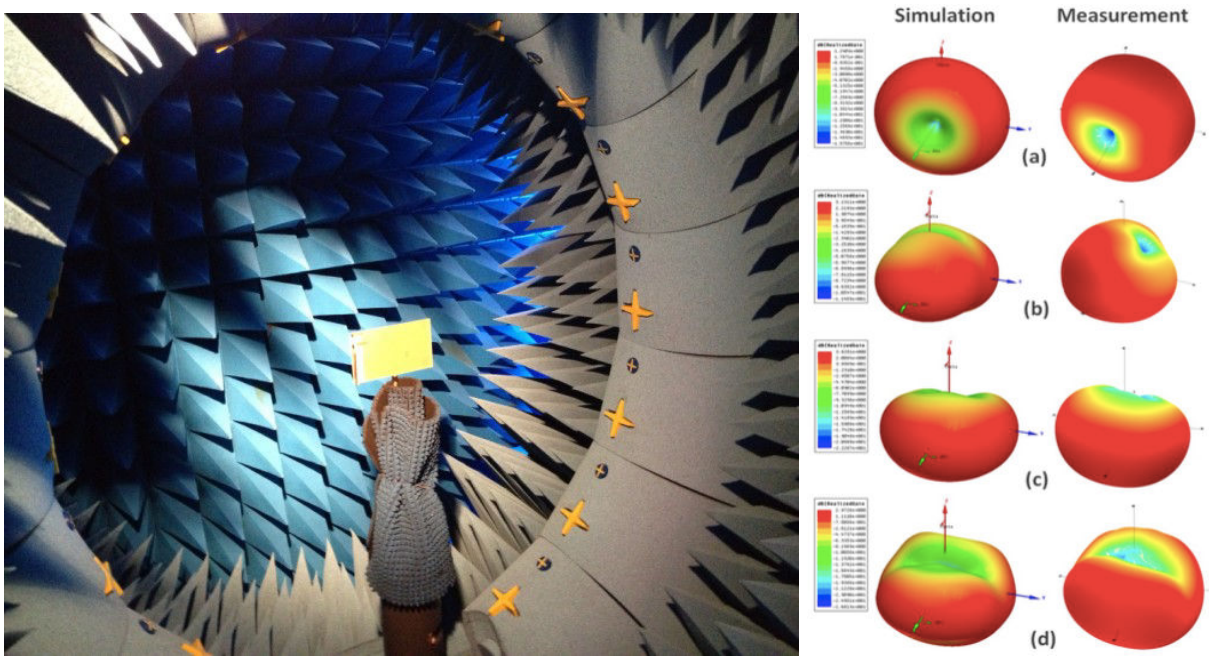

Figure 3.16: Simulated and measured 3D radiation pattern at (a) 700 MHz, (b) 1710 MHz, (c) 2170 MHz, (d) 2700 MHz

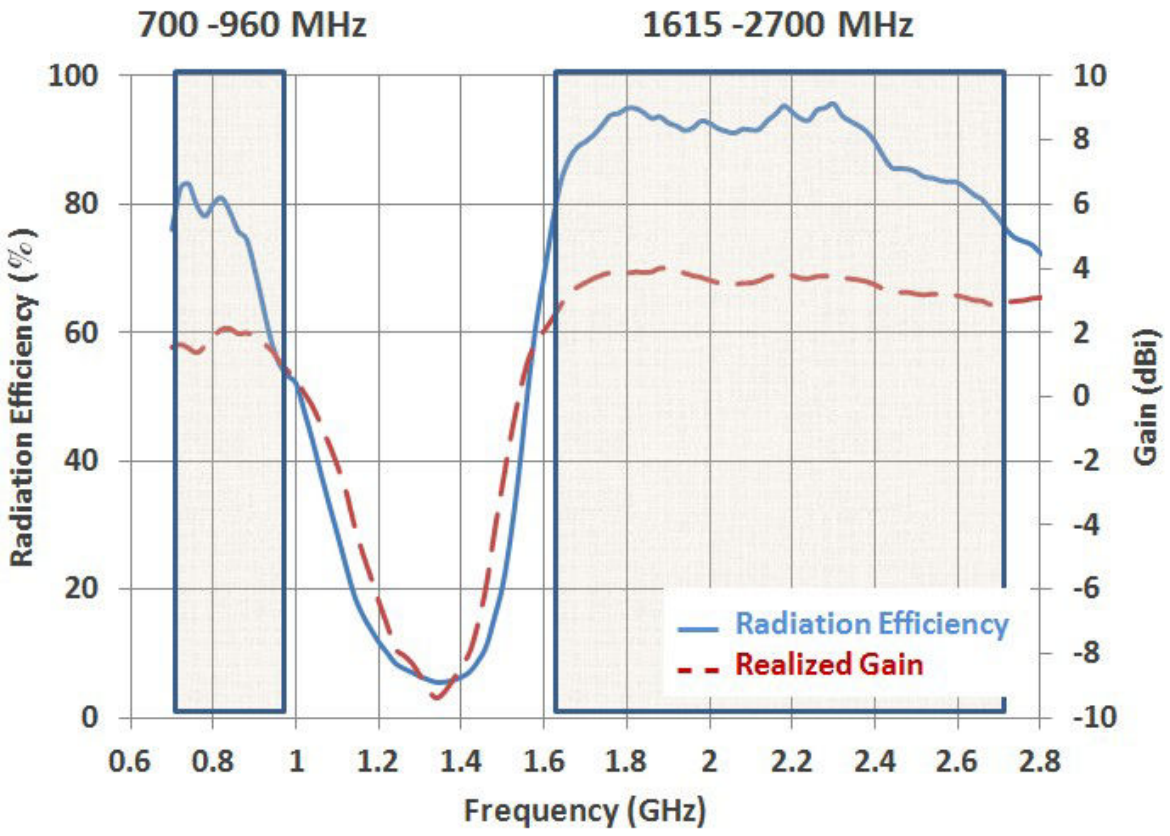

Figure 3.17: Measured radiation efficiency and peak gain of the proposed antenna.

2.3. Conclusion

A multi-band antenna for mobile phone application has been designed. With this concept, the proposed antenna can operate in all frequency bands for mobile phone including the low frequencies in the LTE standard. The dimensions have been optimized to integrate easily this antenna in mobile devices. Moreover, the radiation efficiency greater than 55% ensures that the antenna operates with the good performance.

3. MIMO MULTIBAND ANTENNA FOR SPECTRA PROJECT

SPECTRA is a Celtic Project. It began on September 2010 and will run until August 2014. The primary objective of SPECTRA is to combine new cognitive radio algorithms with innovative approaches on Radio Frequency (RF) front-end and base band components to bring novelties in key areas related to interference-limited and energy-efficient systems, which is going to be demonstrated on a developed proof-of-concept able to communicate cognitively in real time.

To support the target scenario and associated use cases, an antenna system is proposed. The main specifications for the antennas are the frequency bands, the size and the performance.

The antenna system will address the following frequency bands:

- The upper part of TVWS and the Digital Dividend: 700- 862 MHz;
- LTE 2.6 GHz FDD band n°7 and TDD band n°38: 2496-2690 MHz;
- LTE 3.5 GHz TDD band n°42: 3400-3600 MHZ.

Dealing with the design of antennas for portable devices, two main challenges have to be faced: the antenna miniaturization but also the preservation of a large bandwidth in input impedance and correct gain over all the bands of interest. Then the matching circuit will work more correctly, saving return loss effects from the power amplifier and allowing good radiation efficiency. In order to meet these requirements, a MIMO multiband antenna is designed based on the geometry of the previous section.

3.1. Antenna design

Folded monopole has been widely used thanks to their small dimension and low production cost. They are constituted by a folded λ/4 radiating element to decrease its size and also to created multi-resonance frequency. In order to cover entire mobile phone frequency band, parasitic elements were used.

Figure 3.18 shows the geometry of the proposed antenna developed. It includes a folded radiating element to help the matching at the lower frequencies. Thanks to parameter's optimization of folded elements positions, the second resonance frequency appears close to 1700 MHz. In addition, the coupling between main radiating and parasitic elements helps us to cover a higher frequency band from 2400 MHz to 2700 MHz. The proposed antenna is mounted on a 120x200 mm^2 ground plane, typical of mid-size mobile devices. The antenna geometry has been optimized to exhibit a reflection coefficient S_{11} lower than -6dB in the following bands: LTE 700 (790 – 862 MHz), GSM (880 – 960 MHz), DCS (1710 – 1880 MHz), PCS (1850 – 1990 MHz), UMTS 2100 (1920 – 2170 MHz), WLAN (2400-2480) and also LTE 2600 (2500 – 2690 MHz).

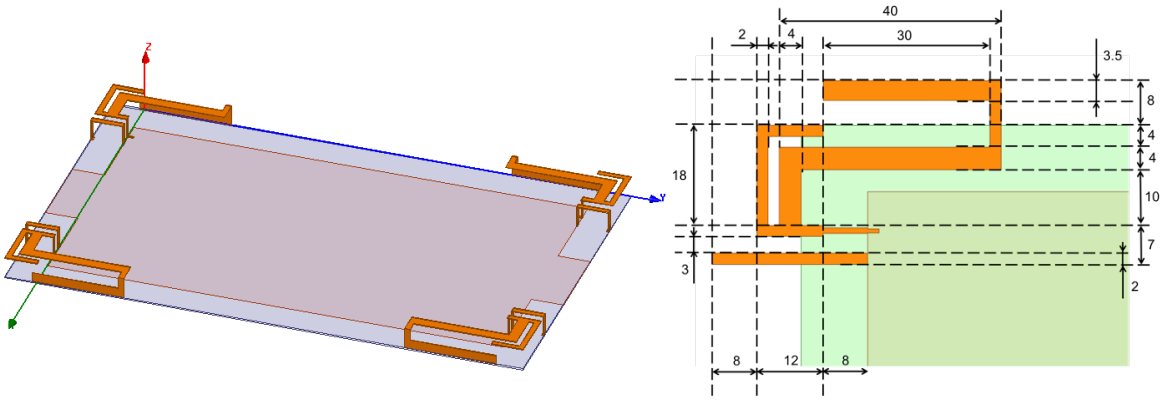

Figure 3.18: SPECTRA antenna geometry.

To understand the proposed antenna performance and also to confirm the explication at the previous section, a parametric study is done. As shown in figure blow, the longest line is presented by the red color part. The length of this line is about 100 mm that is equivalent to $\lambda_1/4$ (with λ_1 is the wavelength at 750 MHz). This branch line creates a resonance to cover the

low frequency band. By changing its length, the influence of this part on the low band is shown in the Figure 3.19.

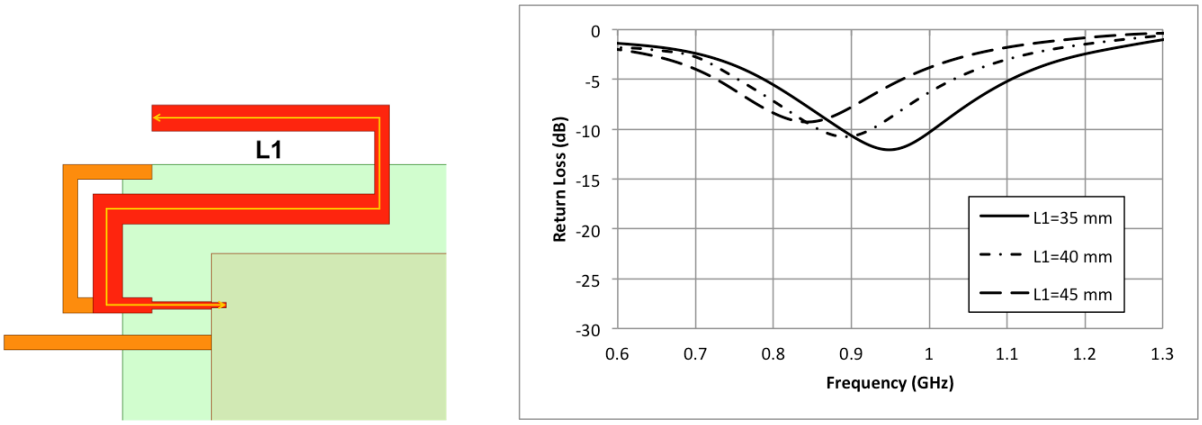

Figure 3.19: The influence of the longest line on the low band

The folded shape of this part helps in reducing the antenna size, as well as to create another resonant frequency in the mid-band. This resonance is appeared by the capacitive effect between two red lines that is shown in Figure 3.20.

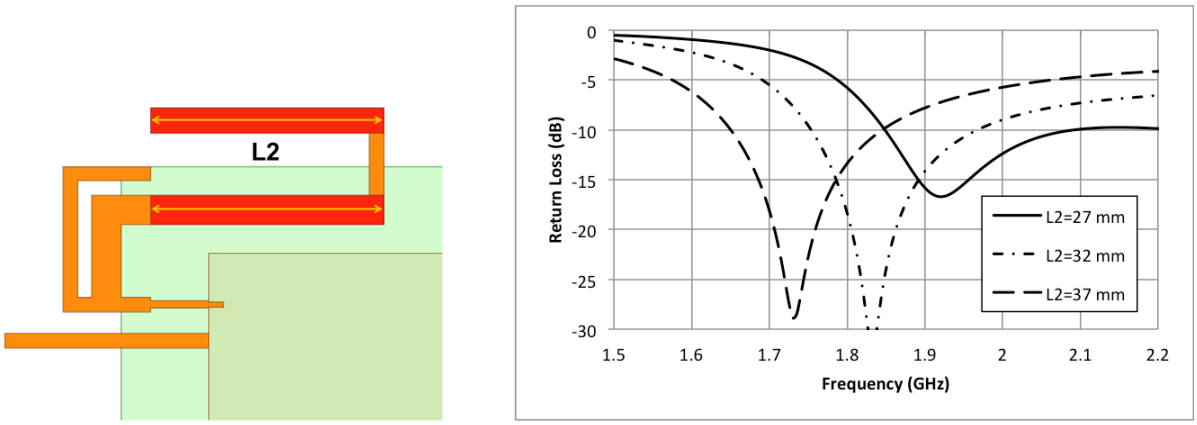

Figure 3.20: The influence of the capacitive effect on the middle band

To assure the proposed antenna can operate at frequency band from 2.4 GHz to 2.7 GHz, an additional ground strip is used. With the length about 28 mm (corresponding to quarter wavelength of 2.7 GHz), a resonance is appeared at 2.7 GHz. Because of frequency band from 1.71 GHz to 2.7 GHz is quite large. The combination of the resonant frequencies that are created by ground strip and capacitive effect of folded shape (has been mentioned in previous paragraph) is not enough to cover this band. To resolve this problem, an additional branch in the folded inverted-L shape is used. The parametric study is shown in figure below that presents the impacts of the ground strip and the additional branch on the high frequency band.

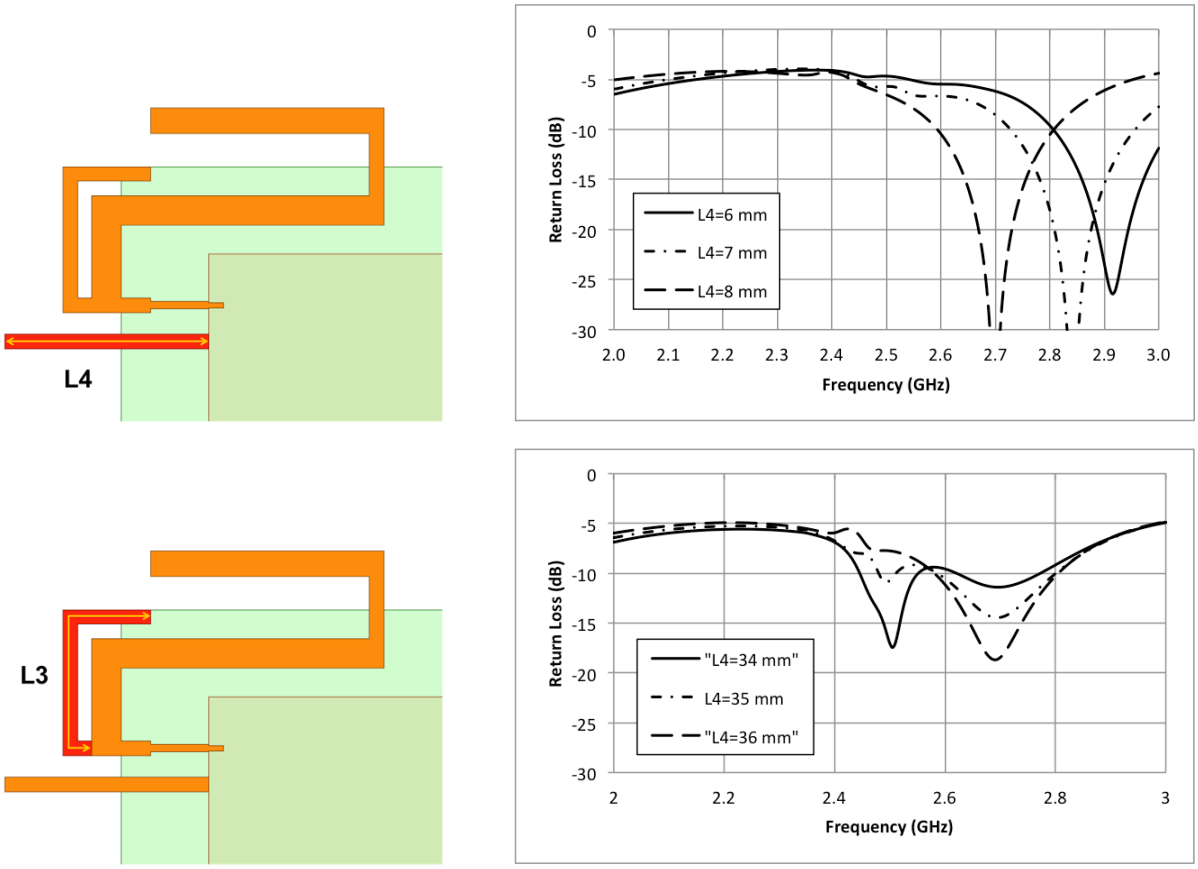

Figure 3.21: The influence of the ground strip and the additional branch on the high band.

After optimize all of parameters, the simulated results of the first final version is presented in the Figure 3.22. From the S-parameters results, this antenna shows the operating frequencies from 790 MHz to 960 MHz for the low band and from 1710 MHz to 2700 MHz for the higher bands (with the S11<-6 dB). Beside, the isolation of antenna is also presented. With the value higher than 8 dB for all of low band and a narrow range around 2.5 GHz, the worst case corresponds to the distance between two antennas that is nearest. For other case, the proposed antenna shows a good isolation (higher than 10 dB).

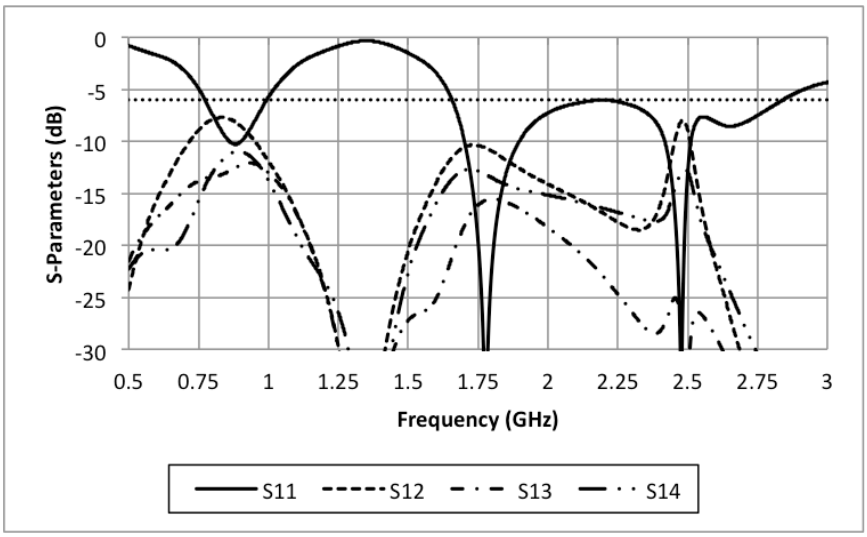

Figure 3.22: Simulated S-parameters of the proposed antenna

3.2. Results and discussion

According to the parameters allowing obtaining an optimized result, a prototype of the proposed antenna was fabricated on a FR-4 Epoxy substrate of permittivity 4.4 and dimensions of 120x200x0.4 mm^3, comparable with modern tablets PCB. This prototype is shown in the following pictures.

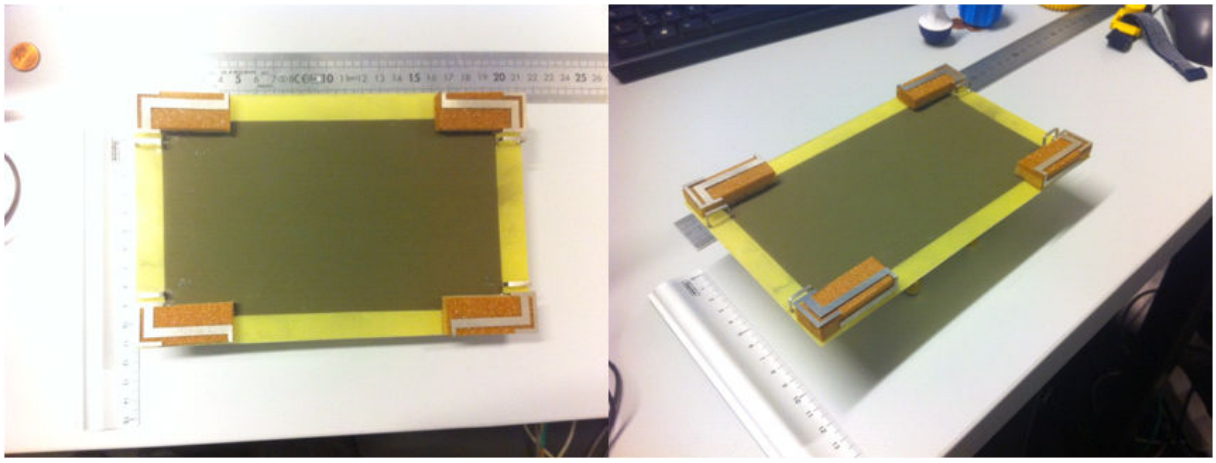

Figure 3.23: Photo of the prototype.

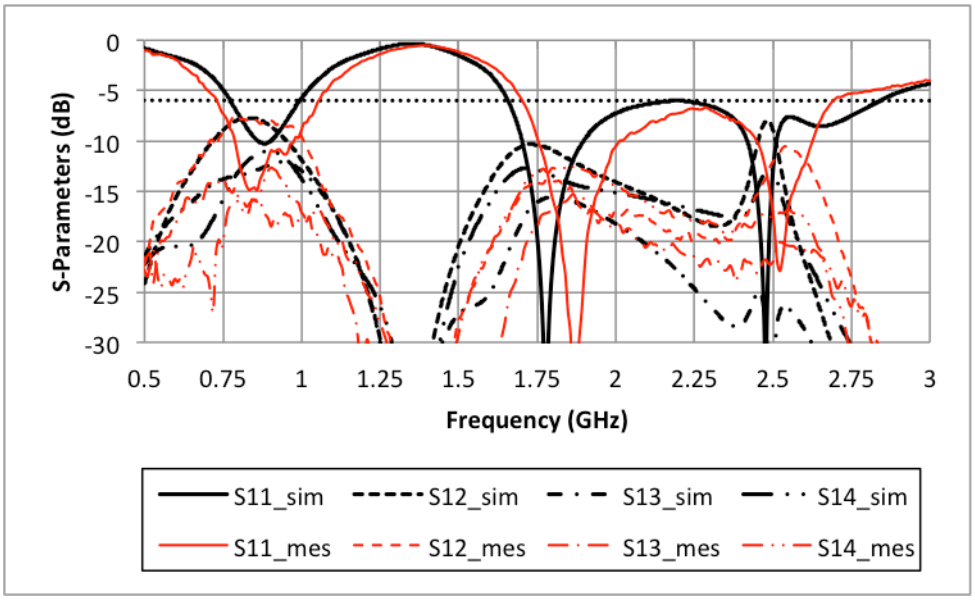

Figure 3.24: The simulated and measured S-Parameters of the proposed antenna.

The figure above presents the comparison between simulated and measured S-parameters of proposed antenna. There are some different between them due to the error of fabrication, however, the results show good agreement. From the measurements, we observe that the impedance bandwidth (defined for S11 < -6 dB) is 270 MHz from 730 MHz to 1000 MHz (about 31%). In the high band, the frequency bandwidth is 990 MHz, from 1710 MHz to 2700 MHz that represents 45% with a reflection coefficient S11 less than -6dB.

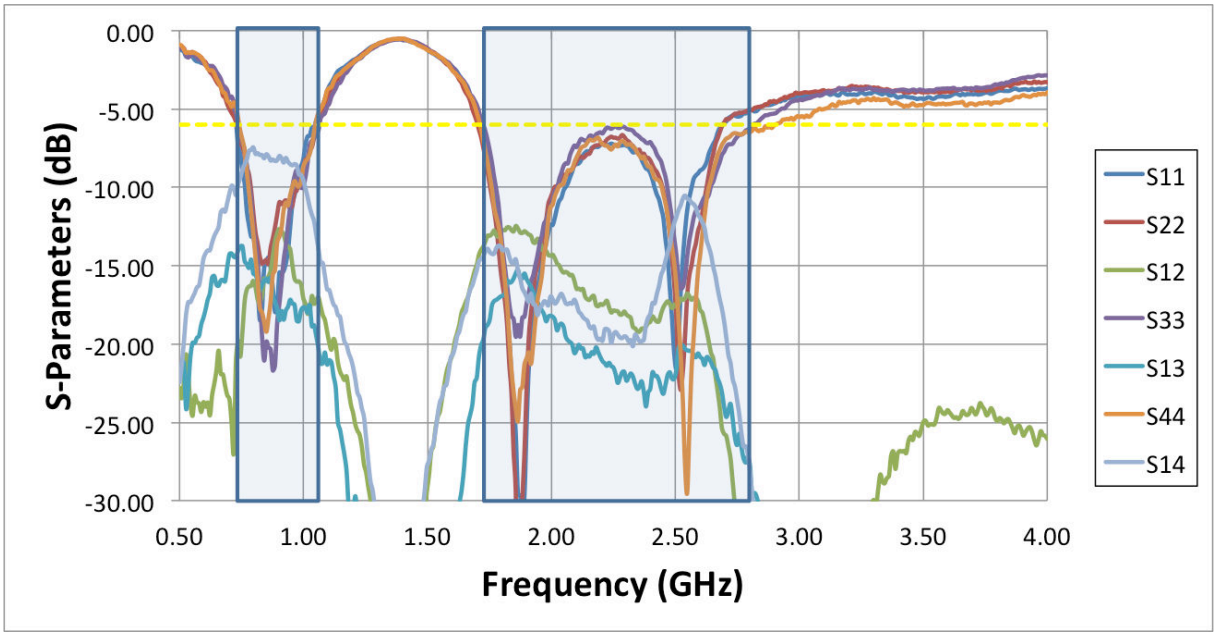

Figure 3.25: Measured S-parameters of the proposed antenna prototype

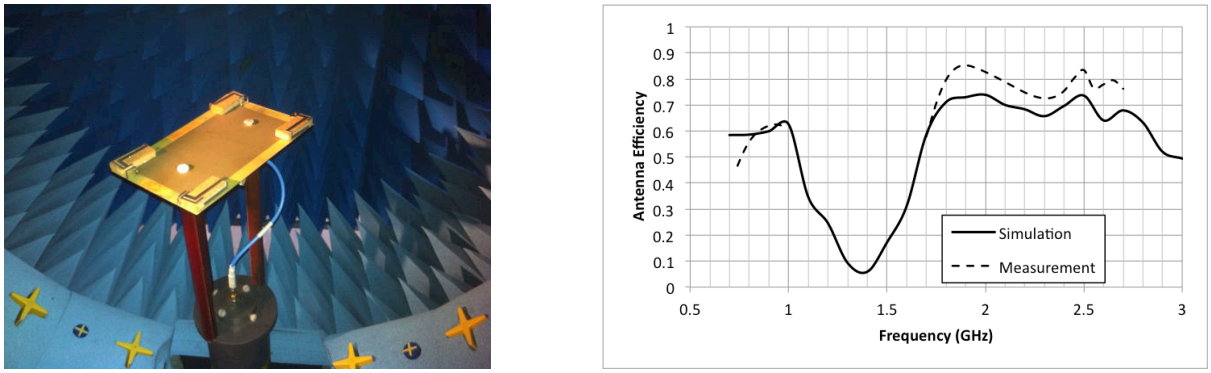

Figure 3.26: Simulated and measured efficiency of the prototype.

The radiation efficiency of the prototype was also measured using the StarLab-Satimo chamber of Orange Labs center in La Turbie (Figure 3.26). There are some different between two results, however, the results show good agreement. We can conclude that the measured antenna efficiency is comprised from 58% to 62% in the lower band and from 59% to 74% in the higher one.

3.3. Conclusion and perspective

In conclusion, a multi-band antenna concept for the MIMO system has been designed. With this concept, the proposed antenna can operate in all frequency bands for mobile phone including the low frequencies in the LTE standard. The dimensions have been optimized to integrate easily this antenna in the mid-size mobile devices. Moreover, the radiation efficiency greater than 58% ensures that the antenna operates with the good performance.

In perspective, a new structure based on the previous antenna is designed. By adding another ground strip on PCB, this structure can cover the 3.5 GHz band. The antenna geometry and simulated results is shown on the figure below. The new prototype will be fabricated and measured.

4. RECONFIGURABLE ANTENNA FOR EXTENSION OF LTE OPERATIONAL MODE OVER TV WHITE SPACES

This section presents a reconfigurable antenna for mobile terminal and TV white space communications, using a Digitally Tunable Capacitor (DTC). The antenna structure is matched permanently over the high frequency bands including DCS/PCS, UMTS, LTE 1800/2600, and 3.5GHz bands. Concerning the sub-GHz bands, several reconfigurable states enable a full coverage of LTE 600/700 and GSM 850/900 standards, as well as future applications on TV White space (TVWS). With dimensions of 40×10×6 mm^3 for the antenna and 130×70×0.8 mm^3 for the whole PCB, this structure is perfectly compatible with any mobile terminal.

In this study, DTC combines high power handling (34 dBm), low power consumption (150 μA) and a good capacitance scale (7.7:1) in a compact packaging. It is controlled with I2C or SPI protocol and has 32 different states [12]

4.1. Antenna design

The geometry of the proposed antenna (Figure 3.27) is based on the capacitive coupling principle between a fed monopole and parasitic elements. The antenna has a compact design (40 mm ×10 mm × 6 mm) and it is placed on top of a FR4-Epoxy substrate with a size of 130 mm × 70 mm × 0.8mm, relative permittivity 4.4, and loss tangent 0.02.

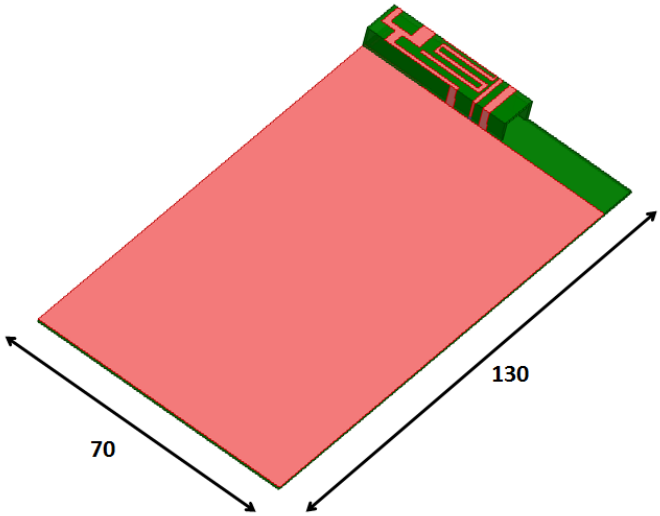

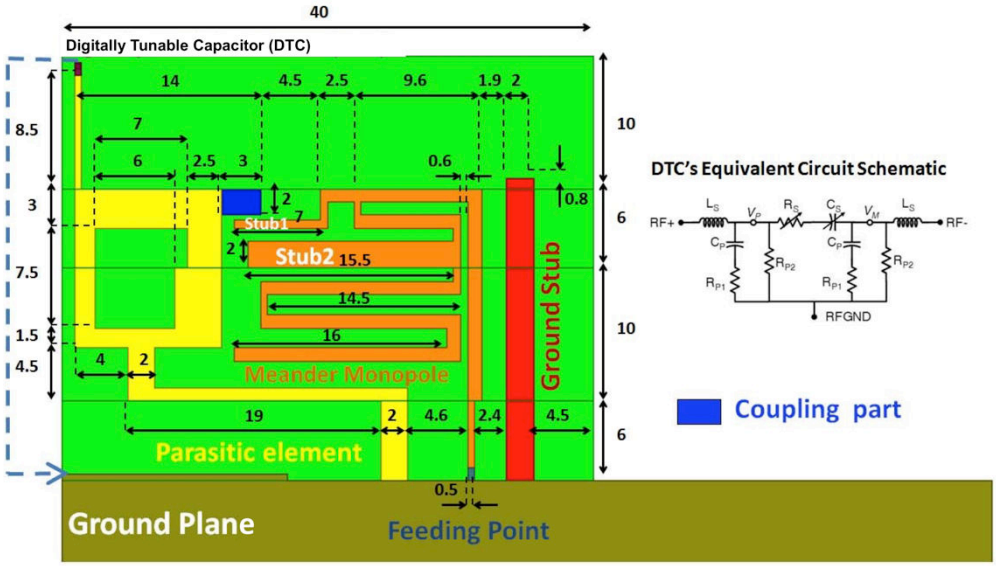

Figure 3.27: The geometry of proposed antenna and chassis dimension.

The proposed antenna consists of three different elements (Figure 3.27). The center element is a meandered monopole fed by a 50Ω microstrip line (orange). The monopole has an overall length of about 84 mm, which creates a resonance around 900 MHz. In the middle of this branch, two strips (pink) are used to provide two resonances at 1750 MHz and 3500 MHz. Moreover, the shunt capacitance effect between the meander monopole and the shorted parasitic element (yellow) generates an additional resonance for the lower band. By tuning the dimension of the "coupled part" (red), the impedance matching in the low-band can be optimized. This shorted parasitic element is connected to the ground plane through a variable capacitor. By tuning its capacitance C_{Tot}, a narrow band can be reconfigured to cover the 630-860 MHz frequency range. On the right side, a ground strip (blue) is used to cover the 2.5 GHz band. Finally, a new resonance is obtained at 2.7 GHz thanks to an optimization of the shape of the meander monopole. The combination of these two different solutions enables the correct matching of the antenna over the middle frequency band.

To understand the proposed antenna performance and also to confirm the explication at the previous section, the simulation for each part of the antenna is done. The antenna's design has only center part. As shown in the simulated results, the first resonance is around 1 GHz, corresponding to the longest trace length. This line also creates third harmonic at 3 GHz. Beside, the strip appeared at the middle of center part radiates at the frequency around 2 GHz.

By adding the ground strip, a new resonant frequency is presented at 2.5 GHz. Due to the combination with another resonance of center part, the bandwidth at the middle band can be extended. Finally, to cover the remaining frequency band, the second strip and the last part are added. This second stub is used to provide a resonant frequency at 3500 MHz. The coupling between the last part and the main strip creates the resonance at the lower frequencies to cover TV White Space band. Thanks to optimizer the antenna parameters, the simulated result is shown in the figure below.

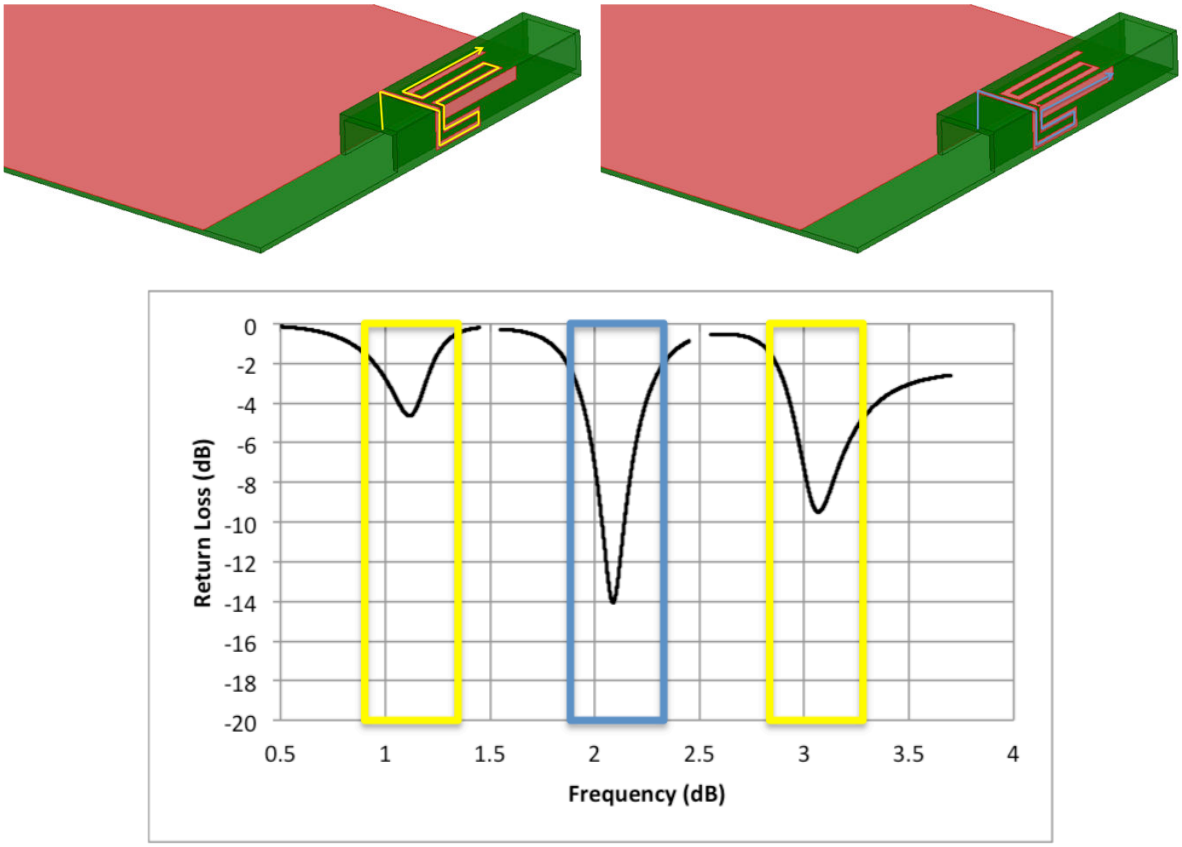

Figure 3.28: The geometry of center part and simulated the reflection coefficient.

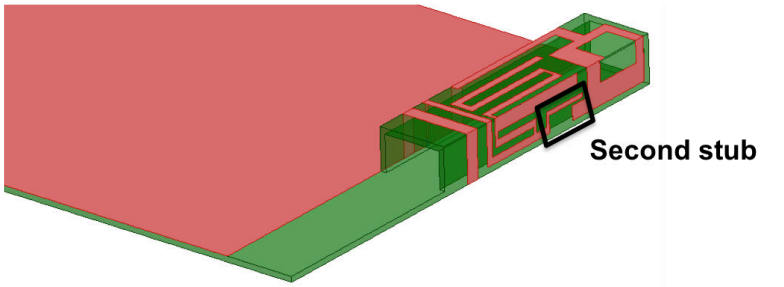

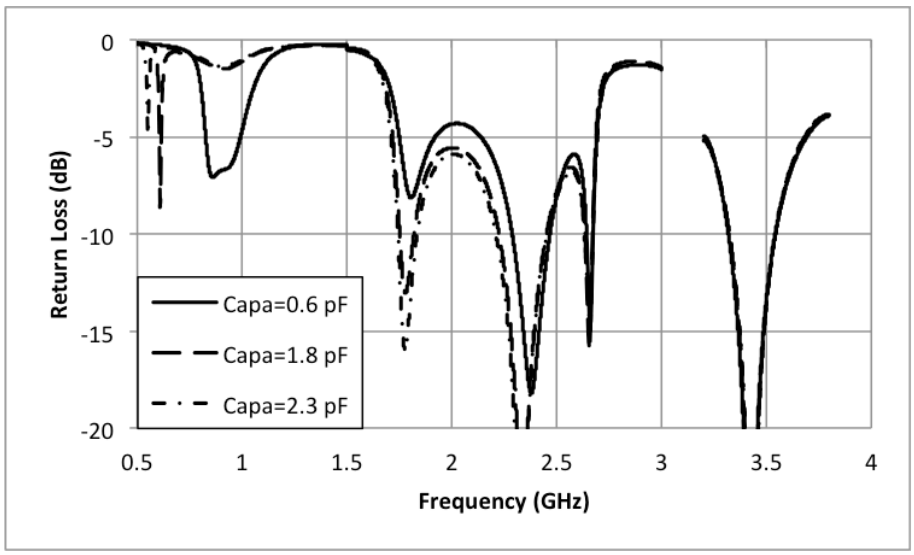

Figure 3.29: The antenna geometry and the simulated reflection coefficient.

4.2. Results and discussion

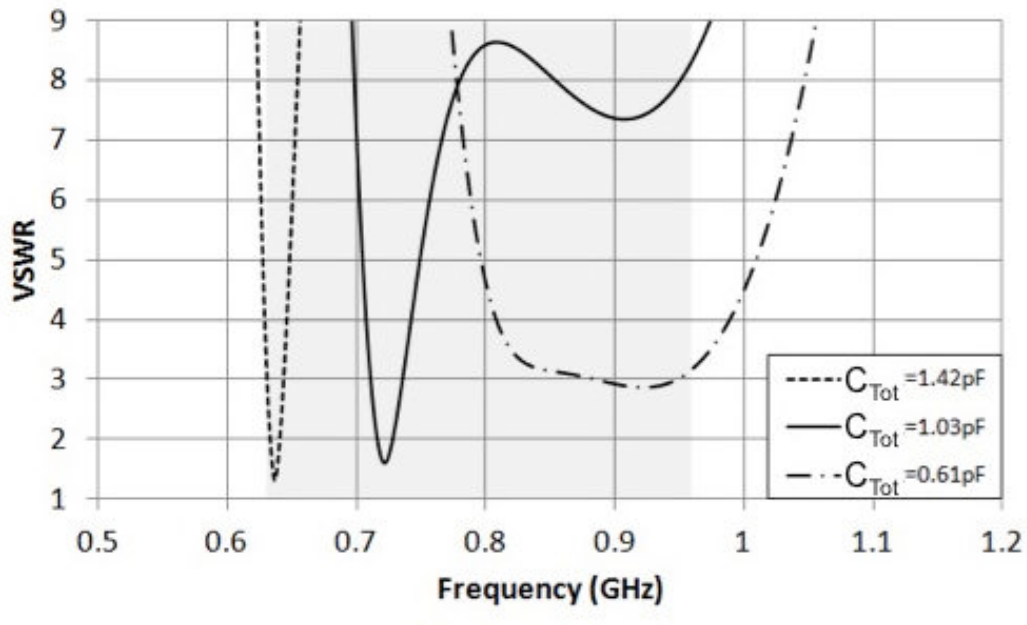

Figure 3.30: Simulated VSWR of proposed antenna at the low frequency bands

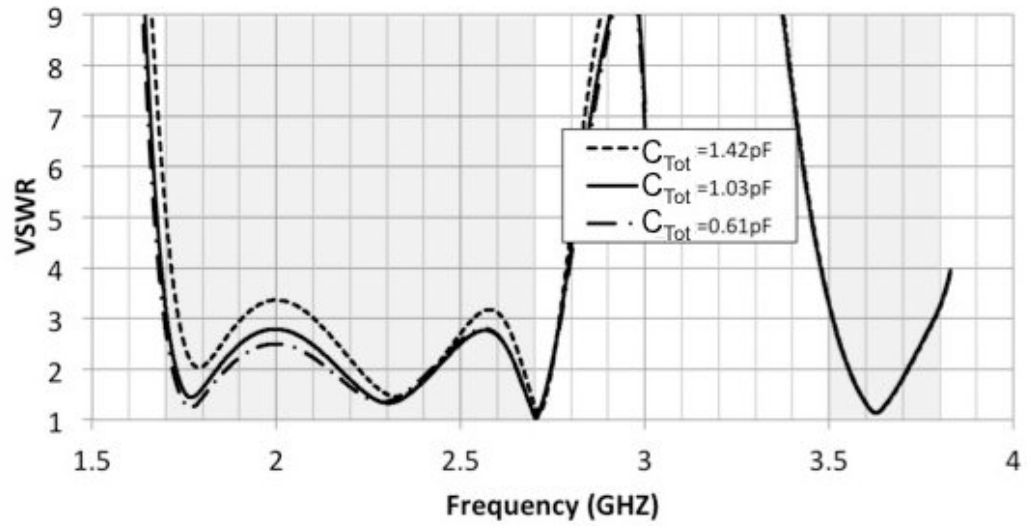

Figure 3.31: Simulated VSWR of proposed antenna at the high frequency bands

By using ANSYS HFFS EM solver, the antenna is simulated. The antenna geometrical parameters are optimized with the aim of obtaining a good impedance matching over all the requested bands. The final parameters values (expressed in mm) are shown in Figure 3.27.

The VSWR curves in the lower frequency bands are presented in Figure 3.30. When the capacitance value of DTC is tuned between 0.6 pF to 1.8 pF, the reflection coefficient of the antenna is modified. For the 0.6pF capacitance, a bandwidth a 100 MHz between 860 MHz and 960 MHz is obtained. For higher capacitance values, a narrow band with a 3:1 VSWR can be tuned from 600 MHz to 850 MHz with an instantaneous bandwidth always higher than 10 MHz. This modification has a small impact on the high frequency band, and the antenna is

constantly matched between 1.6 GHz to 2.7 GHz and 3.3 to 3.6 GHz with a 3:1 VSWR (Figure 3.31).

According to the results shown in Figure 3.32, simulated total efficiencies are roughly -5 dB to -2 dB for the lower band, -3 dB to -0.4 dB for the middle band and -3 dB to -1 dB for the higher band. Thus, it confirms that the proposed antenna is suitable for mobile handset.

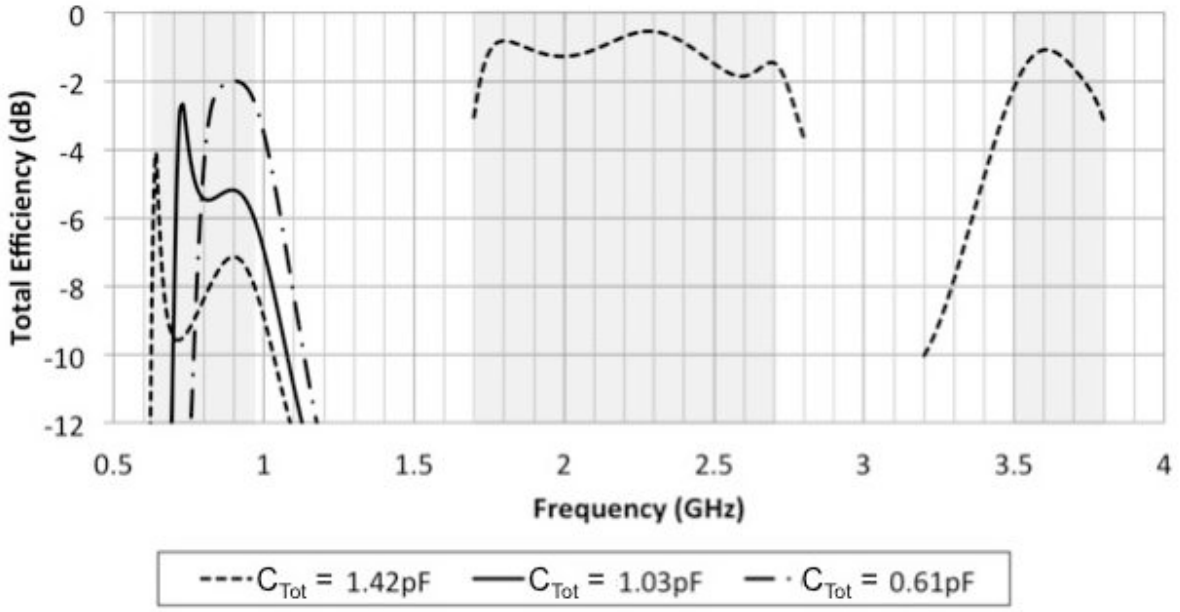

Figure 3.32: Simulated total efficiencies of proposed antenna.

To further confirm the antenna's principle and to clearly show which parts of the antennas are responsible for the radiation in the different bands, the study of the current distribution has been made. As shown in Figure 3.33, four frequencies have been considered. At 630 MHz, the current is mainly located on the meander monopole and the parasitic element, and especially on the strip used to connect the capacitor to the ground plane. At 920 MHz strong currents appear only on the meander monopole. At 2100 MHz, the capacitive effect between the ground strip and the feeding line is clearly visible. Finally, at 3500 MHz, the strongest current density is located on strip 1.

Figure 3.34 shows the prototype of the proposed antenna. The unwrapped radiating structure shown in Figure 3.27 has been printed on the FR4 substrate and successively folded thanks to the mechanical milling of the edges to be bent. The tunable capacitor used to reconfigure the antenna is the Peregrine PE64905 DTC. On the back of the PCB, an I2C system used to control the DTC is placed. It consists of a Mbed NXP LPC 1768 microcontroller and three AA batteries which are placed in the holder. In shunt configuration, the DTC can provide capacitance values from 0.9 pF to 5.6 pF (measured values). Consequently, in order to achieve the needed 0.61 pF capacitance value (Figure 3.30), a series capacitor C_s = 1.9 pF is connected to the DTC. The resulting measured capacitance values ($C_{Tot}=C_{DTC}C_s/(C_{DTC}+C_s)$ as well as the bandwidths of the antenna obtained in the different DTC configurations are summarized in Table 3.1. As it can be noticed, the antenna enables continuous coverage with high frequency resolution control in the low band.

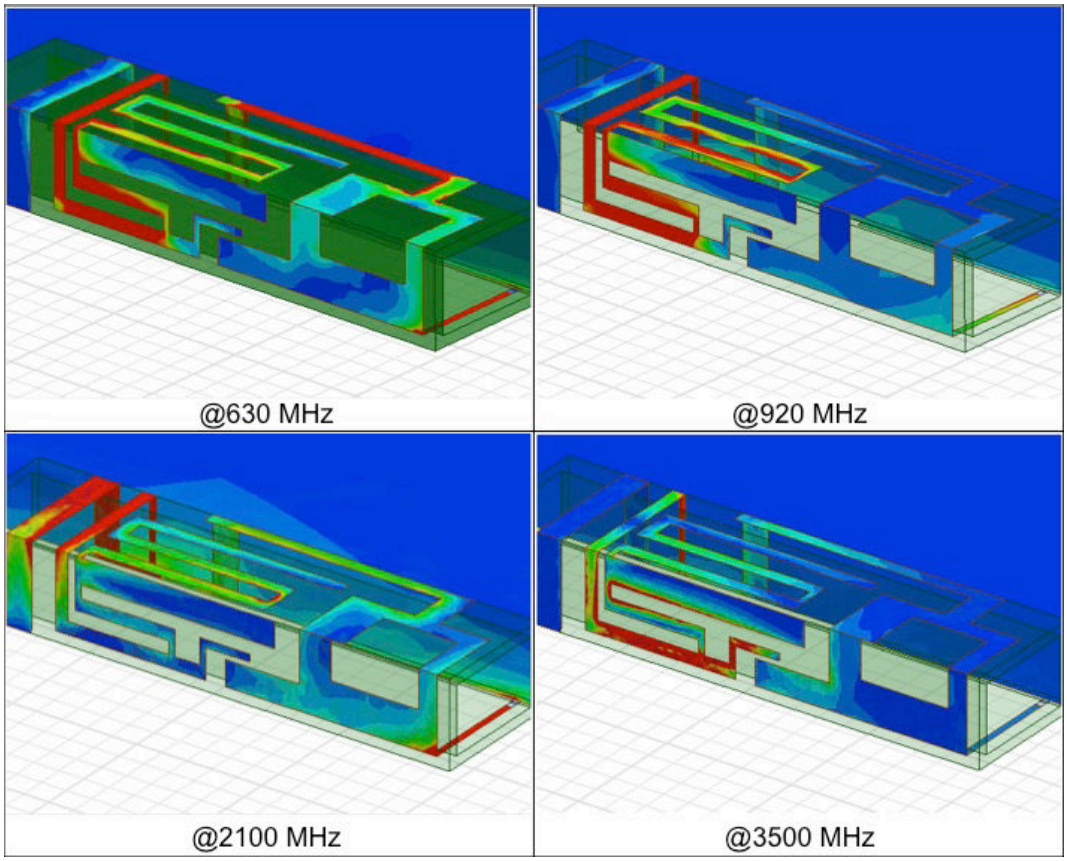

Figure 3.33: Simulated current distribution at different frequencies.

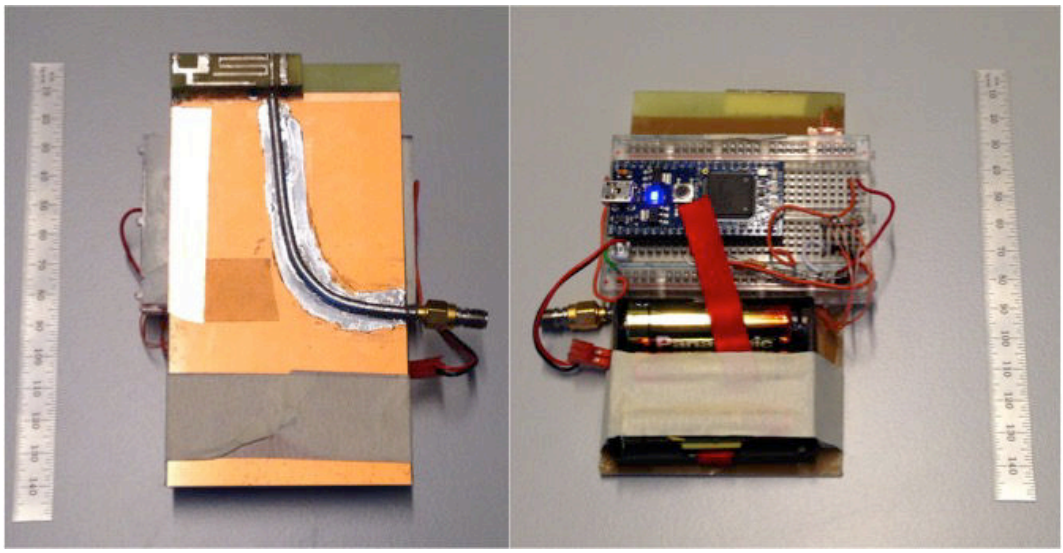

Figure 3.34: The fabricated prototype and the control unit.

DTC State	C_{DTC} (pF)	C_{Tot} (pF)	BW (MHz)	DTC State	C_{DTC} (pF)	C_{Tot} (pF)	BW (MHz)
0	**0.90**	**0.61**	**770-970**	16	3.35	1.21	660-678
1	1.29	0.77	755-795	17	3.49	1.23	657-675
2	1.42	0.81	742-785	18	3.63	1.25	654-671
3	1.56	0.86	732-777	19	3.80	1.27	652-668
4	1.70	0.90	719-769	20	3.94	1.28	649-665
5	1.83	0.93	711-763	21	4.08	1.30	647-662
6	1.96	0.96	703-757	22	4.26	1.31	645-660
7	2.10	1.00	698-753	23	4.39	1.33	643-658
8	**2.24**	**1.03**	**695-748**	24	4.54	1.34	640-655
9	2.37	1.05	686-736	25	4.68	1.35	638-653
10	2.59	1.10	681-721	26	4.85	1.37	636-651
11	2.65	1.11	677-707	27	4.99	1.38	635-649
12	2.78	1.13	673-700	28	5.13	1.39	633-647
13	2.92	1.15	669-691	29	5.27	1.40	632-645
14	3.05	1.17	666-686	30	5.46	1.41	630-643
15	3.19	1.19	663-682	31	**5.60**	**1.42**	**629-642**

Table 3.1: Measured antenna matching for different C_{Tot}

The measured VSWR values of the prototype in the different frequency bands are shown in Figures 3.35 and 3.36. The results in Figure 3.35 show a slight shift in the resonance frequencies with respect to the simulated data, which can be ascribed to fabrication imperfections. A better agreement between simulations and measured is obtained in the higher bands (Figure 3.36).

In the low frequency band, the proposed antenna can operate from 630 MHz to 960 MHz by changing the DTC value with VSWR lower than 3. In the middle frequency band, VSWR is slightly modified when DTC value is tuned, but it is always lower than 3 for capacitance values (C_{Tot}) higher than 1.03 pF. Consequently, the frequency bands from 1700 MHz to 2700 MHz and from 3500 MHz to 3800 MHz are also covered.

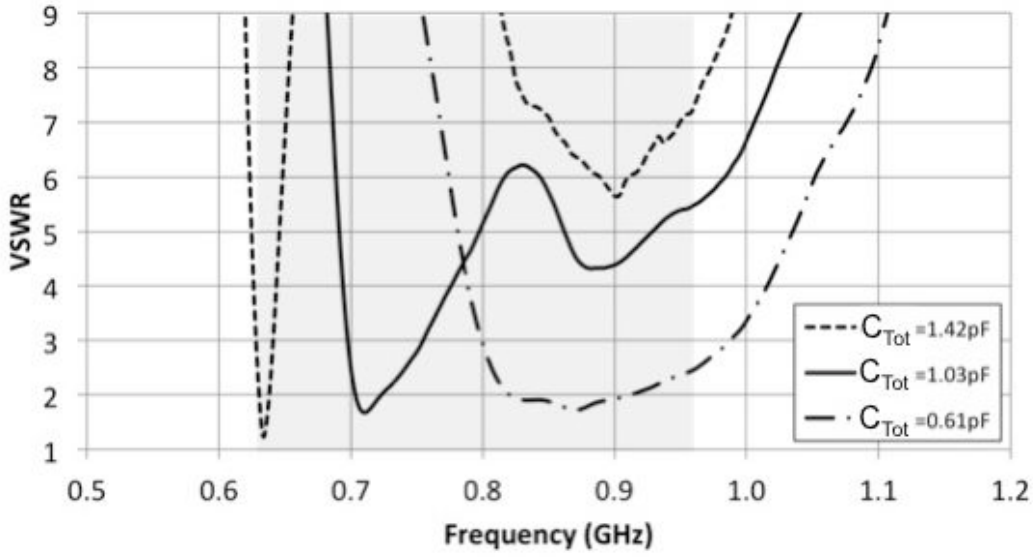

Figure 3.35: Measured antenna VSWR in the low frequency band

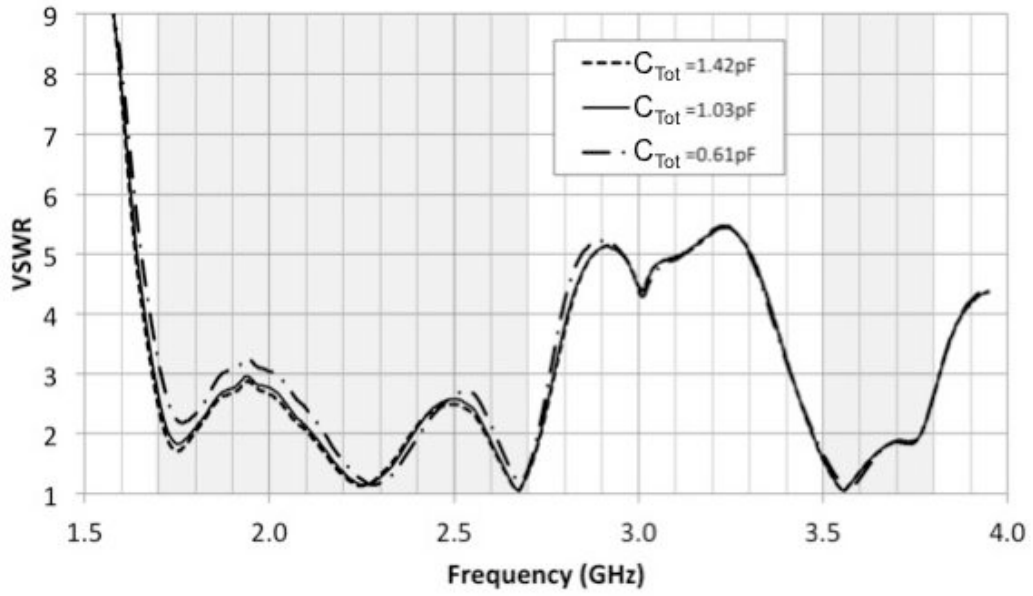

Figure 3.36: Measured antenna VSWR in the middle and high frequency bands

The total efficiency of the antenna has been measured by using a StarLab-Satimo chamber. Since the lower frequency limit of the Starlab-Satimo chamber is 700 MHz, the total efficiency of antenna has been measured only for frequencies above this value. Some slight differences between simulations and measurements are visible in the lower frequency band. However, the agreement is quite fair considering the 1 dB accuracy of the Starlab-Satimo station. The total efficiency level is sufficient for mobile handset applications. It varies from -4 dB at 730 MHz to -2 dB at 860 MHz, from -6 dB to -0.5 dB in the 1710-2700 MHz band and from -2.5 dB to -1.5 dB in the range 3500-3800MHz.

Finally, Figure 3.39 illustrates the simulated and measured radiation patterns of the proposed antenna at 920, 2100, and 3500 MHz, respectively. The measured results fairly

agree with the HFSS simulation. The radiation behavior at the different frequencies is quasi-omnidirectional, thus being suitable for mobile terminal scenarios.

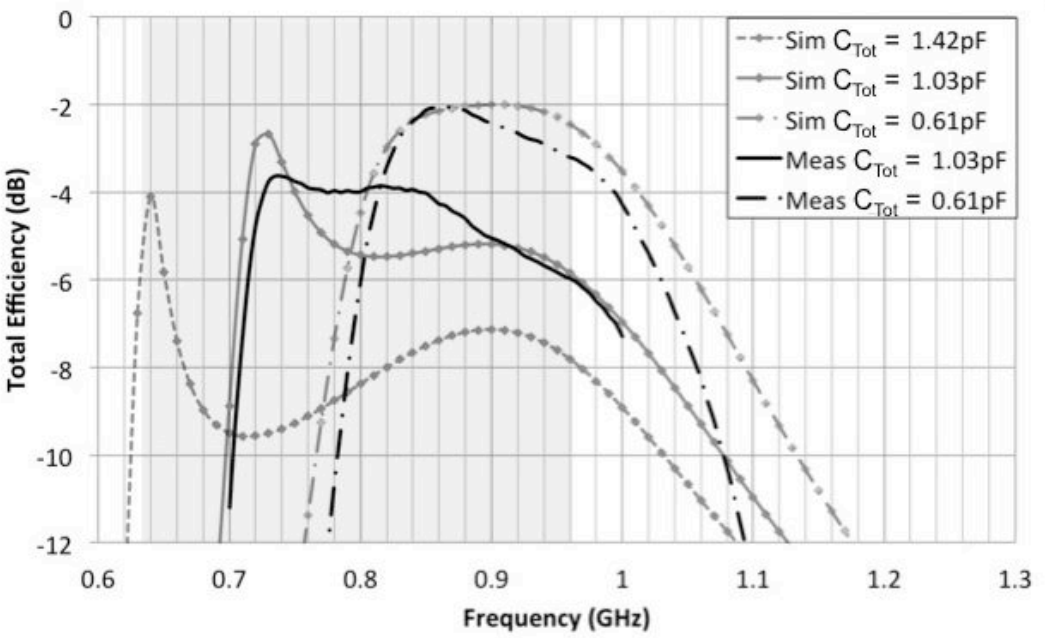

Figure 3.37: Measured and simulated antenna total efficiency in the low frequency band

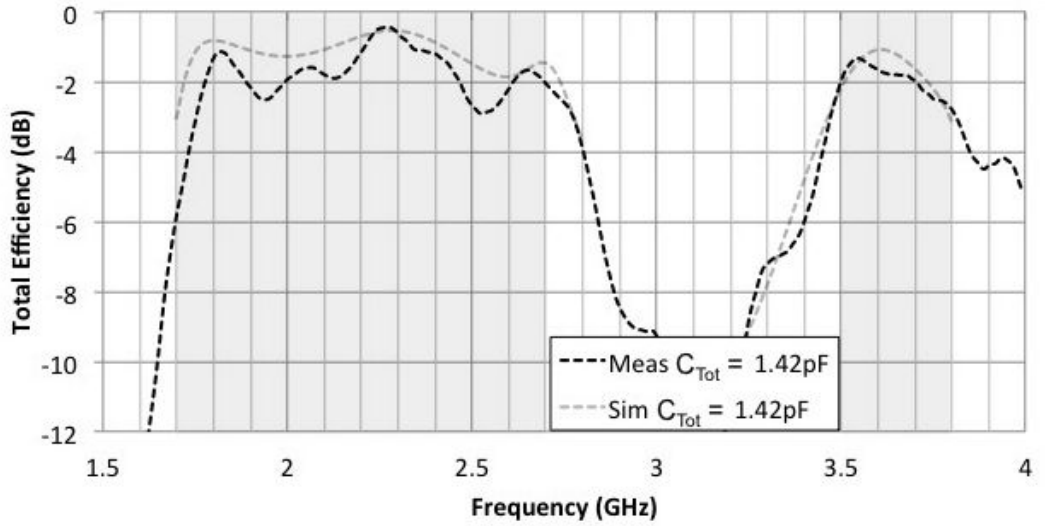

Figure 3.38: Measured and simulated antenna total efficiency in the middle and high frequency band

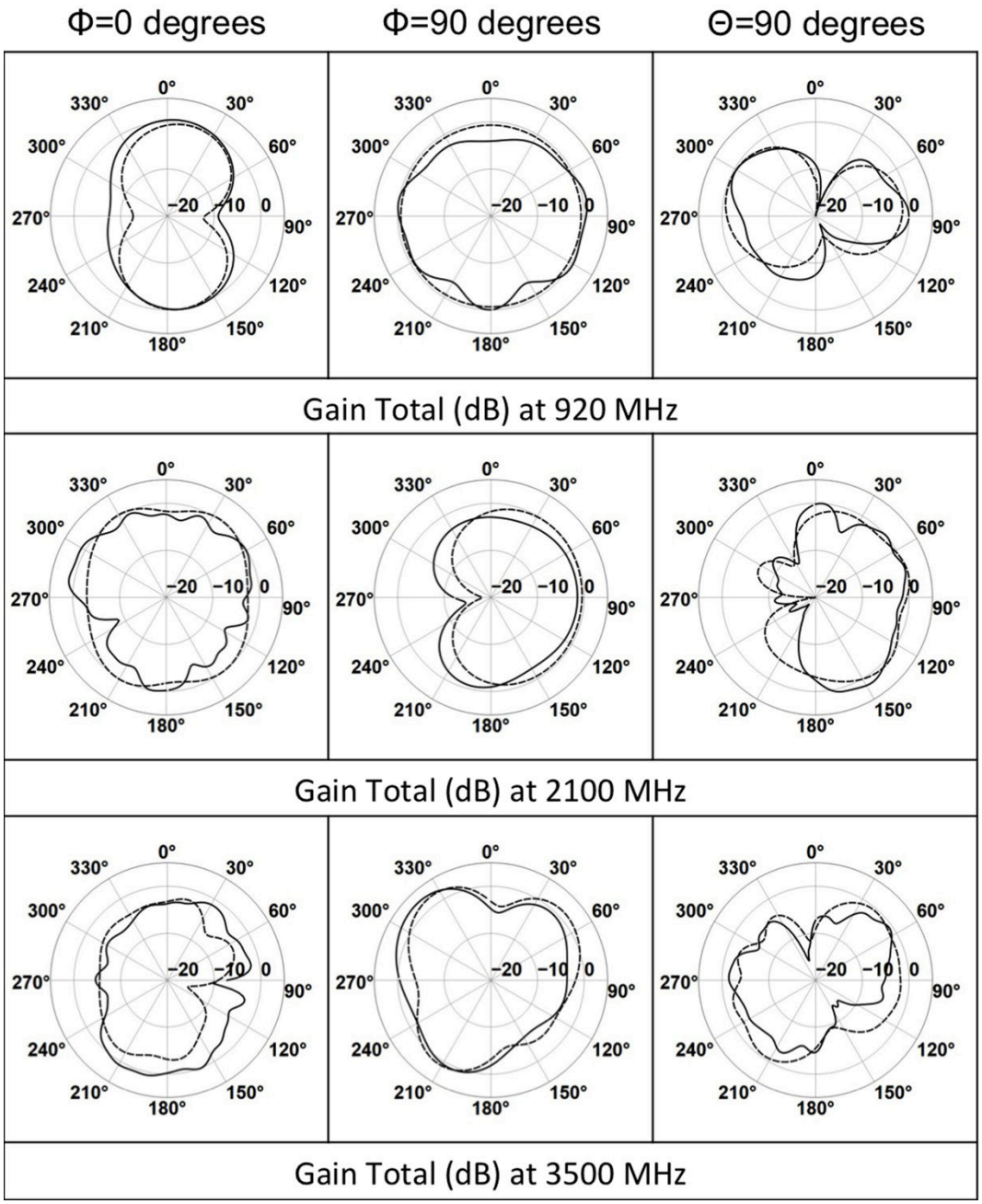

Figure 3.39: Simulated (dotted line) and measured (solid line) radiation pattern of the proposed antenna

4.3. Conclusion

A reconfigurable-multiband antenna is presented for fundamental communication standards and TV White Space. Our proposed structure can cover the main frequency bands with an acceptable efficiency. Thanks to the compact size, this antenna is a good candidate for mobile terminal, and especially MIMO system for which more than one antenna must be integrated in a very small volume.

REFERENCE OF THIS CHAPTER

[1] C. Rowell and E. Y. Lam, "Mobile-Phone Antenna Design" Antennas and Propagation Magazine, vol. 54, pp. 14–34, August 2012
[2] Marta Martinez Vazquez, "Design of antennas for mobile communications devices: practical aspects" IEEE AP-s Distinguished Lecture 2012.
[3] Yonghun Cheon, Jungyub Lee, and Joonghee Lee, "Quad-Band Monopole Antenna Including LTE 700 MHz with Magneto-Dieclectric Material", Antennas and Wireless Propagation Letters, vol. 11, 2012.
[4] C.-H. Ku, H.-W. Liu, and Y.-X. Ding, "Design of Planar Coupled-Fed Monopole Antenna for Eight-Band LTE/WWAN Mobile Handset Application", Progress In Electromagnetics Research C, vol. 33, 185- 198, 2012.
[5] S. Jeon, S. Oh, H.H. Kim and H. Kim, "Mobile handset antenna with double planar inverted-E (PIE) feed structure", Electronics Letters, vol. 48, no 11, May 2012
[6] S. Sesia, I. Toufik, and M. Baker, "LTE-The UMTS Long Term Evolution: From Theory to Practice", U.K.: Wiley, 2009.
[7] Federal Communications Commission, Mobile Spectrum Holdings Report and Order - FCC14-63, Washington, D.C. 20554, June 2014.
[8] R.F. Harrington, "Effect of Antenna Size on Gain, Bandwidth, and Efficiency", Journal of Research of the National Bureau of Standards-D. Radio Propagation, Vol. 64D, No. 1, January-February 1960.
[9] M.A.C Namien, A. Sharaiha, S.Collardey and K. Mahdjoubi, "An Electrically small frequency reconfigurable antenna for DVB-H", Antenna Technology (iWAT), 2012.
[10] F. Canneva, F. Ferrero, .J. Ribero, R. Staraj, "Reconfigurable miniature antenna for DVB-H standard", Antennas and Propagation Society International Symposium (APSURSI), 2010.
[11] B. Mun, C. Jung, M-J. Park, and B. Lee, "A Compact Frequency- Reconfigurable Multiband LTE MIMO Antenna for Laptop Applications", IEEE Antennas Wireless Propag. Lett., vol. 13, 2014.
[12] Peregrine Semiconductor Corp., "UltraCMOS Digitally Tunable Capacitor (DTC) 100-3000 MHz", Document No. 70-0335-06, 2012
[13]

CHAPTER IV
RADIATION PATTERN RECONFIGURABLE ANTENNA FOR WSN

1. STATE OF ARTS

Wireless sensor networks (WSNs) have received a great deal of attention over the past years. This type of systems can remarkably benefit from the integration of pattern-reconfigurable antennas into the sensor nodes. There are three main advantages given by the possibility of steering the beam pattern of the antenna towards specific directions: an increased range, reduced interferences and lower power consumption. Reducing the power consumption is crucial for WSNs, especially when considering nodes only powered by an energy harvesting system such as solar panels or thermal cells [1]. In this case, designers have to deal with a very limited power budget, typically in order of mW, for sending or receiving data packets.

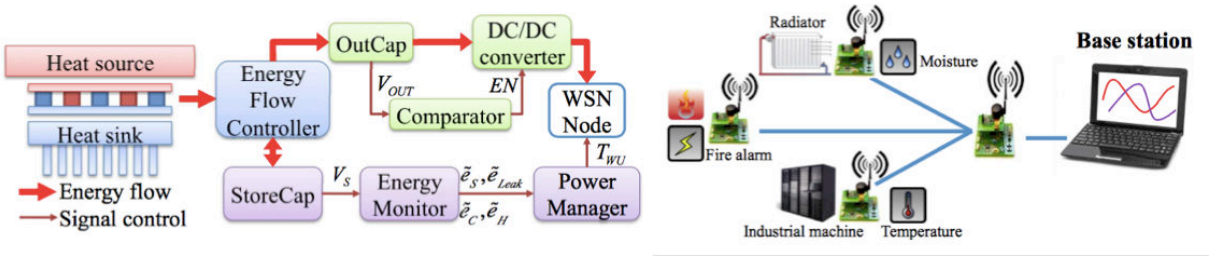

Figure 4.1: Generic architecture of the thermal-powered WSN node [1]

In this context, the possibility of concentrating the radiated energy towards a specific direction allows limiting the transmit power, thus the energy consumption. Moreover, as the antenna radiation pattern can be steered, interferences are reduced, therefore minimizing packet retransmissions. Finally, as the range of the nodes is increased (typically at least twice), error-prone and complex multi-hop transmissions can also be avoided. Despite such advantages, very few solutions specifically intended for integration in wireless sensor nodes have been proposed so far.

Historically, pattern reconfiguration can be obtained by using phased antenna arrays or reflectarrays. Unfortunately, their characteristics make them often unsuitable for applications with strong requirements in terms of cost, dimension, and power consumption. Another possibility is represented by switched antennas.

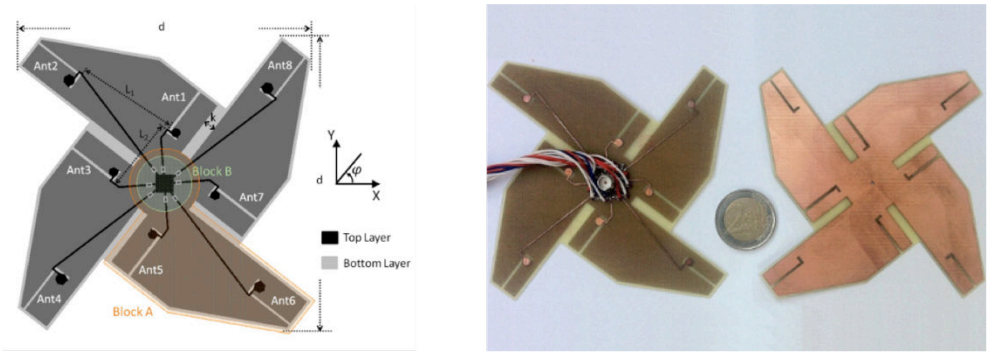

Figure 4.2: Geometry of compact switched-beam steering antenna [2]

In this case, the radiating system is based on the combination of multiple antennas and the reconfiguration mechanism simply consists in the selection of the appropriate elements [2]. However, the number of possible radiation configurations is fixed by the number of available antennas and it cannot be increased without also increasing the complexity and the dimensions of the system. Such a problem is overcome by parasitic elements antennas, in which the mutual coupling between a single active radiator radiation pattern. The reconfiguration is usually obtained through the control of electronic and a certain number of passive elements are properly exploited to generate the requested components that can modify the characteristics of the passive elements [3-4].

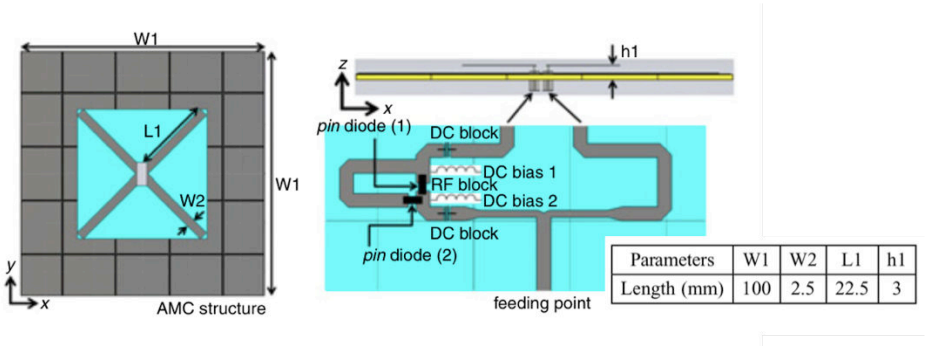

Figure 4.3: Geometry of reconfigurable antenna for wireless sensor network [4].

Another application of WSN is the field of Car-to-car communications. These communications are emerging as a potential solution for improving road safety [5]. Such systems are aimed at reducing the number of vehicle crashes thanks to the early identification of unsafe conditions and the consequent warning of the driver. Recently, several initiatives have been started for the promotion of such cooperative communication solutions in the framework of intelligent transport systems (ITSs). Several countries all over the world have allocated protected frequency bands around 5.9 GHz. In the US, the licensed band is 5.850-5.925 GHz, while in Europe, it is reduced to 5.875-5.925 GHz. However, the immediately below industrial, scientific and medical (ISM) band from 5.855 GHz to 5.875 GHz can be used to extend the available frequency rangefor unprotected services [6].

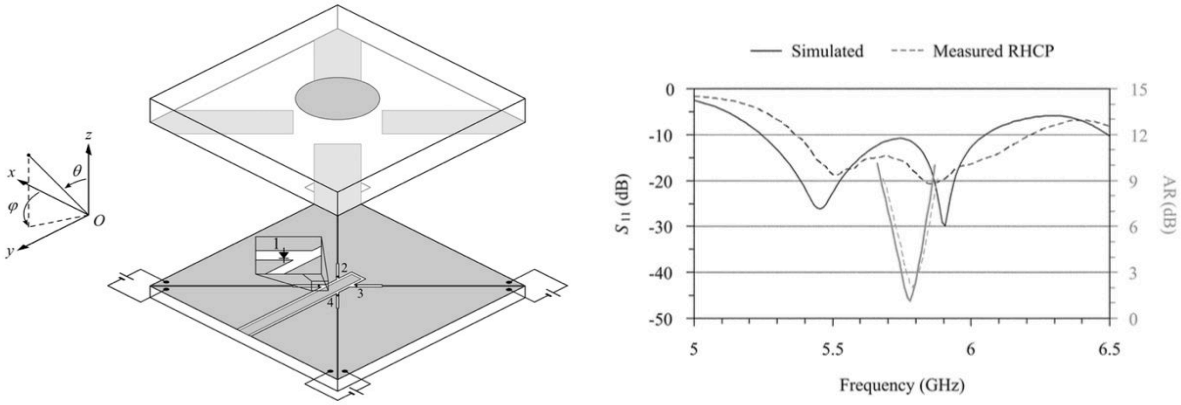

Figure 4.4: Circularly polarized reconfigurable structure and its results [7].

Over the last few years, several antennas operating in the 5.9 GHz frequency band have been proposed. Since the antennas have to be integrated into the vehicles, compactness and low-profile are fundamental requirements. Solutions based on microstrip patch antennas can be found in [7] and [8]. They certainly exhibit a low vertical extension, however, the directive pattern normal to the patch surface makes these solutions unsuitable for C2C communications, where the transmitting/receiving devices are located in almost the same elevation plane.

Consequently antennas radiating omnidirectional patterns in the azimuthal plane are preferred. In [9] and [10] solutions based on a multilayer structure and a shark fin geometry, respectively, have been reported. They both provide multi-standard operation at the cost of a more complicated structure.

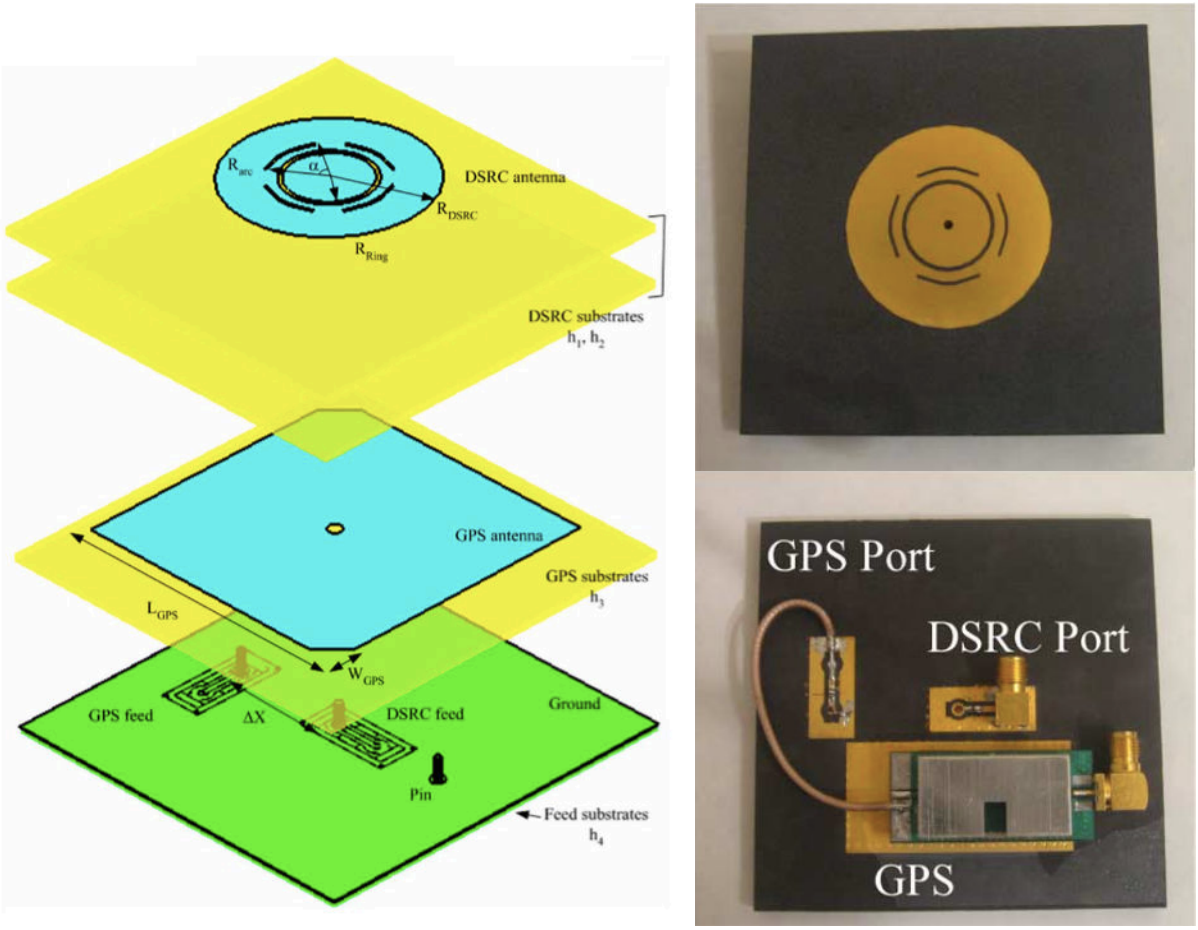

Figure 4.5: Geometry of the low-profile collocated integrated microstrip antenna for GPS and DSRC applications [9].

2. ON ROOF BEAM-STEERING ANTENNA FOR CAR-TO-CAR APPLICATIONS

2.1. The design approach for the synthesis of pattern reconfigurable antenna 1

In this section, an approach for the synthesis of pattern reconfigurable antennas based on the use of parasitic elements is presented. Differently from previously published works, all the elements constituting the antenna system can switch between the active and passive state, thus increasing the number of achievable radiation configurations. This is obtained by a) using element structures that are all identical, and b) applying a feeding network that can be easily reconfigured to change the role of each element.

By following a procedure based on the transmission line theory, the design of the feeding network is performed. It relies on the use of open circuit stubs to provide the correct phase shifts on the parasitic currents flowing on the passive elements in order to achieve a target radiation pattern. For the sake of clarity, the proposed approach is here presented for the representative test case of an antenna system composed by two elements, one active and one passive. However, it can be generalized to take into account any number of elements.

2.1.1. Synthesis approach

The starting point of the proposed synthesis approach is the a priori selection of the single element geometry, which is optimized in order to fulfill some application specific requirements. They usually include a good impedance matching at the working frequencies and suitable dimensions. In addition, as for classical array design problems, the elements must efficiently radiate in the plane where the target behavior is requested so that their patterns can be properly combined. The design procedure can be synthesized in 3 main phases.

A. Phase Shift Optimization:

Two identical elements A_1 and A_2 are arranged in a phased array configuration, so that the shape of the total radiation pattern $\mathbf{E}(\varphi_1, \varphi_2)$ can be modified by varying the phases φ_1 and φ_2 of the feeding signals. An optimization process is performed with the aim of finding the best phase values $\hat{\varphi}_1$ and $\hat{\varphi}_2$ allowing the fitting of the target radiation behavior $\mathbf{E}^T$, i.e.,

$$\varphi_1 = \hat{\varphi}_1, \varphi_2 = \hat{\varphi}_2 \text{ and } \| \mathbf{E}(\hat{\varphi}_1, \hat{\varphi}_2) - \mathbf{E}^T \| < \varepsilon \quad (1)$$

ε being a user-defined threshold. Since, in general, ϕ_1 can be arbitrarily fixed, (1) can be rewritten as

$$\varphi_\Delta = \hat{\varphi}_\Delta \text{ and } \| \mathbf{E}(\hat{\varphi}_\Delta) - \mathbf{E}^T \| < \varepsilon \quad (2)$$

where φ_Δ is the phase shift between the elements, i.e., $\varphi_\Delta = \varphi_2 - \varphi_1$.

B. Stub Design:

Once that the optimal phase shift $\hat{\varphi}_{\Delta}$ has been found, the antenna system is modified to be constituted by a single active element (A1), which is fed by the phased signal, and a parasitic element (A2). Towards this end, A2 is connected to an open circuit stub, whose role is to vary the phase of the current flowing on the element without the need of a dedicated input port. In order to still obtain the optimized $\mathbf{E}(\varphi_1, \varphi_2)$ pattern, the length of the stub is appropriately selected so that

$$\varphi_{st} = \hat{\varphi}_{\Delta} - \varphi_{12} \tag{3}$$

In (3), and are the phase shifts given by the stub and by the distance between the elements, respectively.

C. Reconfigurable Antenna Design:

The final phase consists in arranging the elements and the stub so that the overall antenna system structure could easily enable the pattern reconfiguration. Towards this end, the antenna elements are connected to two copies of the stub designed in the previous phase. However, the stubs open ends are replaced by two diodes that are both connected to the system input port. The reconfiguration mechanism relies on the control of the diodes state. If the diode is ON, then the corresponding element is simply connected to the input port through a transmission line, while if it is OFF; the element is connected to the open circuit stub.

2.1.2. Numerical validation

In order to validate the proposed synthesis approach, it is applied to the design of a low-profile reconfigurable antenna system suitable to be mounted on a large ground plane, such as the vehicle roof in car-to-car applications. The selected element geometry consists of a simple patch fed on the edge by a coaxial probe and grounded through a via. This via allows the antenna to be low profile while enabling the radiation in the azimuth plane.

Figure 4.6 shows the evolution of the antenna structure during the 3 phases of the design process. The design was aimed at obtaining a target radiation pattern $\mathbf{E}^T$ characterized by a minimum 7.5 dB directivity in the azimuth plane.

During phase A, an array of two elements is modeled. The array is simulated using Ansoft HFSS electromagnetic simulator. The phase shift optimized to fulfill the project requirements turns out to be $\hat{\varphi}_{\Delta} = 295°$ ($\hat{\varphi}_1 = 0°$, $\hat{\varphi}_2 = 295°$) and the corresponding φ–plane radiation pattern is shown in Fig. 2 in red. Moreover, by analyzing the simulated transmission coefficient between the two array input ports (S21), φ_{12} is found to be equal to approximately 19°.

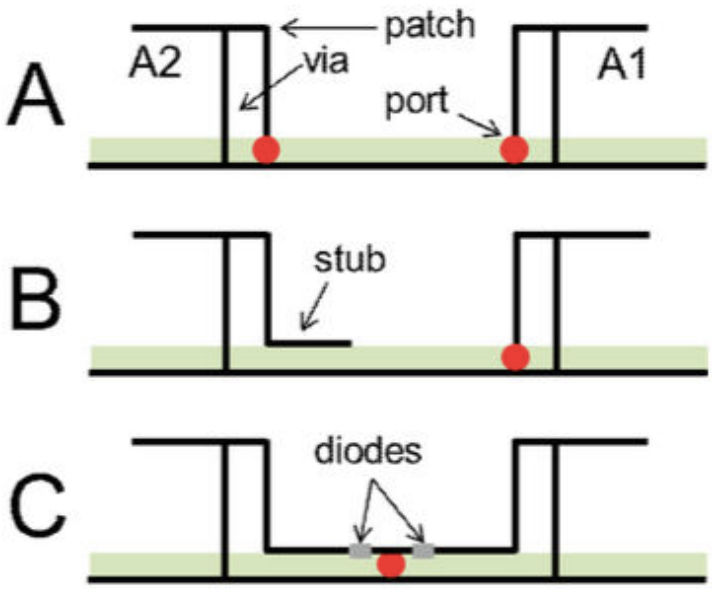

Figure 4.6: The antenna system geometry evolving during the 3 design phases. The view is from the side.

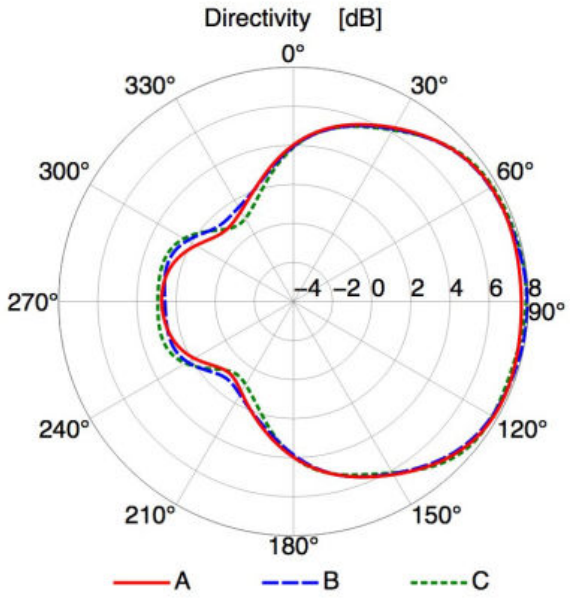

Figure 4.7: Antenna radiation pattern obtained in the three design procedure phases.

By applying simple transmission line theory, the length l_{st} of an open circuit stub printed on a Roger substrate (ε_r = 2.2, tanδ = 0.0009, in green in Figure 4.6) and providing a phase shift $\varphi_{st} = \widehat{\varphi}_{\Delta} - \varphi_{12}$ = 276° = –84° is calculated to be l_{st} = 4 mm. The stub is substituted to the input port of the element A2, as shown in Figure 4.6 – phase B. The simulated directivity pattern of this new antenna configuration is shown in Figure 4.7 in blue. As it can be noticed, the pattern almost perfectly matches the radiation behavior obtained in the array configuration, confirming the correctness of the stub design.

Finally, in order to make the pattern reconfiguration possible, the antenna structure is modified in phase C. More specifically, two stubs are substituted to the input ports of both the radiating elements and connected to the feed by two diodes. The element connected to the diode in the ON state works as the active element, while the one connected to the OFF state diode results to be connected to the stub, thus having the role of the parasitic element. The associated radiation pattern is shown in Figure 4.7 in green. By inverting the states of the two diodes, the antenna can be reconfigured to exhibit a symmetric pattern headed in the opposite direction.

2.2. Antenna design

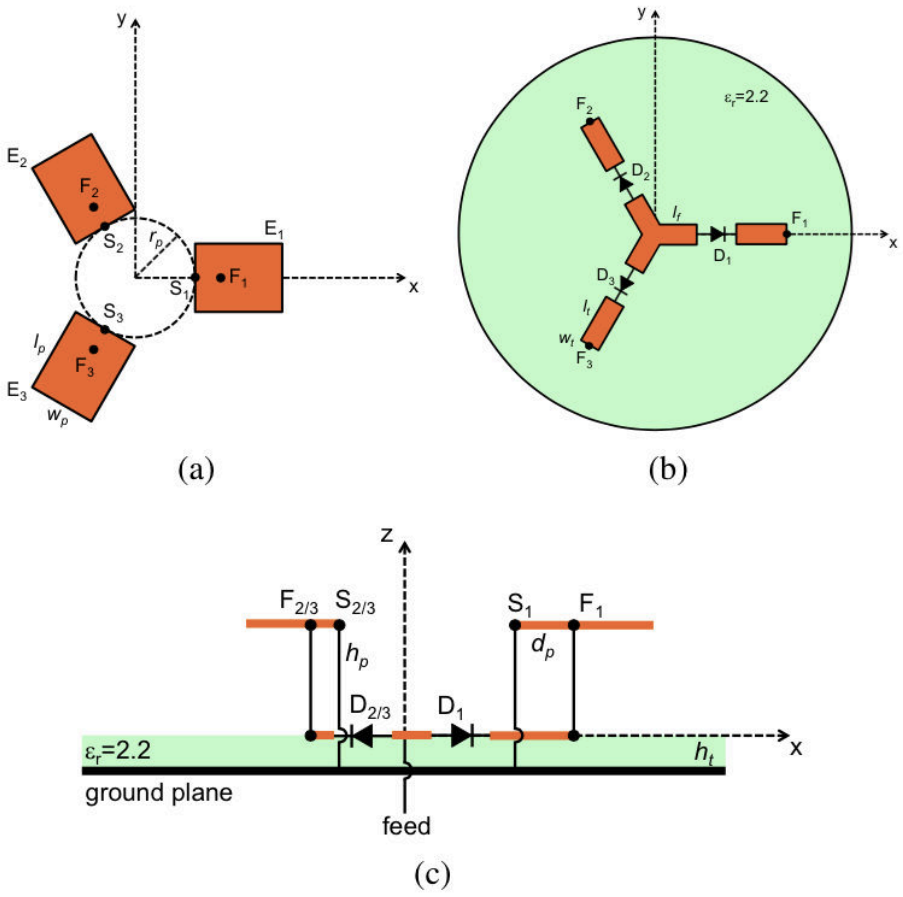

Figure 4.8: Antenna structure. (a) Top view, (b) bottom view and (c) side view.

Based on the design approach as mentioned in the previous section, we proposed an antenna suitable for C2C applications, whose radiation pattern can be electronically and rapidly reconfigured in the azimuthal plane. The use of a pattern reconfigurable antenna provides several advantages. First, because of the effects of the vehicles' fast mobility and the influence of complex urban environment, C2C communications are characterized by a deep multipath, which can substantially decrease the quality of the transmission. Such an effect can be mitigated, and thus the communication quality restored, by adaptively directing the signals towards specific directions. Secondly, the antenna scanning mechanism can be exploited to

collect information on the position of the communicating devices. These additional data can further improve the C2C system danger prevention ability. Finally, the possibility of switching between an omnidirectional and a directive pattern enables particular services like the locking and tracking of specific vehicles.

The proposed antenna is based on the combination of multiple elements, which can act as active radiators or passive reflectors. The control of each element role results in the control of the total antenna radiation behavior. The pattern reconfiguration capability is obtained while maintaining an antenna structure that is low-profile, easy to realize, and specifically intended for roof-top mounting.

The structure of the proposed antenna is shown in Figure 4.8. It is based on 3 main radiating elements E_1, E_2 and E_3 uniformly distributed along the perimeter of a circle of radius r_p = 14 mm. They are located at a distance h_p = 5 mm from a Duroid dielectric substrate (ε_r = 2.2, tandδ = 0.0009) of thickness h_t = 0.508 mm, which is used to support the feeding network. On the backside of the substrate, a large ground plane simulating the car roof is placed. This latter is modeled as a circular plate of radius 500 mm, corresponding to approximately 10λ at 5.9 GHz.

Each radiating element is constituted by a metallic patch of dimensions w_p= l_p= 5.1 mm, which is fed by a via vertically crossing the structure at a distance d_p= 1.5 from the edge of the patch ($F_{1/2/3}$). Each via is connected to a 50 Ω microstrip line (w_t= 1.5 mm), which is linked to the input port by means of a diode acting as a switch. When the switch is ON, the input signal is injected into the microstrip line and led to the corresponding radiating element. When it is OFF, the line is separated from the feed and the antenna becomes a parasitic element. Finally, another via, located at the point $S_{1/2/3}$ is used as short-circuit between the patch and the ground plane.

The pattern reconfiguration mechanism relies on the control of the three diodes D1, D2 and D3. When a diode is in the OFF state, the corresponding radiating element becomes a parasitic element in which the microstrip line roughly acts as a open circuited stub providing a reactive loading. Depending on the length of the microstrip line (l_t) and the location of the diode (l_f), the additional reactive impedance generated by the stub can be either capacitive or inductive. This results in the variation of the distribution of the coupling currents flowing on the passive element. Such variation can be profitably exploited to make the parasitic element providing a reflective or directive effect, similarly to what happens in a Yagi-Uda antenna. In the proposed antenna, the lengths of the 3 lines as well as the distances of the diodes from the input port have been optimized in order to maximize the reflection effect and consequently the front-to- back ratio of the resulting antenna total radiation pattern. The optimal values for l_t and l_f have been found to be 12.85 and 2.5 mm, respectively. The same effects could have been obtained by means of inductors and capacitances integrated on the antenna geometry. However, compared to the proposed solution, the use of additional passive components would have certainly increased the losses and reduced the system efficiency.

Depending on the combination of the diodes' states, the 3 elements antenna here presented can provide up to 7 different radiation pattern configurations. Among them, the 6 directive ones are characterized by different directions of maximum gain in the horizontal plane (D_{max}), resulting in a 60° angular resolution (Table 4.1). However, by reducing the angular separation among the patches, more radiating elements can be employed, and consequently more pattern configurations can be obtained.

As for the other antenna geometrical parameters, such as the patch dimensions, the distance from the ground plane, and the via positions, they have been optimized through a parametric study aimed at obtaining good impedance match all over the 5.850 – 5.925 GHz frequency band for all the radiating configurations, while keeping a compact profile, which does not deteriorate the car aspect and aerodynamics. The final antenna structure occupies a small volume of 38.2 × 38.2 × 5.5 mm^3.

2.3. Results and discussion

In order to assess the antenna performance, a prototype has been built and measured. The employed diodes are MACOM MA4AGSBP907 components, which have very low insertions losses (better than – 0.5 dB) and high isolation (– 28 dB) at the operating frequencies. The correct paths for the DC and RF signals are ensured through a simple bias tee network. The maximum consumption, i.e., when all the 3 diodes are activated to obtain the omnidirectional configuration, is about 3 × 10 = 30 mW, which is negligible in dealing with C2C applications.

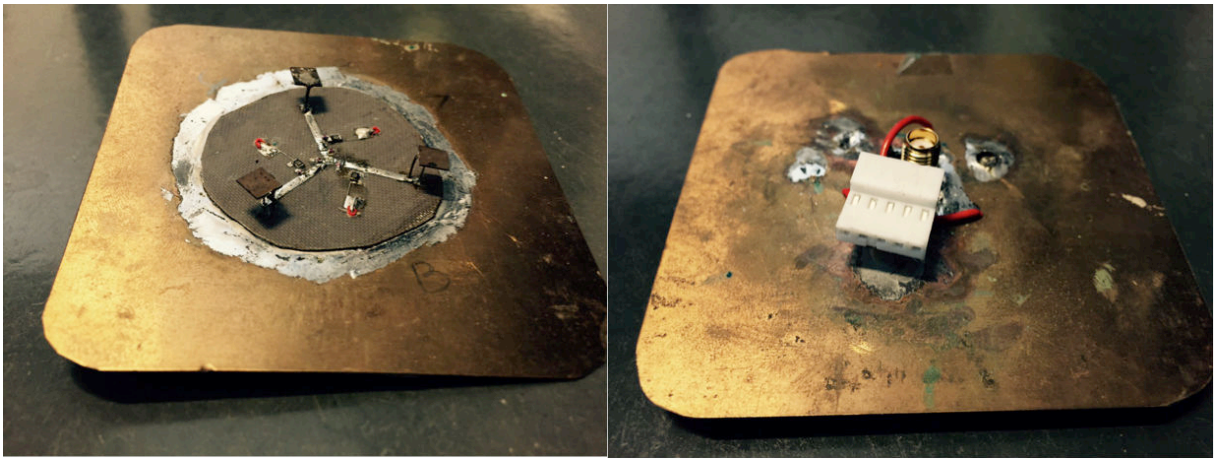

(a) (b)

Figure 4.9: The fabricated antenna prototype: (a) top view; (b) bottom view.

All the possible antenna configurations listed in Table 4.1 have been measured. Because of the symmetry of the geometry, the measurements for the cases C_{11}, C_{12}, C_{13} as well as C_{21}, C_{22}, C_{23} are very similar to each other and differ just for direction of maximum radiation. Consequently, for clarity of the figures, only the results concerning the configurations C_{11}, C_{21}, and C_{33}, representative for the cases where 1, 2 and 3 diodes are ON, are reported.

Configuration	D_1	D_2	D_3	D_{max} (φ)
C_{11}	ON	OFF	OFF	0°
C_{12}	OFF	ON	OFF	120°
C_{13}	OFF	OFF	ON	240°
C_{21}	ON	ON	OFF	60°
C_{22}	OFF	ON	ON	180°
C_{23}	ON	OFF	ON	300°
C_{33}	ON	ON	ON	Omnidirectional

Table 4.1: Radiation pattern configurations.

The measured antenna impedance matching is shown in Figure 4.10. As it can be noticed, the antenna best matching is obtained for the case when only one diode is ON. The $|S_{11}|$ for C_{11} exhibits a minimum around −18 dB at the center of the 5.9 GHz C2C licensed band (highlighted in gray). The impedance matching is slightly worse for C_{21} and C_{31}. This is due to the fact that, when multiple diodes are activated, multiple 50Ω lines are connected to the 50Ω feeding port, resulting in an impedance mismatch. The effects of such a mismatch are visible also through the analysis of the measured total antenna efficiency in the operating band. It is equal to 80% when only one diode is activated and decreases to 62% and 49% for configurations C_{21} and C_{31}, respectively. However, both the $|S_{11}|$ and the efficiency values are still acceptable for C2C applications.

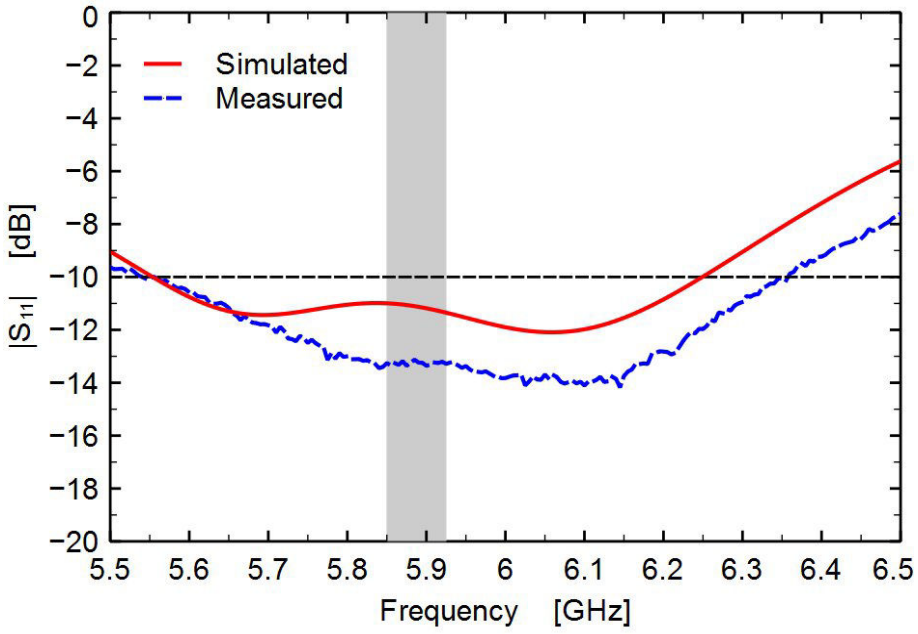

(a)

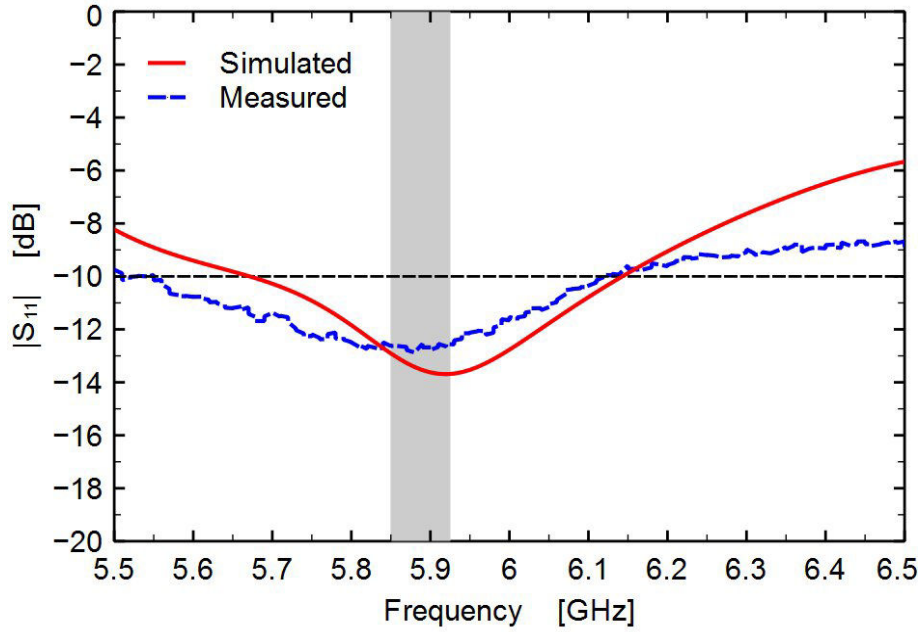

(b)

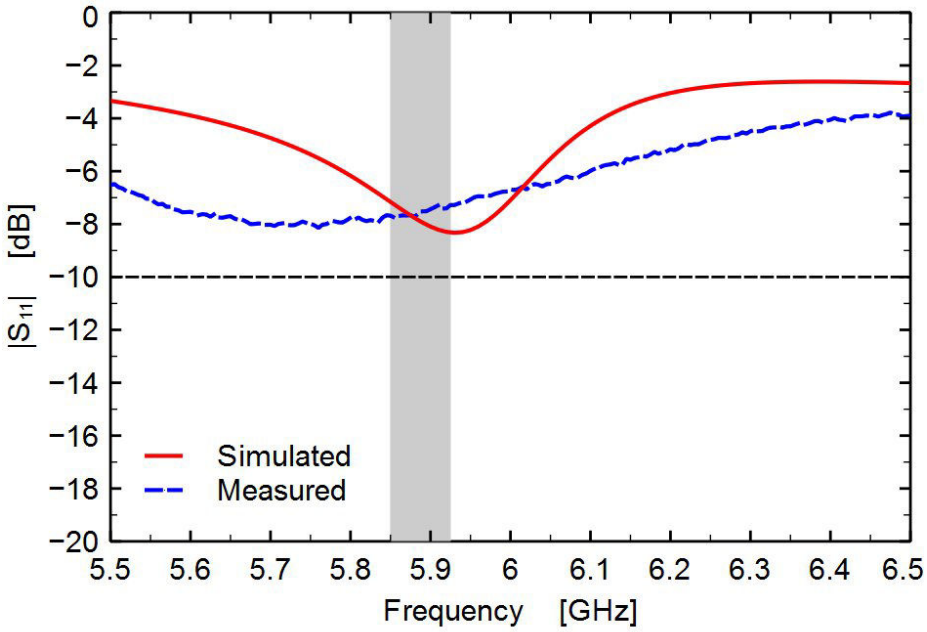

(c)

Figure 4.10: Simulated and measured return loss by the antenna in the different configurations, (a) configuration C11, (b).

Figures 4.11 (a) and 4.11 (b) show the measured realized gain patterns in the elevation and the azimuth planes, respectively. In Figure 4.11 (a) the three cuts at $\varphi = 0°$ (C_{11} and C_{31}) and $\varphi = 60°$ (C_{21}) are reported. Because of the presence of a finite ground plane, the antenna radiation pattern is slightly tilted in the elevation plane with maximum gain at $\theta = 68°$. This θ value is considered in Figure 4.11 (b). However, the pattern lowers down towards the azimuth plane when the antenna is mounted on a larger ground plane, as the car roof.

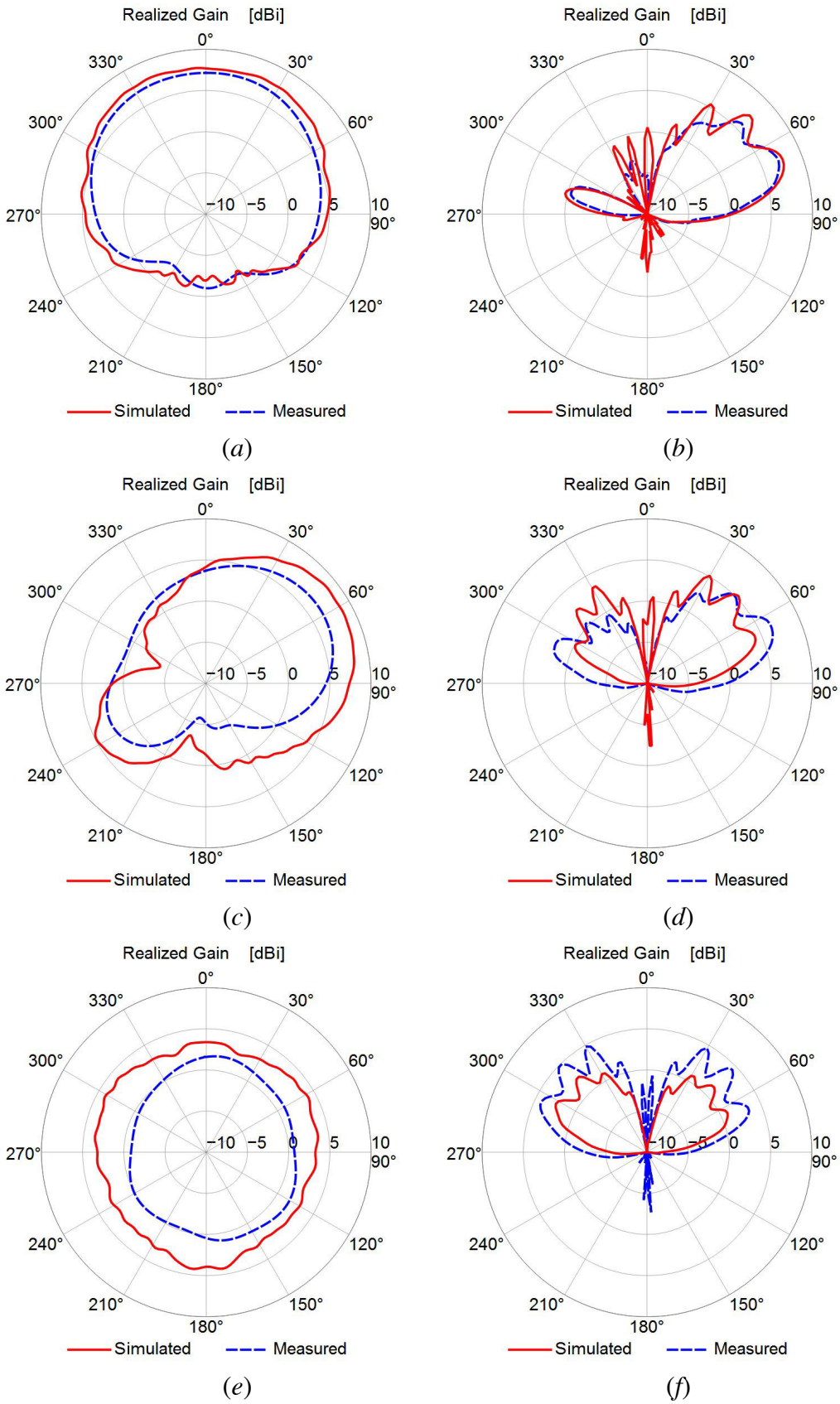

Figure 4.11: Comparison between simulated and measured realized gain pattern of C2C antenna system. (a) Conf. C_{11} at θ = 68°, (b) conf. C_{11} at φ =0°, (c) conf. C_{21} at θ =68°, (d) conf. C_{21} at φ =0°, (e) conf. C_{31} at θ = 68°, and (f) conf. C_{31} at φ =0°.

When 2 out of 3 patches are used as parasitic elements (C_{11}), the antenna radiation pattern is clearly directive with maximum towards the direction of the active diode and minima in the directions of the reflectors. The antenna maximum gain is about 7 dBi with a F/B of more than 8 dB. Moreover, the 160° HPBW allows the antenna to cover the entire azimuthal plane with a minimum gain of 5 dBi by sequentially switching among the C_{11}, C_{12} and C_{13} configurations. When two diodes are simultaneously activated, the antenna radiation pattern is still directive with a maximum gain of about 6.5 dBi, however the F/B is worse because of the increment of the backward radiation level. Finally, an omnidirectional radiation behavior can be obtained by activating all the switches. As shown in Figure 4.11 (b), the gain is quite stable around 0.5 dBi all over the φ values.

	D_{max} (φ)	$Gain_{max}$ [dBi]	F/B [dB]	HPBW (Δ φ)
C_{11}	0°	7.14	8.16	160°
C_{21}	60°	6.52	4.55	100°
C_{31}	––	1.75	––	––

Table 4.2: Radiation measured results.

The main results in terms of maximum direction (D_{max}), maximum gain (G_{max}), front-to-back ratio (F/B) and 3 dB beamwidth (HPBW) are summarized in Table 4.2.

2.4. Conclusion

In this section, a pattern reconfigurable antenna for C2C applications has been presented. The antenna is able to steer the beam towards 6 different directions in the azimuthal plane as well as to exhibit an omnidirectional radiation pattern. The effectiveness of the proposed solution has been validated by measurements performed on a prototype integrating also the reconfiguration control circuit. Future works will be aimed at increasing the number of pattern configurations and still improving the antenna front-to-back ratio.

3. MINIATURE PATTERN-RECONFIGURABLE ANTENNA FOR SMART WIRELESS SENSOR NODES

3.1. The design approach for the synthesis of pattern reconfigurable antenna 2

3.1.1. Synthesis approach

Differently from previously work, in this section, another approach for the synthesis of miniature pattern-reconfigurable antennas suitable for integration into wireless sensor nodes is proposed. The antenna structure is based on the Yagi-Uda concept [3], [4]. A driven element is surrounded by a set of identical parasitic elements, which can act either as reflectors or directors. The beam steering mechanism relies on the use of very low power consuming variable loads located on the parasitic elements. According to the values selected for the loads, the electrical length of each parasitic structure can be increased or decreased, thus realizing a reflector or director, respectively [5]. The antenna radiation pattern can therefore

be steered by selecting the proper configuration of reflectors and directors. The number of possible steering configurations depends on the number of adopted parasitic elements. As a preliminary proof-of- concept, we focus on a simple antenna system constituted by a driven radiator and two parasitic elements located on the opposite sides of the fed one. However the same results will hold for more complex configurations constituted by a larger number or elements uniformly distributed around the driven radiator.

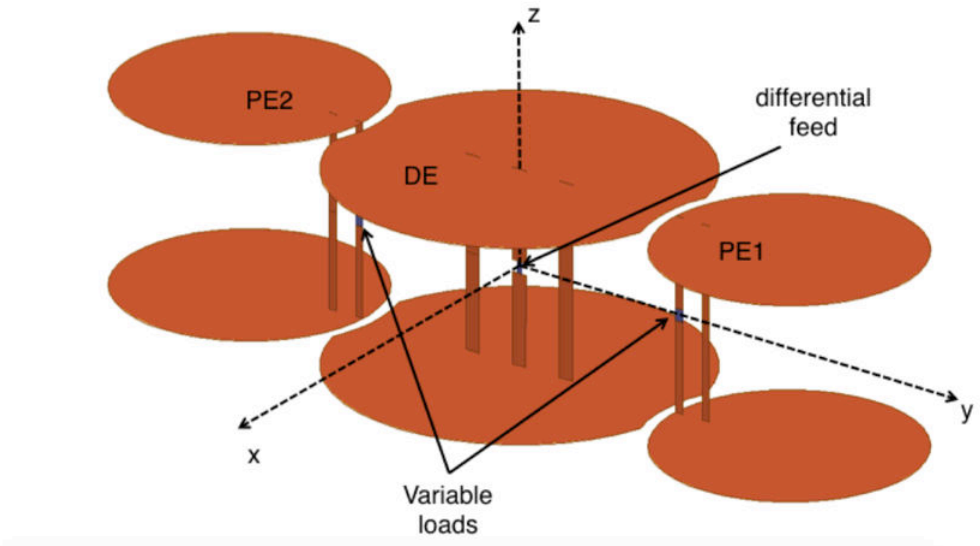

Figure 4.12: Geometry of the proposed antenna.

The geometry of the proposed pattern-reconfigurable antenna is shown in Figure 4.12. In order to enable a differential feed, the geometry is symmetrical with respect to the z-axis. This gives two main advantages: (a) the overall antenna size is reduced since no extended ground plane is needed, and (b) the antenna can be directly matched to the transceiver, which usually has a differential RF output, without the need of a balun and an impedance matching stage that will increase the system losses.

The driven element (DE) is a differential wire-patch antenna, which guarantees an omnidirectional radiation behavior in the azimuthal plane, while keeping a low profile [6]. It is constituted by two circular plates of radius 12 mm separated by a vertical distance of 12.8 mm. The two plates are fed by means of two vertical 1 mm wide metallic strips starting at the center of the plates. Two other strips, symmetrically located along the y-axis at 3.5 mm from the origin, directly connect the two plates. The structure of the parasitic elements PE1 and PE2 is very similar to that of the driven one. The circular plates are slightly smaller (8.5 mm radius) but still separated by the same vertical distance, thus facilitating the realization process. Each parasitic element possesses two vertical strips, one connected to the variable load, and the other one used as short circuit between the plates. The center-to-center distance between the driven and the parasitic elements is 20.25 mm. The plates of DE1 are slightly cut in order to have a minimum 0.8 mm separation from PE1 and PE2.

The optimal values of all the antenna geometrical parameters have been obtained through a parametric study aimed at achieving a good impedance match ($|S_{11}| \leq -10$ dB) in the

Wi-Fi band (2.4–2.485 GHz) as well as a directive pattern along the y-direction. The optimized antenna have an overall size of 57.5 × 24 × 12.8 mm^3, corresponding to 0.47λ × 0.2λ × 0.1λ at the operating band central frequency (2.45 GHz).

3.1.2. Numerical results

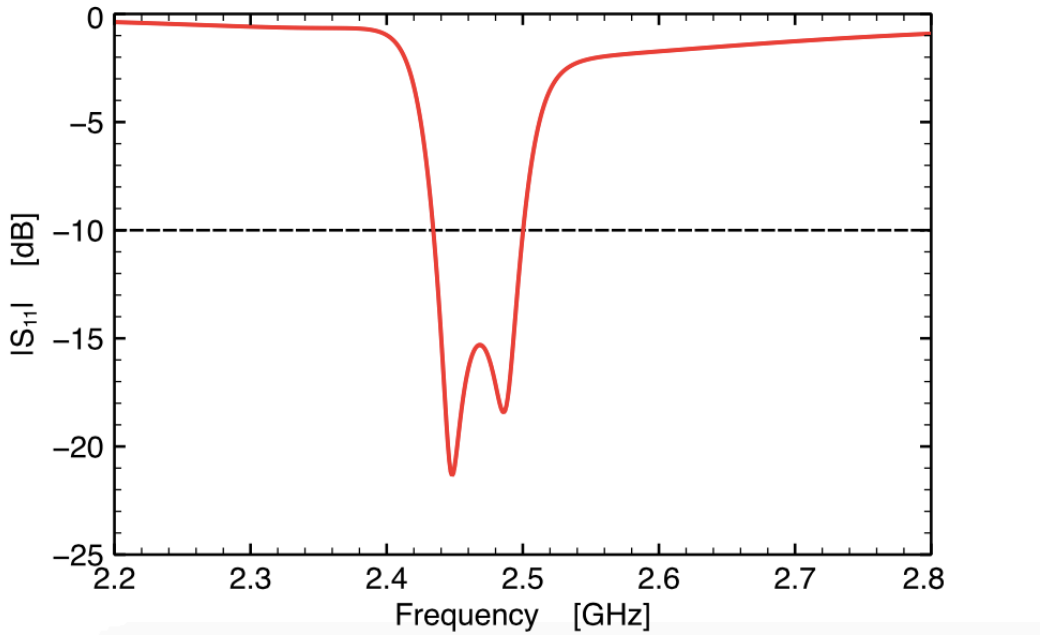

Figure 4.13: Antenna simulated S_{11} parameter.

The variable loads used for the specific antenna design here reported are simple capacitors. Depending on the values of the two capacitors, the antenna can switch between two possible states. In the first state (State 1), the capacitor C_1 located on PE1 is set to 1.3 pF, while the one on PE2 (C_2) is set to 4 pF. This configuration makes PE1 and PE2 acting as a director and reflector, respectively, forcing the main beam of the antenna towards the positive y-direction. Analogously, when the capacitors' values are inverted, the antenna radiation pattern will be directed along the negative y axis (State 2).

The antenna impedance match is reported in Figure 4.13. Since the antenna is perfectly symmetric, only the results related to the State 1 are shown. The combination of two closely spaced resonances provides a 2.7% bandwidth centered at 2.47 GHz for which the $|S_{11}|$ values are lower than −10 dB.

Concerning the radiation behavior, the simulated total realized gain at 2.45 GHz is shown in Figure 4.14. The antenna shows a directive pattern with 7.56 dBi maximum value at ($\theta = 90°$, $\varphi = 90^o$). The front-to-back ratio is approximately 11.26 dB. As expected, the antenna behaves like a Yagi-Uda antenna, where PE1 is the director element and PE2 is the reflector one. This is further demonstrated by the electrical field distribution generated by the antenna at 2.45 GHz, whose vertical cut at x = 0 is shown in Figure 4.15. As it can be noticed, the electrical field clearly radiates towards the direction identified by the director, while it is stopped by the reflector in the negative y-direction.

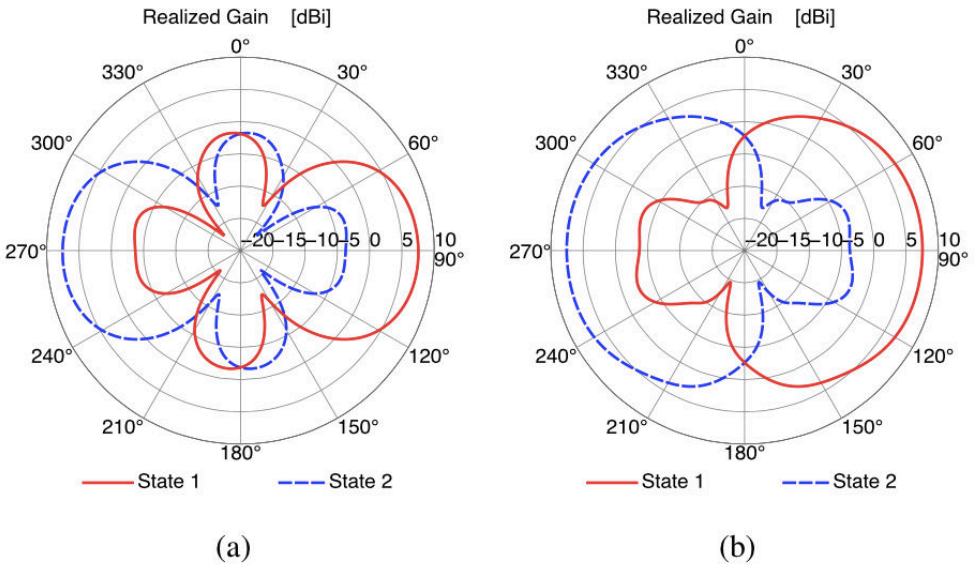

Figure 4.14: Antenna total realized gain at 2.45 GHz. Planes at (a) φ= 90° and (b) θ= 90°.

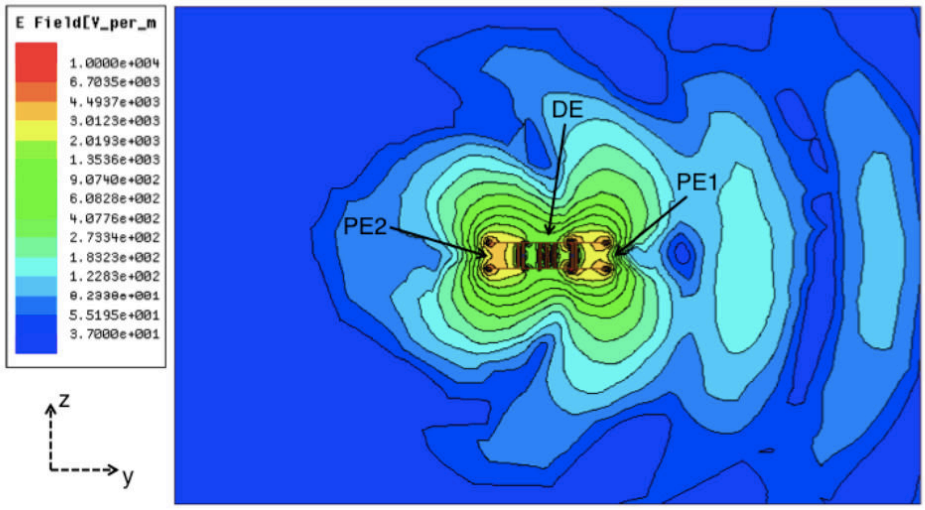

Figure 4.15: Antenna electric field distribution in the z-y plane at 2.45 GHz.

3.2. Antenna design

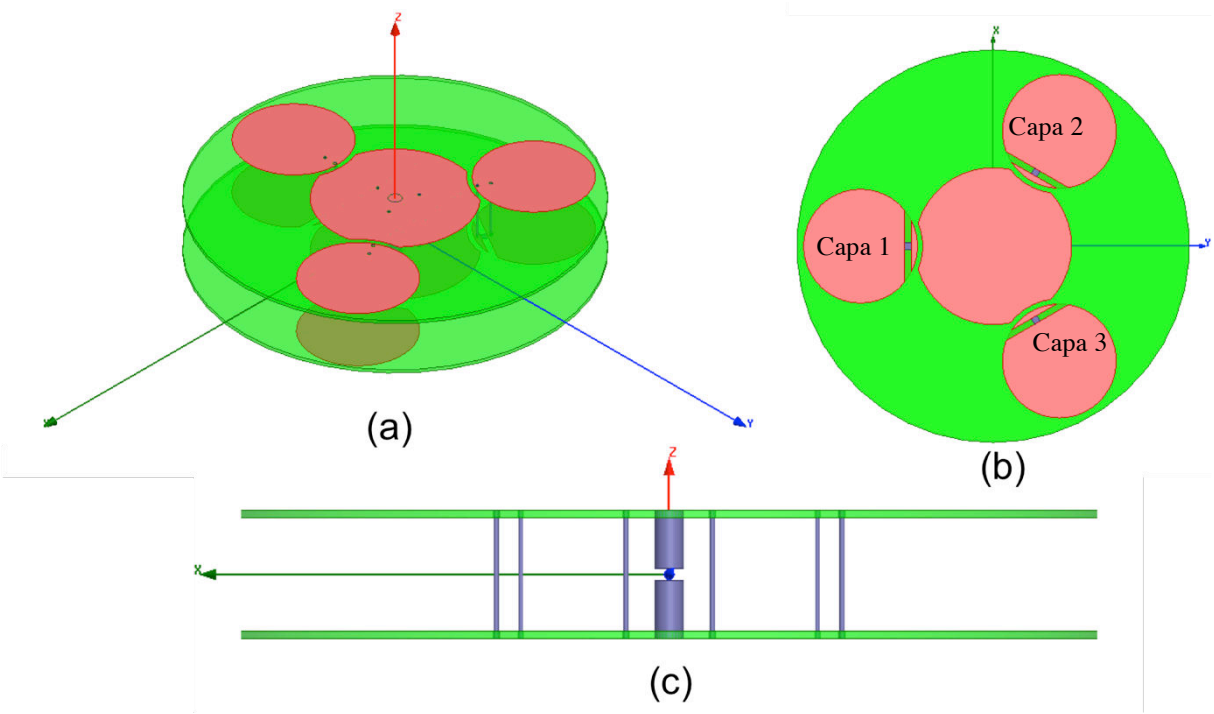

Figure 4.16: The antenna structure. (a) Global view, (b) bottom view, (c) side view

Based on the design approach for the synthesis of pattern reconfigurable antenna 2, a reconfigurable antenna suitable for WSN applications is proposed. The basic shape of antenna structure likes a flattened cylinder, which has two layers. Each layer is place on top of FR4 Epoxy substrate of relative permittivity 4.4 and loss tangent 0.02. The antenna system consists of two parts. At the center of structure, a differential wire-patch antenna is designed as the driven element. It is constituted by two circular plates of radius 12mm separated by a vertical distance of 9mm. At the center of the plates, two vertical metal with the diameter of 2mm is used to feed this element. As well as the wire-patch antenna geometry, three wires with the diameter of 0.35mm located around the feeding cylinder and directly connect the two plates. The distance between the origin to each wire is 3.5mm. The structure of the parasitic elements is quite simple than the driven element. It is constituted by two circular plates of radius 8.5mm (slightly smaller than driven element) and still separated by the same vertical distance. Particularly, the lower plate is divided into two sections due to the slot of width 1mm. This gap is reserved for soldering the DTC. Each parasitic element possesses two vertical wires of diameter 0.35mm that used as short circuit between the plates. The center-to-center distance between the driven and the parasitic elements is about 20.25mm. The plates of driven element are slightly cut in order to have a minimum 0.8mm separation from the parasitic elements.

By using the ANSYS HFSS EM solver, the antenna is simulated. The state of three DTCs defines the pattern reconfigurable mechanism of the proposed antenna. When the capacitor value changes from 1.5pF to 4pF, the parasitic element's characteristic is switched from reflector to director. Thanks to this principle, the antenna radiation pattern will be directed along 6 different directions.

Configuration	Capacitor 1	Capacitor 2	Capacitor 3	D_{max} (φ)
C_1	1.5 pF	2.7 pF	1.5 pF	30°
C_2	1.5 pF	2.7 pF	2.7 pF	90°
C_3	1.5 pF	1.5 pF	2.7 pF	150°
C_4	2.7 pF	1.5 pF	2.7 pF	210°
C_5	2.7 pF	1.5 pF	1.5 pF	270°
C_6	2.7 pF	2.7 pF	1.5 pF	330°

Table 4.3: Radiation pattern configurations.

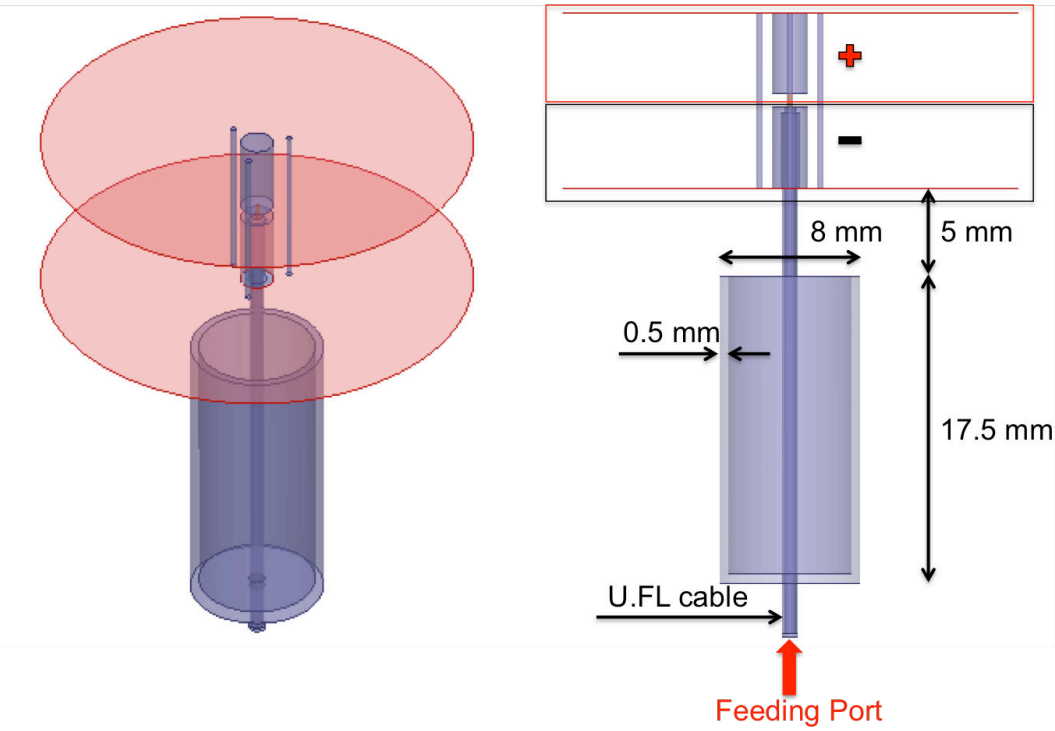

Figure 4.17: The balun structure integrated in the antenna.

Because the antenna feeding method is differential, the measurement is relatively complex. To avoid the reverse current on the cable of VNA, a balun as bazooka type is designed. In theory, a balun is used to BALance UNbalanced systems. In other words, the balun allows us to measure a balance system (differential feed) by using an unbalanced system (VNA). With ANSYS HFSS EM solver, the bazooka balun is designed and simulated. To simplify the simulation, just only the driven element is used to study. The structure and optimizing dimension of balun are shown in Figure 4.17.

The dimension of antenna have been optimized by parametric study aimed at obtain a good impedance match all over the ISM 2.4 GHz band for all the radiating configurations. The final structure occupies a small volume of 60x60x9 mm^3.

3.3. Results and discussion

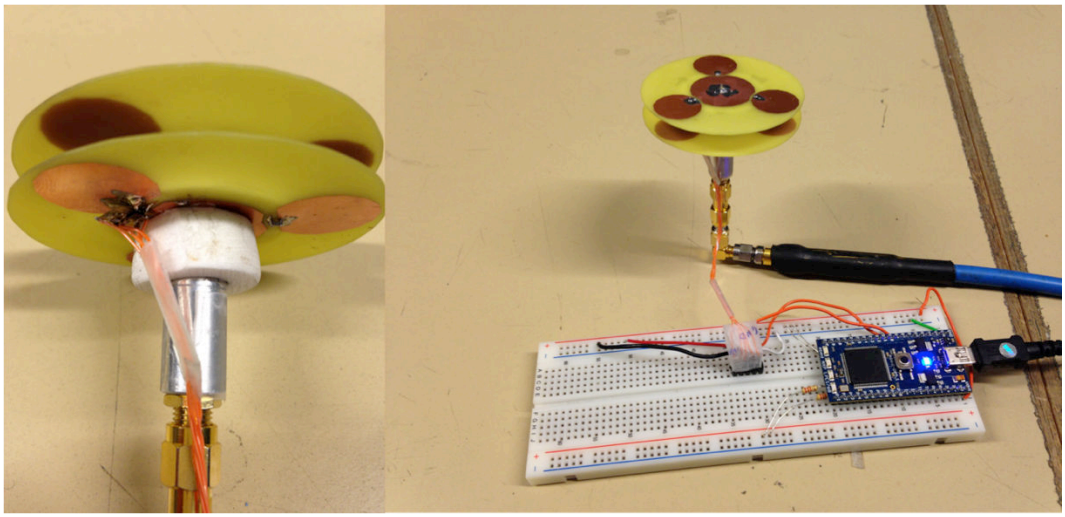

Figure 4.18: The antenna prototype and the control unit

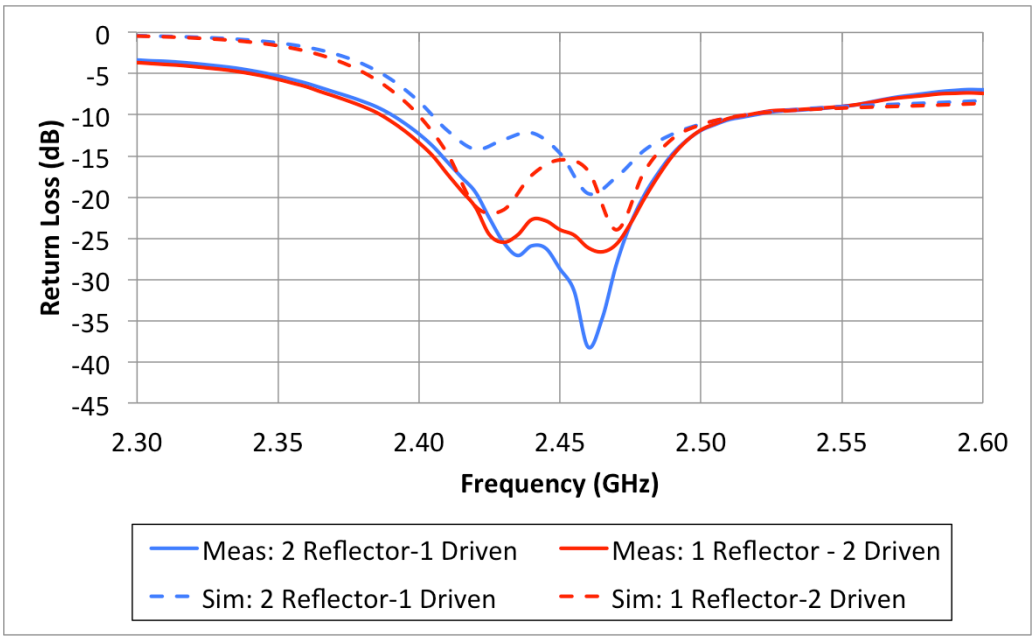

Figure 4.19: Return loss exhibited by the antenna in the different configurations

The prototype of antenna is fabricated as shown in the Figure 4.18. By using Mbed Microcontroller to provide a SPI signal, we can control the DTC on the antenna. Because the antenna geometry is symmetric, so we only need to use a DTC at a parasitic element. The remaining elements have the fix capacitors, one is 1.5 pF and another is 2.7 pF. With this setup, we can measure 2 main configurations of the proposed antenna (1 reflector – 2 drivens and 2 reflectors – 1 driven). From these configurations, the global radiation pattern can be achieved. The simulated and measured S-parameters of 2 configurations is shown on Figure 4.19. The different between simulation and measurement can be explicated by the influence of balun. There is a slightly different between 2 configurations in the impedance matching.

However, the result presents that the proposed antenna operates well in the frequency band required from 2.4-2.48 GHz with the return loss lower than -10 dB.

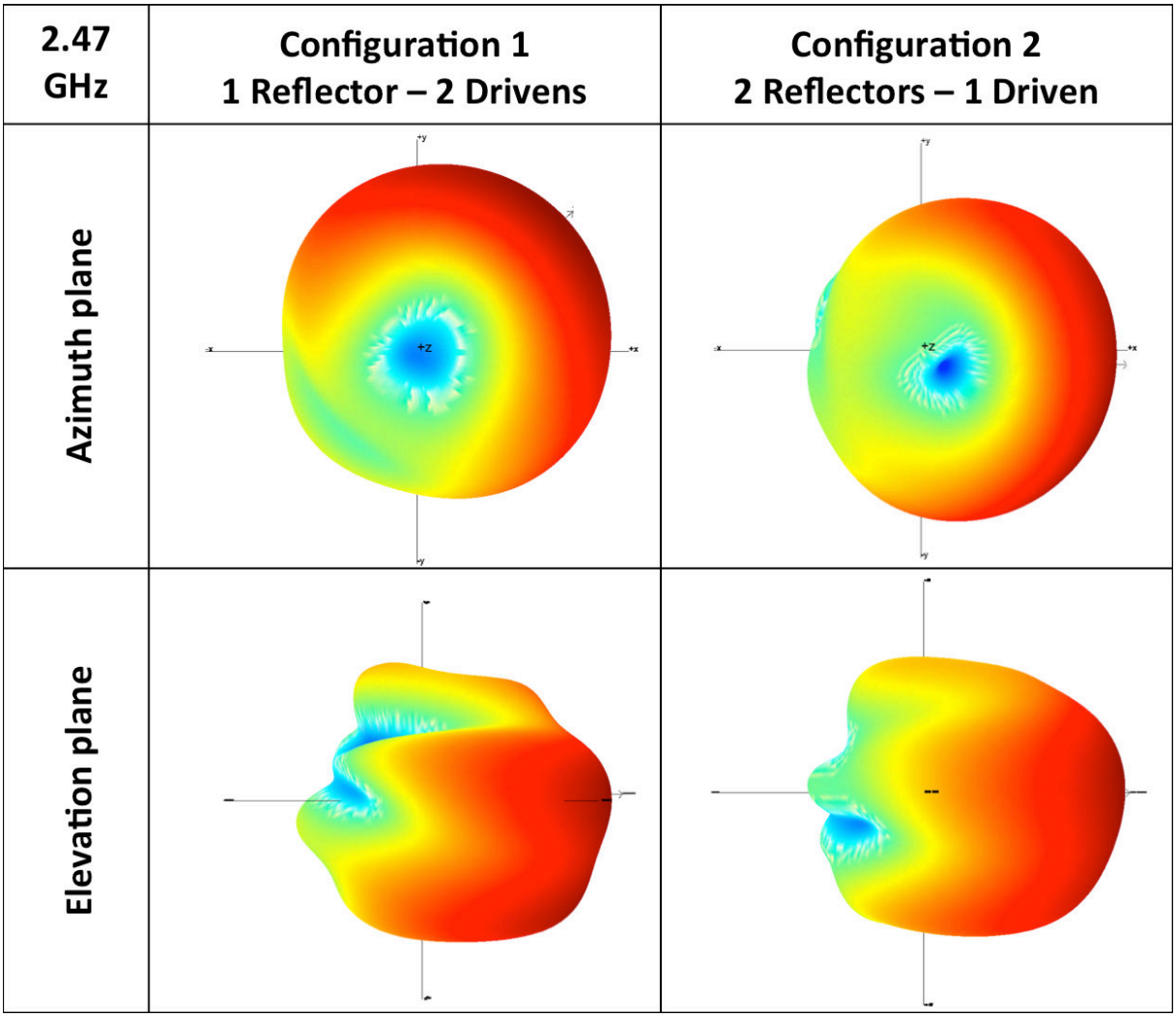

Figure 4.20: Measured 3D realized gain at 2.47 GHz

Figure 4.20 shows the measured realized gain pattern in 3D at 2.47 GHz. From this result, the antenna presents a realized gain with 4.8 dB at the configuration of 2 directors – 1 driven and 3 dB at the configuration of 1 director – 2 drivens. Moreover, the antenna has a good F/B ratio of 10 dB at the first configuration and increase up to 14 dB at the second configuration. However, the total efficiency of antenna seems good, it is around 58% and 69% for configuration 1 and configuration 2, respectively. Because of antenna type is differential feed, we have to add the balun bazooka to measure, this component can degrade the antenna efficiency. Thus when the proposed antenna is mounted directly on the transceiver, the efficiency can be increased. The main results in terms of maximum direction (Dmax), maximum realized gain (Gmax), front-to-back ratio (F/B) and 3dB beamwidth (HPBW) are summarized in Table 4.4.

	D_{max} (φ)	G_{max} (dB)	F/B (dB)	HPBW (Δφ)
Configuration 1	30°	3	10	142°
Configuration 2	90°	4.8	14	124°

Table 4.4: Radiation measured results.

Due to the radiation pattern results, we can deduce the full configuration of antenna when the fix capacitors are replaced by the DTCs.

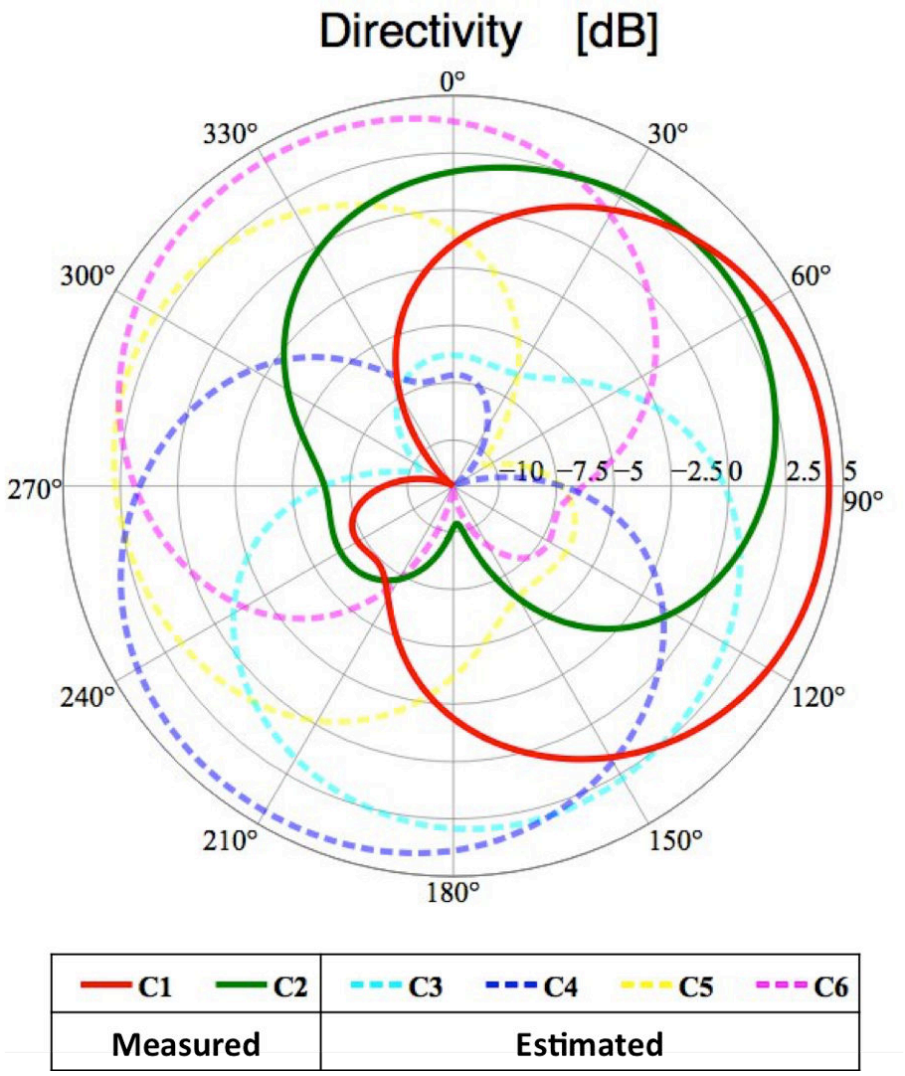

Figure 4.21: Estimated full configuration of the proposed antenna

3.4. Conclusion

In this section, a pattern reconfigurable antenna for PowWow WSN platform has been presented. The antenna has 6 different configurations that can cover all of 360° around the WSN node. The antenna is fabricated and validated by measurements performed on a prototype controlling by Mbed Microcontroller. The future works are implementation the remaining DTCs on the next version. And then, by using PowWow platform, we will measure this antenna system in real environment. This measurement can affirm the great performance of using the directional reconfigurable antenna on the domain WSN. Finally, a final prototype

will be designed and fabricated with all the components that are building in the center of antenna.

4. THE LIGHTHOUSE ANTENNA FOR 2013 IEEE AP-S STUDENT DESIGN CONTEST

The last section in this chapter presents a radiation pattern reconfigurable antenna that has applied for 2013 IEEE AP-S student contest. It has advanced to the semi-final round of this competition.

Goals and Specifications of 2013 AP-S student design contest:

1. Design an antenna system with reconfigurable antenna elements that can adapt to different propagation conditions in order to achieve the best link performance. The performance can be shown in terms of received power or higher level system metric such as symbol error rate.
2. The antenna system should be used to teach how antennas work. Such a system might be used in college undergraduate or graduate courses, and in pre-college ('High School') physics courses.
3. The system must be safe and durable, easily reproducible by others, inexpensive, and portable so that it can be demonstrated at the Symposium.
4. The system must operate at 2.4 GHz, have its own source (i.e. no commercial signal generator can be used), and fit on a table top (roughly 24"x 40") or two closely spaced tables. Readily available software (e.g., student versions of C, Matlab, Visual Basic, LabView) or free software packages may be used. All software must be included in the budget.
5. The total cost for reproduction of the system must be less than $1,500. The use of a laptop computer is allowed and does not have to be included in the $1,500 limit.

Our proposal concerns an inexpensive reconfigurable system with simplicity the influence of the propagation conditions in a wireless link. With this system, concepts of directivity, fading and diversity will become easier to understand for different level of students. The system will be able to interact with any familiar communicating devices with a WiFi transceiver and a web browser (computer, smart phone, tablet…).

4.1. Sophia Team

Sophia team is composed by one PhD student and three under-graduate students and advised by a mentor, list of the team member are below:

1. Trinh Le Huy: Project leader, PhD student at the University of Nice.
2. Belleguie Loic: Undergraduate student, Polytech'Nice, 4th Year, Embedded system specialties.
3. Garret Alexandre: Undergraduate student, Polytech'Nice, 4th Year, Embedded system specialties.
4. Ollivier Loys: Undergraduate student, Polytech'Nice, 4th Year, Embedded system specialties.
5. Fabien Ferrero: Mentor, Associate professor at Polytech'Nice, IEEE member.

4.2. General description of system

The system will focus on the WiFi standard in the 2.4 GHz ISM bands. A directivity reconfigurable antenna topology has to be selected. We especially look for a simple, reliable, light and easy-to-fabricate structure. Main objective is to produce an inexpensive antenna made with very familiar and easy to find material.

The reconfigurable antenna is connected to a Flyport System-on-module solution from OpenPICUS Ecosystem (PIC 16 bit processor and a WiFi Transceiver), and set up on top of a simple 2-wheel robot (with two servo-motors). We can control the operation and the route of robot through the OpenPICUS platform [15]. The Flyport system can embedded a webserver and generate HTML page with AJAX features. Thus, any communicating device with a WiFi transceiver (laptop, tablet, smartphone) could connect to the Flyport and remotely control its operations.

Measurement of the power received on the antenna will be performed by the extraction of the RSSI (received signal strength indicator) given by the WiFi transceiver. Several scenarios to explain concept of directivity, fading and diversity will be proposed. We will present three different scenarios to show the different physical effects.

The first scenario will concern the concept of line of sight (LOS) and non-LOS. The system moves in a 100 cm straight line. RSSI for each radiation configuration is cyclically measured and plotted on a graph on the webpage. One absorber is placed between the emitter and the receiver. At the moment the path from emitter to receiver become an unobstructed view, the configuration that has a beam focusing on emitter is always the best solution to communicate. But in the case of NLOS, the absorbers block the direct path, and other configurations have a better signal.

Second scenario will emphasize the concept of directive antenna. The 2-wheel robot spins at a fixed position in a LOS communication. During the rotation movement, the RSSI of each configuration is measured and traced on the webpage graph. The RSSI for each antenna will reach a maximum value at a different angle.

Finally, the third scenario will explain the concept of fading and diversity. The robot will move straightly by 10 cm steps. For each step, RSSI for each configuration will be measured and thanks to OpenPICUS device, the graph RSSI versus positions for all configurations will be generated directly on the browser. We observe fading effect on the RSSI value of the different configurations. At the end of the measurement, the system will plot on the graph choosing the best configuration for each position (Selection Combining method). At the end of the process, we can deduce the CDF versus RSSI to extract roughly the diversity gain. With this outcome, the interest of directivity diversity is simply shown.

4.3. Antenna concept

Nowadays, as wireless communications have grown rapidly and become an ubiquitous part of modern life, improving quality of signal transmission is greatly necessary. This is a

real challenge for researchers, especially in multi-propagation environment. With the effect of multipath, the fading problem caused by destructive interference always exists. It is considered to propose a multi-directional antenna or one has ability to choose the best channel to communicate. On the basis of a monopole antenna as a driven element and additional the parasitic element as a director, an antenna's concept is presented.

The proposed antenna is fabricated from a metallic cylinder with a hole etched on its base. A coaxial port is placed into this hole in order to feed a monopole inside the cylinder. Three slots are cut evenly onto the cylinder side. In the middle of each slot, a switch system composed by a PIN diode and a bias circuit is soldered on the edge.

Thanks to these switches, the box can be "electromagnetically closed or opened" on one side. Thus, three beams in three different directions can be formed. Hence with this design, the antenna concept is divided into three parts: the monopole antenna, the slotted cylinder and three switch systems.

4.3.1. Monopole Antenna

To have an omnidirectional radiation pattern, the monopole antenna is a reasonable choice. In theory, the resonance frequency is defined by the monopole height. A parametric study of the monopole height influence is presented on Figure 4.22, resonance frequency can be tuned to 2.45 GHz with a height of 30 mm.

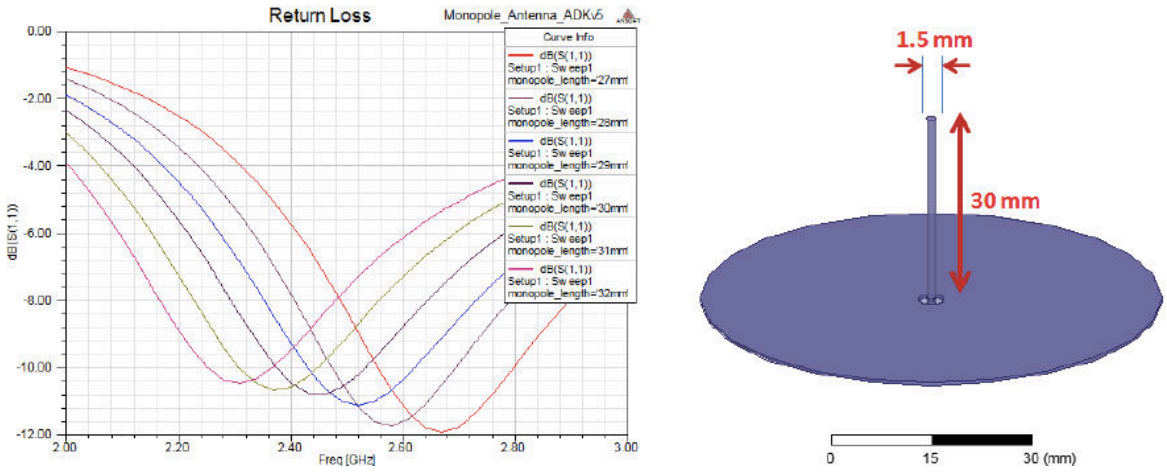

Figure 4.22: Return loss of different antenna length and the view of monopole structure.

4.3.2. The Metallic Cylinder

Similar to the principle of Yagi-Uda antenna, utilizing additional parasitic element can guide the radiation beam to desire directions. And in theory, a horizontal slot on metal can be seen as a vertical monopole. Hence we propose to add parasitic elements around the monopole, which are the horizontal slots, etched on the metallic cylinder. While length of the slots defines the antenna's resonance frequency, its width defines antenna matching. Antenna model and radiation patterns for the different configuration are presented on Figure 4.23.

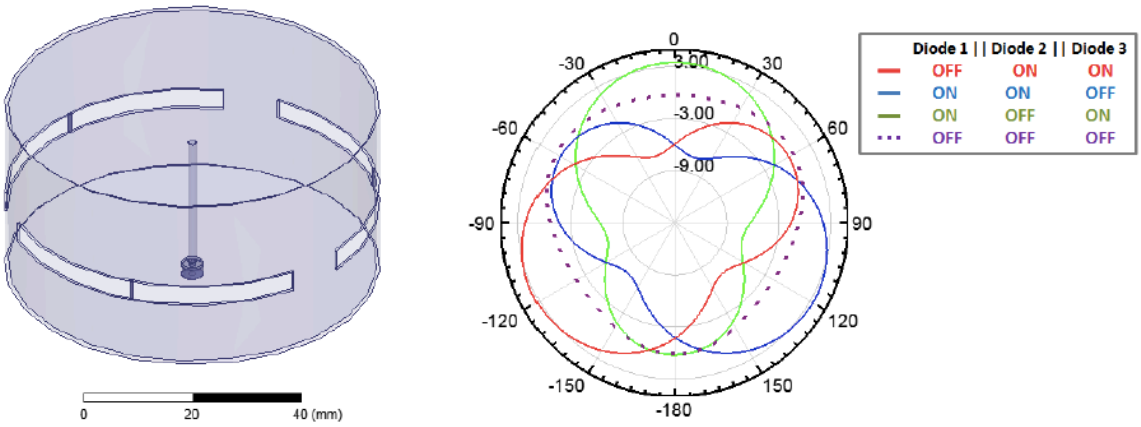

Figure 4.23: Antenna structure and the simulated radiation pattern for different configurations.

4.3.3. Switch System

To prevent a slot to radiate, it is short-circuited at its center by means of a PIN diode. To allow the polarization of the diode, an inductor of "choke" and capacity are used as shown in the diagram below. The reflection coefficient simulation for the different configurations using a PIN diode model is presented on Figure 4.24. The antenna is matched on the 2.4 GHz band with a -10 dB criteria for each configuration.

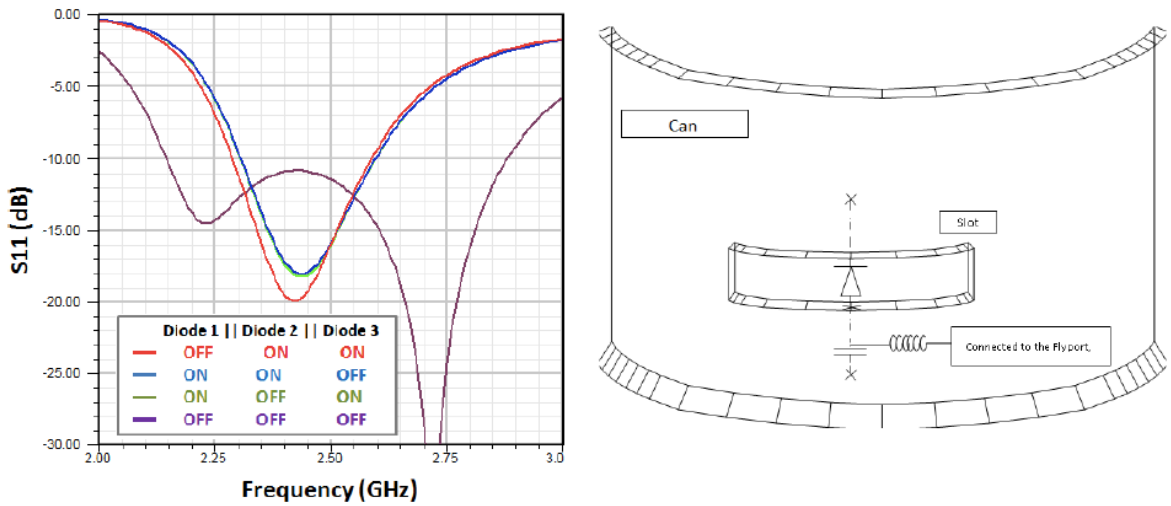

Figure 4.24: Simulated reflection coefficient and switch system topology.

The PIN diode operates like a switch. When the diode is reverse-biased, its resistance is very high (> 1k Ohm) and the diode behaves like an open circuit. Otherwise, its resistance is small (around 1 Ohm), the diode is presented as a short circuit. The DC voltage bias PIN diode is provided from Flyport OpenPICUS. When PIN diode is biased, to assure that the DC source doesn' t interfere with the RF source, the DC block and RF block are integrated. We use capacitor to isolate RF source from the current which activate PIN diode. In the same way RF block, which is a choke coil,

attenuates high frequencies completely. We chose PIN diodes from MACOM with a very small package: MA4SPS502 (ODS-1270) in order to limit as much as possible the impact on the slot radiation [16].

4.3.4. Antenna fabrication

To satisfy the requirements about easily reproducible and inexpensive of contest's subject, we chose the standard coffee can (70 mm of diameter) as the cylinder. Thanks to the HFSS software, the dimension of antenna is optimized. Then, the proposed antenna is presented in Figure 4.25. Measurements have been realized with a SATIMO station. The radiation patterns of all configurations are presented in Figure xx .

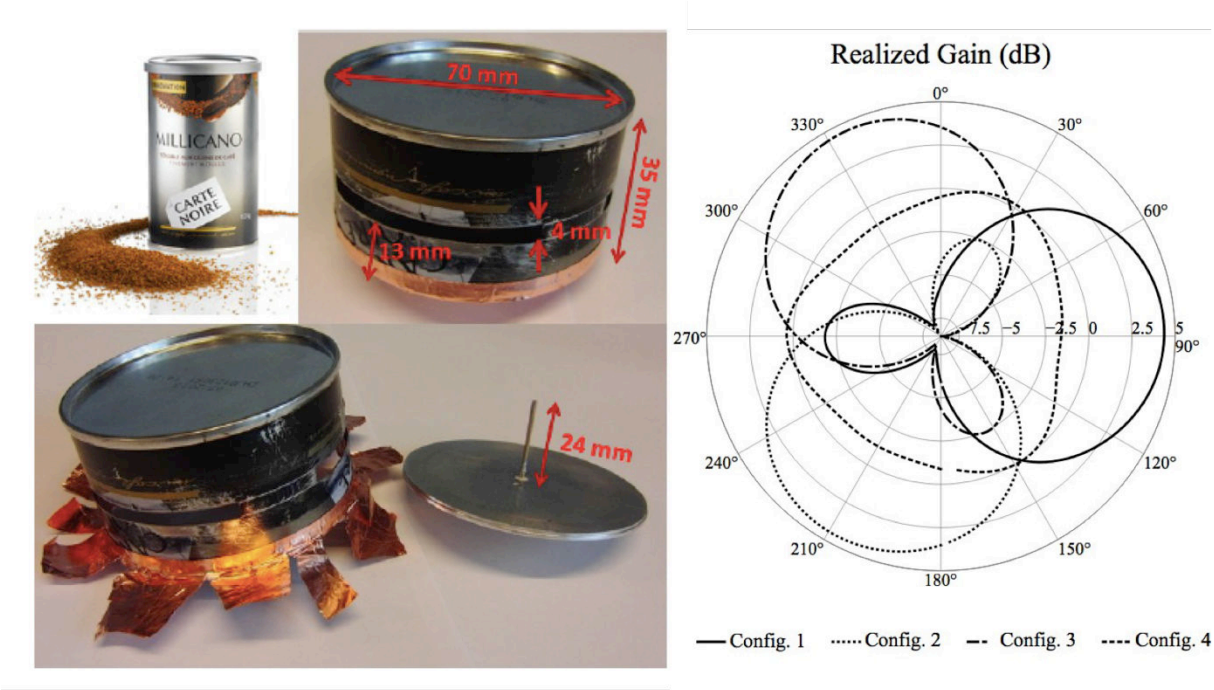

Figure 4.25: The antenna prototype and the azimuth plane of measured radiation pattern.

4.4. Communication system design

4.4.1. OpenPICUS platform

Wi-Fi is a very popular wireless technology to inter-connect electronic devices by using the radio waves at 2.4 GHz. In this project, we used a miniature system named Flyport Wi-Fi (Figure 4.26 (a)) that associates a microchip microcontroller and WiFi transceiver. Flyport provides an easy way to connect sensors/devices to the Internet by programming with the OpenPICUS IDE software. The software stack as well as the IDE is released as open source software. We can measure the received RF power based on the RSSI information. A WiFi scan has to be executed to compute the RSSI for all the different WiFi networks available. On the other hand, the Flyport shows a great feature that is a customizable webserver. This webserver can provide a webpage to any device

that is connected to the Flyport. Thanks to this interface, the user can interact with the proposed system, control the Flyport and plot graph of RSSI. The schematic view of the system is presented on Figure 4.26 (b). To develop all these functionalities we have used some different programming languages as C, HTML, pHp and JavaScript.

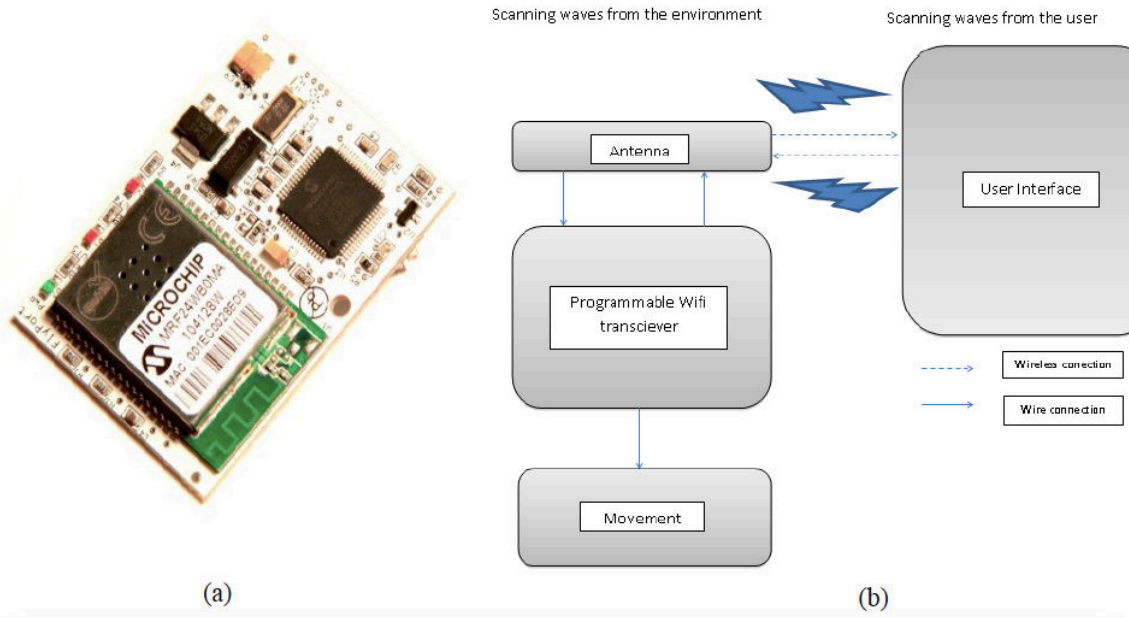

Figure 4.26:(a) Programmable WiFi transceiver and (b) the schematic view of proposed system.

4.4.2. RSSI measurement

The WiFi standard provides mechanisms implemented at both the physical and data link layers to estimate the power of a received signal. This estimate value of the received power is called Received Signal Strength Indicator (RSSI). Absolute accuracy of the RSSI reading is not specified. This definition is implemented by manufacturers in the different ways. The RSSI is computed by estimating the power in the preamble of a Wi-Fi beacon [17]. An Access Point (AP) transmits this beacon repeatedly at fixed intervals, broadcasting basic information about the Wi-Fi network that the AP is creating. Receiving devices generate an estimate of the incident signal power. This mechanism allows us to obtain not only a received power estimate, but also to discriminate between different networks, and obtain a measure with improved noise immunity. To link the RSSI value with the absolute received power, a calibration will be needed.

4.4.3. Movement function

To work on the three scenarios our antenna has to move in straight line or turn by controlling two DC motors. If the two motors are switched on, the robot is going straight line, if only one motor is switched on, the robot is turning on itself. These movements are implemented on the Flyport by using the software OpenPICUS IDE. To

allow these movements, the pins required are matched to a microcontroller. With the software we have defined first which pins are output, then which are switched on or off. To simplify the development of the robot platform, we used an existing robotic board compatible with Arduino microcontroller. Then another board is used to connect the OpenPICUS socket with the Arduino shield socket.

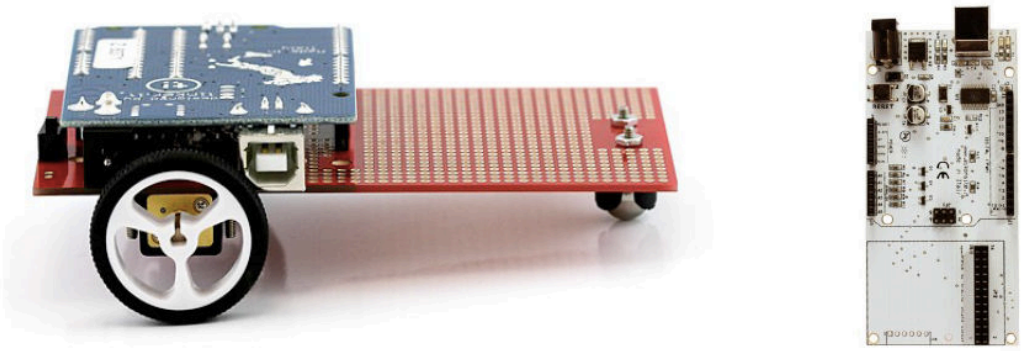

Figure 4.27: The Arduino robot platform

4.4.4. Webserver and control webpage

For more ergonomics and ease of understanding of the phenomena highlighted, a webpage is designed. In addition, this webpage allows accessing the scenarios, controlling the robot, simulating and analyzing the RSSI that indicates the received signal strength. The graph has been designed from an open source AJAX code available on http://www.flotcharts.org/.

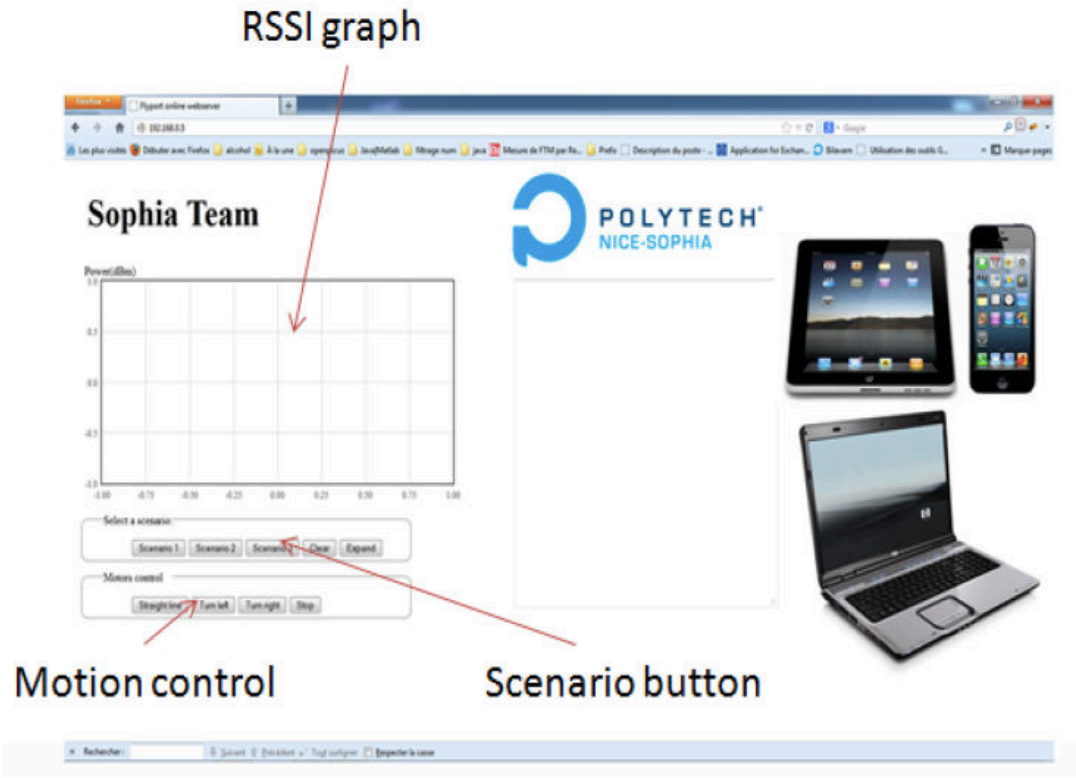

Figure 4.28: The interface of webpage and some device that can communicate with system.

The webpage is presented on Figure 4.28 with a simple interface. There are 4 buttons are used to control the motion of the robot (straight, turn left, turn right and stop), and 5 buttons are used to start scenarios and clear the graph. To access to this webpage, the IP address of the Flyport is entered in a web browser.

4.5. Fabrication and calibration

4.5.1. A. System assembly

The antenna, the Flyport WIFI module, Robot platform board and prototyping board were assembled. The final system is presented on Figure 4.29. As you can see, the antenna is placed over the robot platform using a FR4 PCB. Assembly is not perfectly clean, but it will be improved in the next weeks. The system is powered with 3 AA batteries.

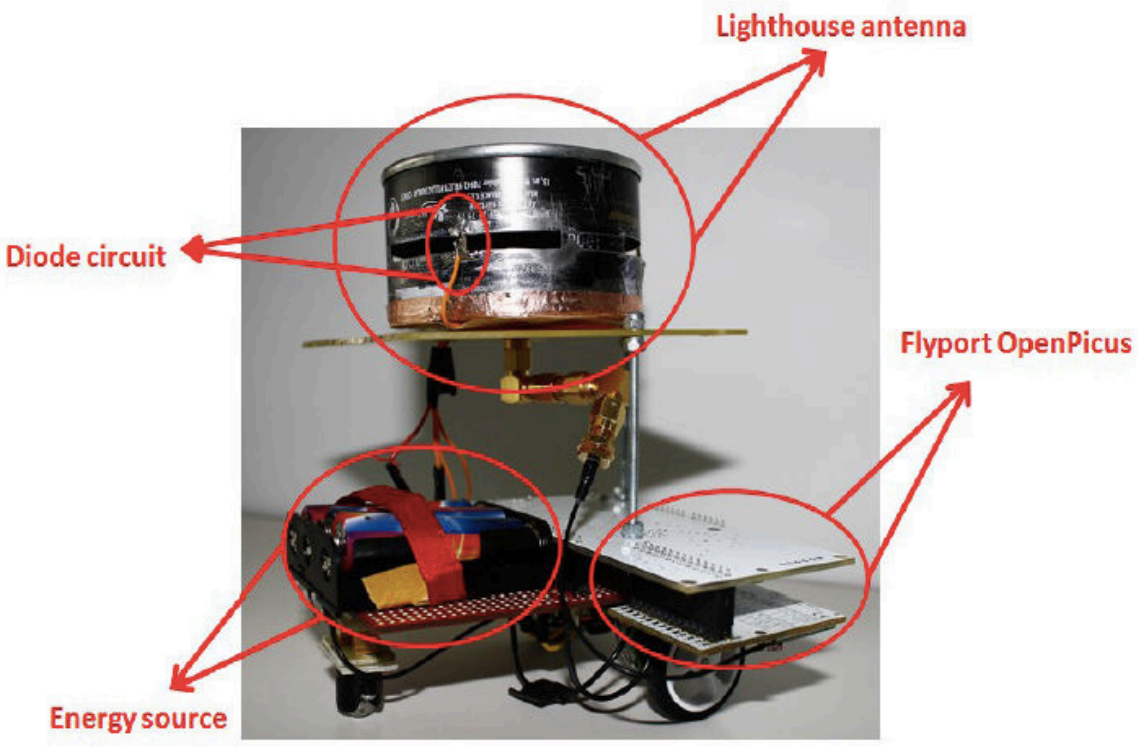

Figure 4.29: Completed system of the lighthouse on wheel antenna

4.5.2. Calibration of OpenPICUS power sensing

We make the calibration in an anechoic chamber to avoid parasitic reflection and to get a stable response of the channel. We realize measurement for different distance between the WiFi gateway and the robot. From the measured result, we deduce a simple formula to convert the RSSI value to the power received in dBm, as it is shown on the Figure 4.30. This formula is only valid on the -50 to -80 dBm range, thus we have 30 dBm of dynamic:

$$P_{dBm} = RSSI - 215$$

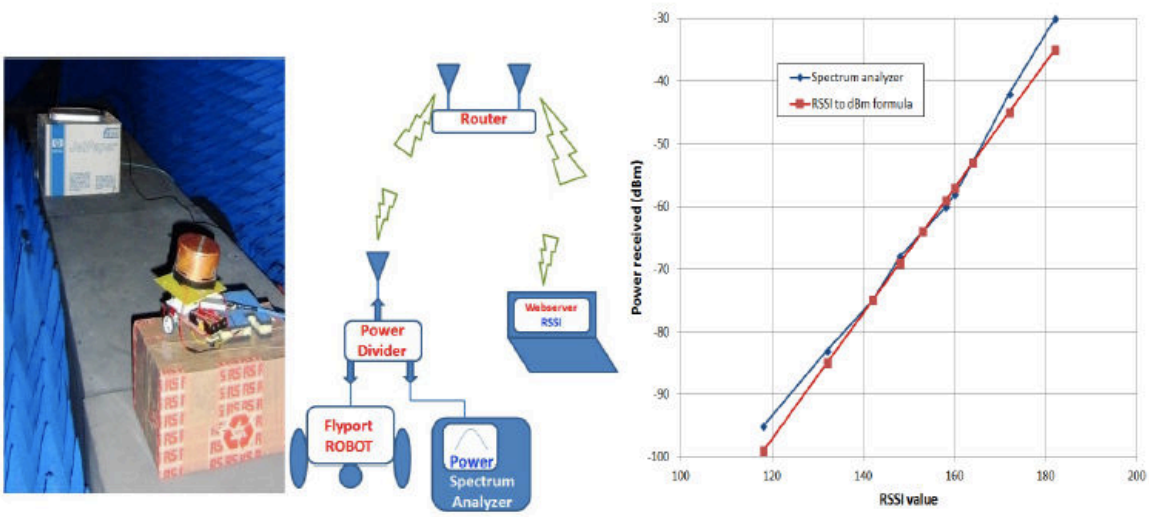

Figure 4.30: The procedure of calibration and received power with respect to RSSI value.

4.6. Scenarios validation test

The different scenarios have been tested to verify the functionality of the system.

4.6.1. Scenario 1

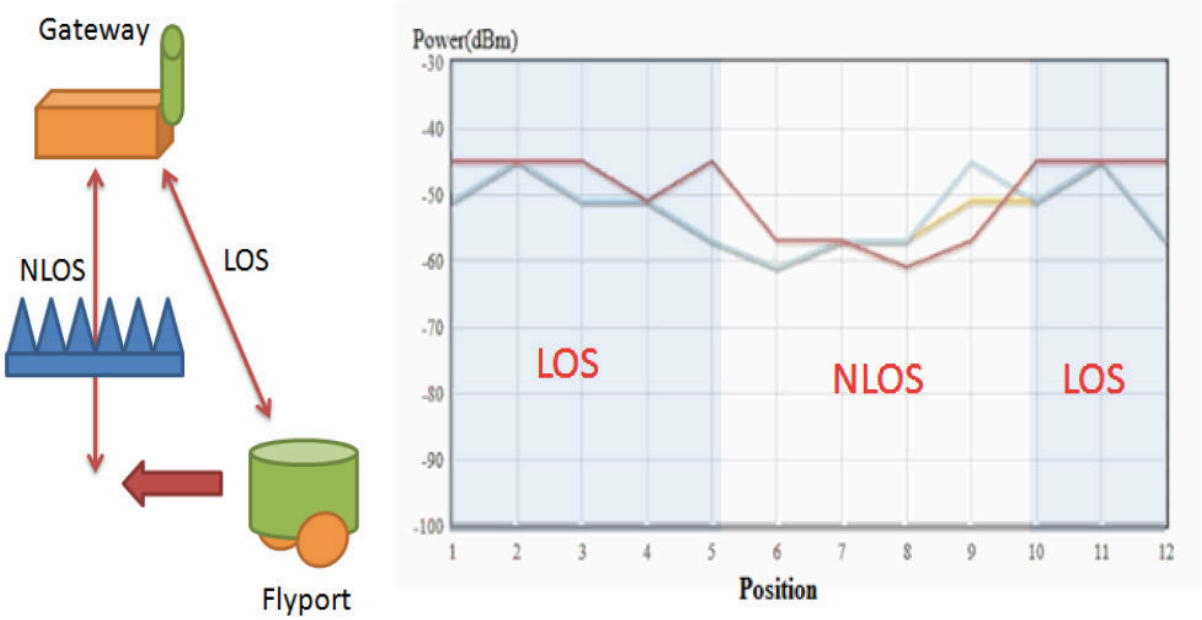

Figure 4.31 : Scenario 1 description and received powers at different positions

The first scenario will concern the concept of LOS and NLOS. The system moves in a 50-cm straight line. RSSI for each radiation configuration is cyclically measured; the best configuration is indicated by the corresponding LED. Several absorbers are placed between the emitter and the receiver. The reflector is also added on the side to maximize NLOS communication. At the moment the path from emitter to receiver become an unobstructed view, the configuration that has a beam focusing on emitter is always the best solution to communicate. But in the case of NLOS, the absorbers block the direct path, so we have to switch to other configurations in order to find the best way for communication. By using the LEDs, we can easily see which configuration have the highest RSSI. The result is presented on the Figure 4.31. It shows the received power for a slot pointing toward the gateway (red curve). When the absorber blocks the line of sight path, the red curve decreased from -45dBm to -60 dBm. In the LOS configuration the received power is not perfectly flat due to the multi-path effect.

4.6.2. Scenario 2

In the second scenario, the 2-wheel robot spins at a fixed position. The absorbers are placed around the gateway to create a clean LOS communication. During the rotation movement, the RSSI of each configuration is measured and traced a graph that is available on the OpenPICUS Webserver. Each rotation step is about 35°, then, the

robot spin completely in 10 steps. We experience a lot of problem with the scenario due to the reflections in the lab room. However, in the graph presented, we can see that optimal received power for each slot in different rotation angles. Results would have been better in an anechoic chamber. We are still trying to find a better solution to clearly show this concept of directivity in a simple demonstration.

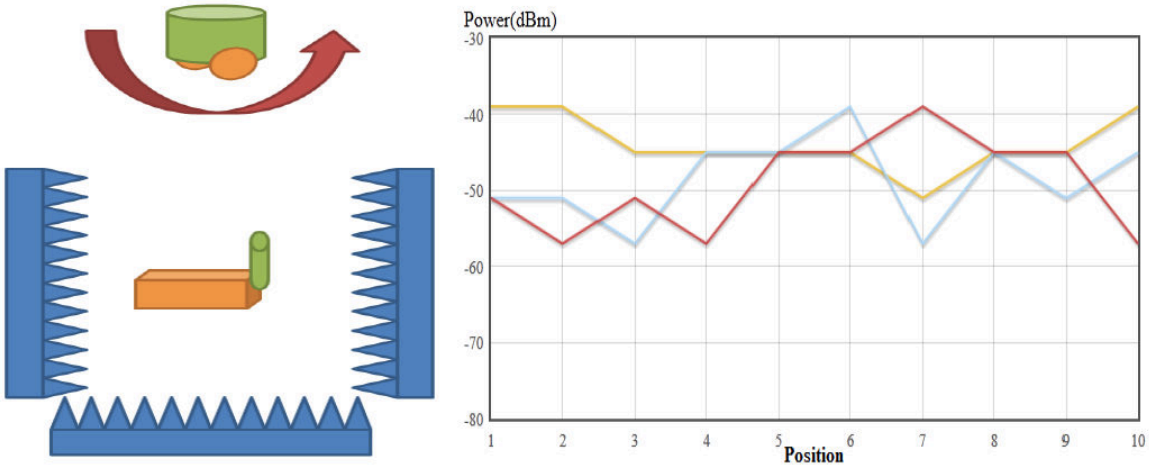

Figure 4.32: Scenario 2 description and received powers at different positions

4.6.3. Scenario 3

With the third scenario, we will try to explain the concept of fading and diversity. The robot will move straightly by 10mm steps. For each step, RSSI for each configuration will be measured and thanks to OpenPICUS device, the graph RSSI versus positions for all configurations will be generated directly on the browser. The experiment has been realized in the electronic labs room of the school. It is a large room (6*9*3m3) with many metallic objects (whiteboard, lab tables, metallic ceiling, etc). Thus, this environment should generate a string multi-path effect. As shown on the Figure 4.33, we observe deep fading effect on the RSSI of the different configurations. Strong attenuations, higher than 15dB, are observed. However, we can see that deep fading effect does not occur at the same time on the different configuration. Then, by selecting the configuration with the strongest received power, it is possible to limit fading effect. With this outcome, the interest of directivity diversity is simply shown.

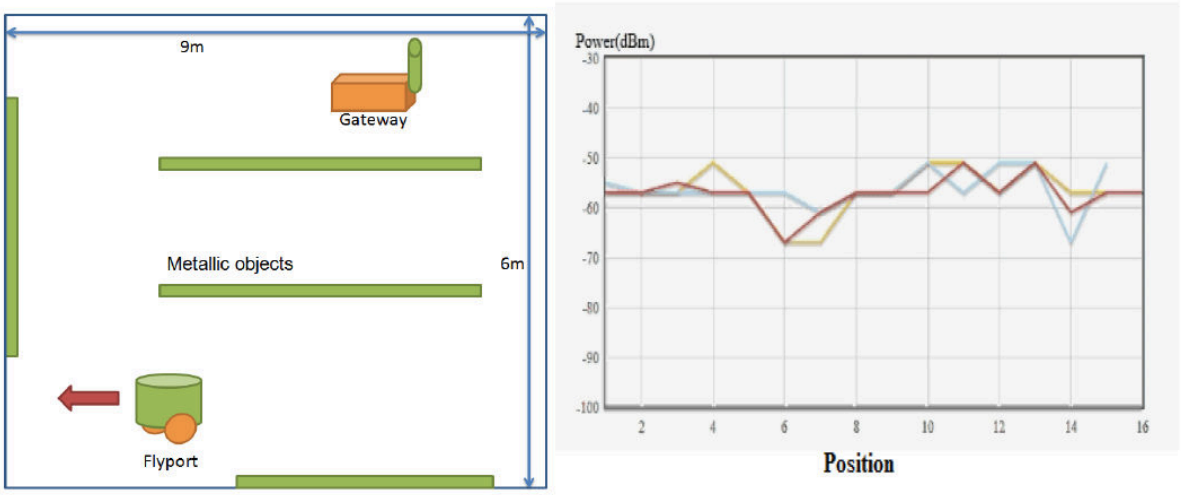

Figure 4.33: Scenario 3 description and received powers at different positions

4.7. Conclusion and perspectives

Several items have not been implemented for now, but will be added in the future as the indicated LED above each slot to show which slot is closed or opened. In the different scenario, the omnidirectional configuration with all diodes switched off, will be used as a reference configuration. The actual prototype has still some bugs that have to be corrected for the final demonstration

REFERENCE OF THIS CHAPTER

[1] T. N. Le, A. Pegatoquet, O. Sentieys, O. Berder, and C. Belleudy, "Duty- Cycle Power Manager for Thermal-Powered Wireless Sensor Networks", *24th IEEE Int. Symp. Personal, Indoor and Mobile Radio Comm.*, pp. 144-149, London, UK, Sept. 8-11, 2013.

[2] L. Catarinucci, S. Gugliemi, R. Colella, and L. Tarricone, "Compact switched-beam antennas enabling novel power-efficient wireless sensor networks", IEEE Sens. Journ., vol. 14, no. 9, pp. 3252-3259, 2014.

[3] C. Kittiyanpunya and M. Krairiksh, "A four-beam pattern reconfigurable Yagi-Uda antenna", IEEE Trans. Antennas Propag., vol. 61, no. 12, pp. 6210-6214, 2013.

[4] K. Kim, K. Hwang, J. Ahn, and Y. Yoon, "Pattern Reconfigurable Antenna for Wireless Sensor Network System", *Electron. Lett.*, vol. 48, no. 16, pp. 984-985, 2012.

[5] Pontes, J., Reichardt, L., andZwick, T., ''Investigation on antenna systems for car-to-car communication", *IEEE Journ. Sel. Areas Comm.*, 2011, 29, (1), pp. 7-14.

[6] Alexander, P., Haley, D., and Grant, A.: ''Cooperative intelligent transport systems: 5.9-GHz field trials", *Proc. IEEE*, 2011, 99, (7), pp. 1213-1235.

[7] Aïssat, H., Cirio, L., Grzeskowiak, M., Laheurte, J.-M., and Picon, O., "Reconfigurable circularly polarized antenna for short-range communication systems", *IEEE Trans. Microw. Theory Tech.*, 2006, 54, (6), pp. 2856-2863.

[8] Leonardi, O., Pavone, M., Cadili, T., Sorbello, G., and Isernia, T., "Monolithic patch antenna for dedicated short-range communications", *Electron. Lett.*, 2013, 49, (2), pp. 85-86.

[9] Rafi, G. R., Mohajer, M., Malarky, A., Mousavi, P., and Safavi-Naeini, S., "Low-profile integrated microstrip antenna for GPS-DSRC application", *IEEE Ant. Wireless Propag. Lett.*, 2009, 8, pp. 44-48.

[10] Gallo, M., Bruni, and S., Zamberlan, D., "Design and measurement of automotive antennas for C2C applications", Proc. 6th European Conf. Antennas Propag. (EUCAP), Prague, Czech Republic, 2012, pp. 1799-1803.

[11] S. Lim, "Design of a multidirectional, high-gain compact Yagi antenna," *IEEE Antennas Wireless Propag. Lett.*, vol. 8, pp. 418-420, 2009.

[12] R. Schlub and D. V. Thiel "Switched parasitic antenna on a finite ground plane with conductive sleeve," *IEEE Trans. Antennas Propag.*, vol. 52, no. 5, pp. 1343-1347, 2004.

[13] C.-H. Ko, I.-Y. Tarn, and S.-J. Chung, "A compact dual-band pattern diversity antenna by dual-band reconfigurable frequency-selective reflectors with a minimum number of switches," *IEEE Trans. Antennas Propag.*, vol. 61, no. 2, pp. 646-654, 2013.

[14] L. Lizzi, F. Ferrero, J.-M. Ribero, and R. Staraj, "Low-profile TETRA wire-patch antenna for automotive applications," *Microw. Opt. Techn. Lett.*, vol. 54, no. 7, pp. 1711-1714, 2012.

[15] http://www.openpicus.com/

[16] PIN diodes MA4SPS502 : http://www.macomtech.com/DataSheets/MA4SPS502.pdf

[17] Picco, V.; Martin, K., "An Automated Antenna Measurement System Utilizing Wi-Fi Hardware," Antennas and Propagation Magazine, IEEE , vol.53, no.6, pp.173,184, Dec. 2011

CHAPTER V
CONCLUSION

Several reconfigurable antenna designs have been proposed in this manuscript. The chapter 2 presented an overview of active devices, and especially digitally tunable capacitor (DTC) that was used in this thesis. measurement RF characterization of the device has been presented, and main advantages of this component have been highlighted: high power handling (34 dBm), low power consumption and low ESR. Component control method is more complex than classical device like PIN or varactor diode, but most modern communication devices are supporting SPI or I2C protocol, so the integration of these components in the communicating terminal is feasible. In addition, due to the low DC power consumption (0.7 mW/DTC), this component is suitable for the applications requiring very low power as WSN. A reconfigurable antenna for White Space applications has been designed to demonstrate the capability of DTCs. The proposed antenna consists in two resonators with a DTC that is integrated on each element. The antenna operation frequency range is 470-710 MHz that is used for DVB-T but could be used for White-space communication using cognitive radio system in the next years.

In chapter 3, we have introduced three different antennas; the first is a passive multiband antenna that operates at the frequency bands such as 700-960 MHz for LTE 700/GSM 900, 1710-2170 MHz for GSM 1800/LTE 1800/UMTS bands, 2400-2700 MHz for ISM, Bluetooth, Wi-Fi and LTE 2600 applications. Due to the relative small size ($68\times130\times1.6$ mm^3), this antenna becomes a good candidate for the mobile devices. The radiation efficiency greater than 55% ensures that the antenna operates with good performances. Based on the principle of this antenna, we propose a MIMO design with four elements. The shape and size of the antenna is changed and optimized for a mid-size device like tablet. This antenna system operates at the frequency bands of 790-960 MHz for LTE 800/GSM 900, 1710-2170 MHz for GSM 1800/LTE 1800/UMTS bands, and 2400-2700 MHz for ISM, Bluetooth, Wi-Fi, LTE 2600. Due to the radiation efficiency greater than 58%, we can assert that this antenna system can work well for this application. A demonstration of 4x4 MIMO LTE communications was realized in Monaco in the frame of Spectra project.

Considering that passive antenna is reaching its limit, the continue expansion of antenna operating band, especially at low frequencies is impossible. Therefore, the last antenna in this chapter is a reconfigurable-multiband antenna that can operate for fundamental communication standards and TV White Space. The antenna structure is matched permanently over the high frequency bands including DCS/PCS, UMTS, LTE 1800/2600, and 3.5GHz bands. Concerning the sub-GHz bands, by using DTC component, several reconfigurable states enable a full coverage of LTE 600/700 and GSM 850/900 standards, as well as future applications on TV White space (TVWS). Thanks to the compact size ($40\times10\times6$ mm^3), this antenna is a good candidate for 5G mobile terminal, and especially MIMO system..

Then, in chapter 4, three directivity reconfigurable antennas for WSN applications were introduced. The first one is an antenna for Car-to-Car applications. Thanks to the design of a low-profile, antenna system is suitable to be mounted on a large ground plane, such as the vehicle roof. The proposed antenna is based on the combination of multiple elements, which can act as radiators or reflectors by using the reconfiguration control circuit. The proposed

antenna is able to steer the beam towards 6 different directions in the azimuthal plane as well as to exhibit an omnidirectional radiation pattern. The next antenna is a pattern reconfigurable antenna for PowWow WSN platform. The antenna system consists of two parts. At the center of the structure, an antenna wire-patch acts as a main element. Around it, three parasitic elements are placed. On each element, a variable capacitor (DTC) is integrated, depending on the capacitor value; the role of parasitic elements is changed between director and reflector mode. Thus, this antenna can cover all of 360° around the WSN node with 6 different configurations. And finally, we have presented a directivity reconfigurable antenna that has applied for 2013 IEEE AP-S student contest. With this antenna system, our team reached the semi-final round of this competition. The proposed antenna is fabricated from a metallic cylinder with a hole etched on its base. A coaxial port is placed into this hole in order to feed a monopole inside the cylinder. Three slots are cut evenly onto the cylinder side. In the middle of each slot, a switch system composed by a PIN diode and a bias circuit is soldered on the edge. By changing the state of these PIN diodes, the radiation pattern of antenna can be reconfigured and enables the antenna system to cover all of 360° around the system.

Some possible improvement for the antennas presented in this thesis can be the optimization of the reconfigurable-multiband antenna (that is presented on chapter 3) for the MIMO applications. Firstly, antenna dimensions have to be miniaturized as much as possible. And then, by analysis of characteristic modes on the chassis of antenna, the optimal position of second antenna can be found. By using a MIMO test bench, the performance of the proposed antenna system can be evaluated.

In addition, for the directivity reconfigurable antenna that is introduced on chapter 4, a WSN simulator is being developed and tested thanks to a collaboration with MCSOC team in LEAT. A single hop network with one Base Station (BS) and eight End Devices (ED) are implemented in OMNET+. The EDs are randomly distributed around the BS. All the nodes are equipped either with omnidirectional or directive antennas (2, 3, 4, 6 directions). Based on a realistic protocol for exchanging data in the network, a comparison of the performance of the different types of antenna is performed. Some parameters are extracted such as the total power consumption and the collision between the nodes. First results, shown in Table 5.1, demonstrated the advantage of directional antenna compared with omnidirectional antenna on WSN applications. A 42% reduction of the total power consumption is observed for 4 directions case compared with ommnidirectional case. .

	Number of connected nodes	Collision (%)	Consumption (mJ)	RSSI (dBm)
Omnidirectional	8	48.03	1.67	-79.02 for 50m
2 directions	6	26.77	1.13	-91.97 for 100m
3 directions	7	8.16	0.74	-85.03 for 100m
4 directions	8	2.08	0.71	-74.13 for 100m
6 directions	8	0	0.98	-71.56 for 100m

Table 5.1: Results of WSN simulator.

LIST OF FIGURES

LISTE OF TABLES

APPENDIX 1: MBED Compiler Code

```
#include "mbed.h"
 #include <iostream>
 #include <iomanip>

 //Configuration of the different port used
 I2C i2c1(p9, p10);// sda(data), scl(clock)
 I2C i2c2(p28,p27);

// slave's address with the R/W bit (1 bit ('0' for write) left shifted), original address is 0x71
 const int addr1 = 0xE2;
 const int addr2 = 0xE0;

 int data1=2; //Writing data on i2c1
 int data2=19; //Writing data on i2c2

 int main() {
    i2c1.frequency(10000);

   // int data1;
   // bool flag = false;

     while(1){

       //Writing data on i2c1 bus (p9, p10)
       i2c1.start();
       i2c1.write(addr1);
       i2c1.write(data2);
       i2c1.stop();

       wait_ms(2);

       //Writing data on i2c1 bus (p28, p27)
       i2c2.start();
       i2c2.write(addr2);
       i2c2.write(data2); // 0 <=> C=0.6pF and 19 <=> C=3pF
       i2c2.stop();

       wait(2);
   }
 }
```

APPENDIX 2: Scilab Code to calculate ECC

```
clear()
 close()
 clc

 A=fscanfMat('conf1_470.tab');
 B=fscanfMat('conf3.tab');

 taille=size(A)
 n=taille(1,1)-1;
 m=(taille(1,2)-5)/4;
 res_theta=180/n;
 res_phi=360/m;

 Eph1=A(:,(m+3):(2*m+3))+%i*A(:,2:(m+2));
 Eph2=B(:,(m+3):(2*m+3))+%i*B(:,2:(m+2));
 Eth1=A(:,(3*m+5):(4*m+5))+%i*A(:,(2*m+4):(3*m+4));
 Eth2=B(:,(3*m+5):(4*m+5))+%i*B(:,(2*m+4):(3*m+4));

 for i=1:n+1
    for j=1:m+1

 A0(i,j)=(Eth1(i,j)*conj(Eth2(i,j))+Eph1(i,j)*conj(Eph2(i,j)));
 end
    end

 //discretisation de theta et phi
 theta=0:res_theta:180;
 sinus_theta=sin(theta*%pi/180)';
 A1=A0(1,:)*sinus_theta(1);
 for i=1:n+1
 A1(i,:)=A0(i,:)*sinus_theta(i,:);
 end

 B0=((abs(Eth1)).^2+abs(Eph1).^2);
 C0=((abs(Eth2)).^2+abs(Eph2).^2);
 B1=B0(1,:)*sinus_theta(1);
 C1=C0(1,:)*sinus_theta(1);
 for i=1:n+1
 B1(i,:)=B0(i,:)*sinus_theta(i,:);
 C1(i,:)=C0(i,:)*sinus_theta(i,:);
 end

 A=(sum(A1*5*(%pi/180)*10*(%pi/180)));
 B=(sum(B1*5*(%pi/180)*10*(%pi/180)));
 C=(sum(C1*5*(%pi/180)*10*(%pi/180)));
 coeff_cor=A./(sqrt(B).*sqrt(C))
 ro.nom=(abs(A))^2./(abs(B).*abs(C))

 envcor=(abs(A))^2./(abs(B).*abs(C))

 //S-parameters

 S11=0.51+0.278*%i;
 S21=-0.275-0.094*%i;

 envcorr2= abs(((conj(S11)*S21*2).^2)/((1-S11.^2-S21.^2).^2))
```

PUBLICATIONS

INTERNATIONAL JOURNAL PAPERS

[1] **L.H. Trinh**, L. Lizzi, F. Ferrero, R. Staraj, J-M Ribero, "Reconfigurable Antenna for Future Spectrum Reallocations in 5G Communications", IEEE Antennas and Wireless Propagation Letters, April 2015. (Submitted)

[2] L. Lizzi, **L.H. Trinh**, F. Ferrero, R. Staraj, J-M Ribero, "S-Parameters Based Methodology for the Design of Pattern Reconfigurable Antennas", IEEE Transactions on Antennas and Propagation, Mai 2015. (Submitted)

INTERNATIONAL CONFERENCE PAPERS

[1] **L.H. Trinh**, F. Ferrero, R. Staraj, J-M. Ribero, " 700-960MHz MIMO antenna for picocell applications ", IEEE International Symposium on Antennas and Propagation and USNC-URSI National Radio Science Meeting, Florida, July 2013.

[2] **L.H. Trinh**, F. Ferrero, R. Staraj, J-M. Ribero, " Mobile phone antenna for 2G, 3G and 4G standards ", The International Conference on Advanced Technologies for Communications, Ho Chi Minh, Oct. 2013.

[3] L. Belleguie, A. Garret, L. Ollivier, **L.H. Trinh**, F. Ferrero, " The Lighthouse on Wheel Antenna ", Sophia Antipolis Microelectronics Conference, Oct. 2013.

[4] T.Q.V. Hoang, **L.H. Trinh**, F. Ferrero, Tan-Phu Vuong, J-L Dubard, " Space Diversity for Robust Wireless Power Transmission in Multipath Environments ", IEEE International Symposium on Antennas and Propagation and USNC-URSI National Radio Science Meeting, Memphis, July 2014.

[5] Leonardo Lizzi, **L.H. Trinh**, F. Ferrero, A. Pegatoquet, J-M Ribero, R. Staraj, " Synthesis of Miniature Pattern-Reconfigurable Antennas for Smart Wireless Sensor Nodes "", IEEE International Symposium on Antennas and Propagation and USNC-URSI National Radio Science Meeting, Memphis, July 2014.

[6] Van Hoang, T.Q.; **Trinh, L.H**.; Ferrero F.; Seguenot, E.; Tan-Phu Vuong; Dubard, J.-L., " Rectenna measurement in a realistic environment ", IEEE Conference on Antenna Measurements & Applications (CAMA), Juan les Pins, Nov 2014.

[7] **L.H. Trinh**, F. Ferrero, R. Staraj, J-M Ribero , "Reconfigurable Antenna for Extension of LTE Operational Mode Over TV White Spaces", IEEE European Conference on Antenna and Propagation, Lisbon, Avril 2015.

[8] **L.H. Trinh**, F. Ferrero, R. Staraj, J-M Ribero , “Influence of Component ESR on a 4g Frequency Reconfigurable Antenna”, IEEE International Symposium on Antennas and Propagation and USNC-URSI National Radio Science Meeting, Vancouver, July 2015.

NATIONAL CONFERENCE PAPERS

[1] **L.H. Trinh**, E. Le Guen, F. Ferrero, R. Staraj, J-M. Ribero, J-L. Mattei, “ Miniaturisation d’antenne IFA avec un matériau magnéto-diélectrique pour l’application LTE 700-GSM dans une picocell ”, Journées Nationales Microondes, Paris, May 2013.

[2] **L.H. Trinh**, L. Lizzi, F. Ferrero, R. Staraj, J-M Ribero , “Antenna reconfigurable pour l’appilcation Car-to-Car”, Journées Nationales Microondes, Bordeaux, Juin 2015.